



DISSERTATION

# Changes of EEG Synchrony in the Course of Alzheimer's Disease Markers Based on the Multivariate Spectral Density

ausgeführt zum Zwecke der Erlangung des akademischen Grades eines  
**Doktors der technischen Wissenschaften**

unter der Leitung von

**Em.O.Univ.Prof. Dipl.-Ing. Dr.techn. Manfred Deistler**

E105 - Institut für Wirtschaftsmathematik

eingereicht an der Technischen Universität Wien

Fakultät für Mathematik und Geoinformation

von

**Dipl.-Ing. Markus Waser**

Matrikelnr.: 0426023

Promenadegasse 11-13/3/11, 1170 Wien

Wien, am 19.09.2013

---

(Markus Waser)



---

## Kurzfassung

---

Die Alzheimer Krankheit – die Hauptursache von Demenz – ist eine neurodegenerative Erkrankung die gravierende soziale, gesellschaftliche und ökonomische Folgen mit sich zieht. In dieser Dissertation werden Synchronitäts-Veränderungen im Elektroenzephalogramm (EEG) von Alzheimer-Patienten untersucht. Synchronität wird dabei mit verschiedenen Maßen, die auf die multivariate spektrale Dichte des EEG basieren, untersucht. Ziel ist es die Möglichkeit aufzuzeigen, Marker für EEG-Synchronität als Ergänzung zu bestehenden klinischen Diagnose- und Prognose-Prozeduren zu verwenden.

Für diese Studie wurden 79 EEG-Aufnahmen von Alzheimer-Patienten aus der PRODEM-AUSTRIA Datenbank verwendet. Die Aufnahmen unterliegen einem klar definierten klinischen Paradigma das eine Ruhephase und ein kognitives Testverfahren beinhaltet. Der Krankheitsgrad wurde durch den neuropsychologischen Mini-Mental State Examination Test Score quantifiziert. Alter, Geschlecht, Bildungsgrad und Krankheits-Dauer wurden als Kovariable eingesetzt.

Die multivariate spektrale Dichte wurde mittels eines indirekten Schätzverfahrens ermittelt. Auf Basis dieses Schätzers wurden Kohärenzen, partielle Kohärenzen, bivariate und bedingte Granger Kausalitäten, statische und dynamische kanonische Korrelationen und Hauptkomponenten zur Analyse von EEG-Synchronität berechnet. Die Maße wurden zwischen Einzelelektroden, zwischen Gruppen von Elektroden und innerhalb dieser Gruppen ermittelt. Die Maß-Änderungen wurden mit quadratischer Regression ( $p$ - und  $R^2$ -Werte) bewertet.

Synchronität zwischen den Elektrodengruppen zeigte die meisten signifikanten Änderungen. In der Ruhephase waren dynamische kanonische Korrelationen und Granger Kausalitäten vielversprechend. Während des kognitiven Tests brachten Kohärenzen und statische/dynamische kanonische Korrelationen hochsignifikante Resultate, vor Allem zwischen linken temporalen und zentralen/parietalen Elektrodengruppen. Bei den meisten Maßen war ein Synchronitäts-Anstieg zu Beginn der Krankheit evident. Dies könnte auf neuronale Kompensationsmechanismen zurückzuführen sein. Die Ausnahme bildeten Granger Kausalitäten, die eine durchgehende Synchronitäts-Abnahme zeigten.

Insgesamt erwies sich die Analyse von EEG-Synchronität als vielversprechender Ansatz zur Beschreibung des Grades der Alzheimer Krankheit. Longitudinale Studien sind notwendig um zu entscheiden, ob EEG-Marker auch zur Prädiktion des Krankheits-Verlaufes einsetzbar sind. Eine Kombination von EEG-Maßen mit anderen Markern, z.B. aus klinischen bildgebenden Verfahren, könnte das Verständnis von funktionellen und strukturellen neuronalen Veränderungen, die mit der Alzheimer Krankheit einhergehen, erweitern.



---

## Abstract

---

Alzheimer's disease (AD) – the main cause of dementia – is a progressive neurodegenerative disorder that entails severe social and economic consequences. In this thesis, synchrony changes in the electroencephalogram (EEG) in the course of AD are investigated with the objective of demonstrating the capability of EEG markers to serve as supplements to existing clinical diagnostics. Thereby, EEG synchrony is quantified by measures that are based on the multivariate spectral density of the EEG.

For this study, 79 EEG recordings of "probable" AD patients from the PRODEM-AUSTRIA database were used. Samples were conducted according to a clinically predefined paradigm including resting state and cognitive tasks. AD severity was measured by the neuropsychological Mini-Mental State Examination (MMSE) score. Age, sex, degree of education, and duration of AD were used as covariables.

The multivariate spectral density was estimated by an indirect estimation procedure. Based on the estimate, coherences, partial coherences, bivariate and conditional Granger causalities, and both static and dynamic canonical correlations and principal components were derived. The measures were analyzed between single EEG channels, between groups of EEG channels, and within these groups. Correlations between the measures and MMSE scores were assessed by a quadratic regression model ( $p$ - and  $R^2$ -values).

Synchrony between groups of EEG channels yielded the most significant changes. In resting state, dynamic canonical correlations and Granger causalities were the most promising measures. During the cognitive task, highly significant findings for coherences and both static and dynamic canonical correlations were observed, mainly in left hemispheric temporal and central/parietal channels. Most measures showed an increase of synchrony for MMSE scores from 26 to 20; this phenomenon may be attributed to compensatory mechanisms in the brain. Granger causalities formed an exception, they revealed a decrease of synchrony with descending MMSE scores.

The investigation of EEG synchrony changes in AD proved to be a promising approach for supplementary classification of AD severity. Longitudinal studies need to determine as to whether EEG markers are also capable of predicting AD progression. A combination of EEG measures with other markers for AD severity, e.g. from clinical imaging procedures, could improve the understanding of functional and structural neuronal changes that come along with AD.

**Keywords:** EEG Synchrony, Alzheimer's Disease, Multivariate Spectral Density, Coherence, Partial Coherence, Granger Causality, Canonical Correlation.



---

## Danksagung

---

An dieser Stelle möchte ich mich bei einigen Menschen bedanken, deren Unterstützung mir die Fertigstellung dieser Arbeit ermöglicht hat.

An vorderster Stelle sollen hier meine beiden Betreuer erwähnt werden: auf der einen Seite Manfred Deistler (Technische Universität Wien), der mich oft durch statistische Unklarheiten geleitet und mir hilfreiche Denkanstöße zu den EEG-Analysen gegeben hat; auf der anderen Seite Heinrich Garn (AIT Austrian Institute of Technology), der mich bei der Umsetzung der Analysen unterstützt und mir die Möglichkeit gegeben hat, diese Arbeit im Rahmen meiner Forschungstätigkeit am AIT zu verfassen.

Anschließend möchte ich zwei meiner Kollegen, die zu guten Freunden geworden sind, hervorheben: zum einen Beatrice Jobst, die mir in unzähligen Diskussionen wertvolle Impulse gegeben und deren unvergleichliche Penibilität auch die kleinste sprachliche Ungenauigkeit aufgedeckt hat; zum anderen Matthias Dorfer, der in der EEG-Vorverarbeitung wesentliche Arbeit geleistet und durch seine Programmier-Expertise eine effiziente Umsetzung ermöglicht hat. Gemeinsam mit anderen Kollegen, hier möchte ich besonders Manuel Lechner erwähnen, haben sie für ein angenehmes Arbeitsklima gesorgt und auch dafür, dass das Mittagessen immer pünktlich um 12 Uhr auf dem Tisch stand.

Christian Schmid danke ich für inhaltliche und semantische Korrekturen, die wesentlich zur Qualität und Lesbarkeit des Geschriebenen beigetragen haben.

Einen großen Anteil an der Fertigstellung dieser Arbeit hat meine Familie, bei der ich mich für ihre bedingungslose Unterstützung im Studium und in allen sonstigen Lebenslagen bedanken möchte.

Diese Arbeit ist im Rahmen des von der *Österreichischen Forschungsförderungsgesellschaft FFG* geförderten Projektes "*Advanced*" *EEG in der Vorhersage des Verlaufs der Alzheimerdemenz* (Projekt Nr. 827462, BRIDGE Programm) entstanden. Die verwendeten EEG-Daten stammen von der PRODEM-AUSTRIA Datenbank der Österreichischen Alzheimer Gesellschaft und wurden aufgenommen an den Medizinischen Universitäten Graz, Wien, Innsbruck und dem Allgemeinen Krankenhaus Linz. Die Algorithmen zur EEG-Analyse sind am AIT Austrian Institute of Technology GmbH entstanden. Finanziell wurde das Projekt außerdem unterstützt von Dr. Grossegger & Drbal GmbH, Wien.

Markus Waser





---

## **Statutory Declaration**

---

I hereby certify that no other than the sources and aids referred to were used in this thesis. All parts which have been adopted either literally or in a general manner from other sources have been indicated accordingly.

I certify that the main contribution of this thesis, the development of algorithms for measuring changes of EEG synchrony in the course of Alzheimer's disease, is my own work.

Vienna, September 2013

Markus Waser



---

# Contents

---

<b>List of Figures</b>	<b>xi</b>
<b>List of Tables</b>	<b>xiii</b>
<b>1 Introduction</b>	<b>1</b>
1.1 Alzheimer's Disease . . . . .	1
1.2 Changes in the EEG of AD Patients . . . . .	3
1.3 Research Questions . . . . .	4
1.4 Thesis Outline . . . . .	5
<b>2 Materials and Methods</b>	<b>7</b>
2.1 Sample Data . . . . .	7
2.2 EEG Preprocessing . . . . .	10
2.2.1 Description of Artefacts . . . . .	10
2.2.2 Artefact Removal . . . . .	13
2.2.3 Segmentation . . . . .	18
2.3 Stationary Processes in Time Domain . . . . .	18
2.3.1 Foundations . . . . .	18
2.3.2 Hilbert Space . . . . .	21
2.3.3 Autoregressive Processes . . . . .	22
2.4 Stationary Processes in Frequency Domain . . . . .	23
2.4.1 Discrete Time Fourier Transform . . . . .	23
2.4.2 Spectral Representation of Stationary Processes . . . . .	24
2.4.3 Multivariate Spectral Density . . . . .	25
2.5 Dependence Measures Derived from the Multivariate Spectral Density	26
2.5.1 Framework . . . . .	26
2.5.2 Coherence . . . . .	27
2.5.3 Partial Coherence . . . . .	27
2.5.4 Bivariate Granger Causality . . . . .	28
2.5.5 Conditional Granger Causality . . . . .	29
2.5.6 Static Canonical Correlation Analysis . . . . .	29
2.5.7 Dynamic Canonical Correlation Analysis . . . . .	30
2.5.8 Static Principal Component Analysis . . . . .	31
2.5.9 Dynamic Principal Component Analysis . . . . .	32
2.6 Estimating the First and Second Moments . . . . .	33
2.6.1 Mean . . . . .	33
2.6.2 Autocovariance Function . . . . .	34

2.7	Estimating the Multivariate Spectral Density . . . . .	35
2.7.1	Periodogram . . . . .	35
2.7.2	Direct Spectral Estimates . . . . .	37
2.7.3	Indirect Spectral Estimates . . . . .	39
2.7.4	Implementation . . . . .	40
2.7.5	Spectral Estimation in this Study . . . . .	45
2.8	Implementation of the Dependence Measures . . . . .	46
2.8.1	Coherence . . . . .	46
2.8.2	Partial Coherence . . . . .	47
2.8.3	Bivariate Granger Causality . . . . .	47
2.8.4	Conditional Granger Causality . . . . .	50
2.8.5	Static Canonical Correlation Analysis . . . . .	50
2.8.6	Dynamic Canonical Correlation Analysis . . . . .	51
2.8.7	Static Principal Component Analysis . . . . .	52
2.8.8	Dynamic Principal Component Analysis . . . . .	52
2.9	Analyzing EEG Synchrony . . . . .	53
<b>3</b>	<b>Results</b>	<b>57</b>
3.1	Synchrony Between Single EEG Channels . . . . .	57
3.1.1	Main Results . . . . .	58
3.1.2	Detailed Results: Resting State . . . . .	63
3.1.3	Detailed Results: Cognitive Task . . . . .	76
3.2	Synchrony Between Groups of EEG Channels . . . . .	91
3.2.1	Main Results . . . . .	91
3.2.2	Detailed Results: Resting State . . . . .	100
3.2.3	Detailed Results: Cognitive Task . . . . .	110
3.3	Synchrony Within Groups of EEG Channels . . . . .	120
3.3.1	Main Results . . . . .	120
3.3.2	Detailed Results: Resting State . . . . .	122
3.3.3	Detailed Results: Cognitive Task . . . . .	125
<b>4</b>	<b>Discussion and Conclusion</b>	<b>129</b>
4.1	Discussion . . . . .	129
4.2	Conclusion . . . . .	134
	<b>Bibliography</b>	<b>137</b>

---

## List of Figures

---

1.1.1	Structural changes in the brain in AD . . . . .	2
1.1.2	Projected incidence rates of dementia and AD . . . . .	3
2.1.1	Empirical distribution of demographic variables . . . . .	8
2.1.2	Empirical distribution of MMSE scores . . . . .	9
2.1.3	Electrode names and positions . . . . .	10
2.2.1	EEG with artefacts from blinking . . . . .	11
2.2.2	EEG with artefacts from muscle tension . . . . .	12
2.2.3	EEG with artefacts from cardiac activity . . . . .	13
2.2.4	EEG with artefacts from sweating . . . . .	14
2.2.5	EEG with artefacts from poor electrode contact . . . . .	15
2.2.6	Gain and phase of high-pass FIR filter . . . . .	15
2.2.7	EEG preprocessing step 1 . . . . .	16
2.2.8	EEG preprocessing step 2 . . . . .	16
2.2.9	EEG preprocessing step 3 . . . . .	17
2.2.10	EEG preprocessing step 4 . . . . .	17
2.2.11	EEG preprocessing step 5 . . . . .	17
2.7.1	Window closing . . . . .	42
2.7.2	Rectangular window and corresponding spectral window . . . . .	43
2.7.3	Triangular window and corresponding spectral window . . . . .	43
2.7.4	Hann window and corresponding spectral window . . . . .	44
2.7.5	Hamming window and corresponding spectral window . . . . .	44
2.7.6	Parzen window and corresponding spectral window . . . . .	45
2.9.1	Electrode channel pairs . . . . .	55
2.9.2	Electrode channel groups . . . . .	55
3.1.1	Partial coherences between C3-P7, $\delta$ , resting state . . . . .	58
3.1.2	Coherences between P4-P8, $\theta$ , cognitive task . . . . .	61
3.2.1	Dynamic canonical correlations, Post.-T.L., $\theta$ , resting state . . . . .	92
3.2.2	Cond. Granger causalities, Cent. $\rightarrow$ Post., 1 <sup>st</sup> PCs, resting state . . . . .	93
3.2.3	Cond. Granger causalities, Cent. $\rightarrow$ T.L., 2 <sup>nd</sup> PCs, resting state . . . . .	94
3.2.4	Coherences, Cent.-T.L., 2 <sup>nd</sup> PCs, $\delta$ , cognitive task . . . . .	96
3.2.5	Static canonical correlations, Cent.-T.L., cognitive task . . . . .	97
3.2.6	Dynamic canonical correlations, Cent.-T.L., $\theta$ , cognitive task . . . . .	98
3.3.1	Dynamic PCA, T.R., $\beta_0$ , cognitive task . . . . .	121



---

## List of Tables

---

2.9.1	Frequency bands names and borders . . . . .	53
3.1.1	Significant changes between channels in resting state . . . . .	60
3.1.2	Significant changes between channels during the cognitive task . . . . .	62
3.1.3	Results: far intrahemispheric channel pairs, $\delta$ , resting state . . . . .	63
3.1.4	Results: far intrahemispheric channel pairs, $\theta$ , resting state . . . . .	64
3.1.5	Results: far intrahemispheric channel pairs, $\alpha$ , resting state . . . . .	64
3.1.6	Results: far intrahemispheric channel pairs, $\beta_0$ , resting state . . . . .	65
3.1.7	Results: far intrahemispheric channel pairs, total, resting state . . . . .	66
3.1.8	Results: far interhemispheric channel pairs, $\delta$ , resting state . . . . .	67
3.1.9	Results: far interhemispheric channel pairs, $\theta$ , resting state . . . . .	68
3.1.10	Results: far interhemispheric channel pairs, $\alpha$ , resting state . . . . .	68
3.1.11	Results: far interhemispheric channel pairs, $\beta_0$ , resting state . . . . .	68
3.1.12	Results: far interhemispheric channel pairs, total, resting state . . . . .	69
3.1.13	Results: local anterior channel pairs, $\delta$ , resting state . . . . .	70
3.1.14	Results: local anterior channel pairs, $\theta$ , resting state . . . . .	71
3.1.15	Results: local anterior channel pairs, $\alpha$ , resting state . . . . .	71
3.1.16	Results: local anterior channel pairs, $\beta_0$ , resting state . . . . .	72
3.1.17	Results: local anterior channel pairs, total, resting state . . . . .	72
3.1.18	Results: local posterior channel pairs, $\delta$ , resting state . . . . .	73
3.1.19	Results: local posterior channel pairs, $\theta$ , resting state . . . . .	74
3.1.20	Results: local posterior channel pairs, $\alpha$ , resting state . . . . .	74
3.1.21	Results: local posterior channel pairs, $\beta_0$ , resting state . . . . .	75
3.1.22	Results: local posterior channel pairs, total, resting state . . . . .	75
3.1.23	Results: far intrahemispheric channel pairs, $\delta$ , cognitive task . . . . .	76
3.1.24	Results: far intrahemispheric channel pairs, $\theta$ , cognitive task . . . . .	77
3.1.25	Results: far intrahemispheric channel pairs, $\alpha$ , cognitive task . . . . .	77
3.1.26	Results: far intrahemispheric channel pairs, $\beta_0$ , cognitive task . . . . .	78
3.1.27	Results: far intrahemispheric channel pairs, total, cognitive task . . . . .	79
3.1.28	Results: far interhemispheric channel pairs, $\delta$ , cognitive task . . . . .	80
3.1.29	Results: far interhemispheric channel pairs, $\theta$ , cognitive task . . . . .	80
3.1.30	Results: far interhemispheric channel pairs, $\alpha$ , cognitive task . . . . .	81
3.1.31	Results: far interhemispheric channel pairs, $\beta_0$ , cognitive task . . . . .	81
3.1.32	Results: far interhemispheric channel pairs, total, cognitive task . . . . .	82
3.1.33	Results: local anterior channel pairs, $\delta$ , cognitive task . . . . .	83
3.1.34	Results: local anterior channel pairs, $\theta$ , cognitive task . . . . .	84
3.1.35	Results: local anterior channel pairs, $\alpha$ , cognitive task . . . . .	84

---

3.1.36	Results: local anterior channel pairs, $\beta_0$ , cognitive task . . . . .	85
3.1.37	Results: local anterior channel pairs, total, cognitive task . . . . .	86
3.1.38	Results: local posterior channel pairs, $\delta$ , cognitive task . . . . .	87
3.1.39	Results: local posterior channel pairs, $\theta$ , cognitive task . . . . .	88
3.1.40	Results: local posterior channel pairs, $\alpha$ , cognitive task . . . . .	88
3.1.41	Results: local posterior channel pairs, $\beta_0$ , cognitive task . . . . .	89
3.1.42	Results: local posterior channel pairs, total, cognitive task . . . . .	90
3.2.1	Significant changes between channel groups in resting state . . . . .	95
3.2.2	Significant changes between channel groups during the cognitive task . . . . .	99
3.2.3	Results: between 1 <sup>st</sup> PCs of channel groups, $\delta$ , resting state . . . . .	100
3.2.4	Results: between 2 <sup>nd</sup> PCs of channel groups, $\delta$ , resting state . . . . .	101
3.2.5	Results: between channel groups, $\delta$ , resting state . . . . .	101
3.2.6	Results: between 1 <sup>st</sup> PCs of channel groups, $\theta$ , resting state . . . . .	102
3.2.7	Results: between 2 <sup>nd</sup> PCs of channel groups, $\theta$ , resting state . . . . .	103
3.2.8	Results: between channel groups, $\theta$ , resting state . . . . .	103
3.2.9	Results: between 1 <sup>st</sup> PCs of channel groups, $\alpha$ , resting state . . . . .	104
3.2.10	Results: between 2 <sup>nd</sup> PCs of channel groups, $\alpha$ , resting state . . . . .	104
3.2.11	Results: between channel groups, $\alpha$ , resting state . . . . .	105
3.2.12	Results: between 1 <sup>st</sup> PCs of channel groups, $\beta_0$ , resting state . . . . .	105
3.2.13	Results: between 2 <sup>nd</sup> PCs of channel groups, $\beta_0$ , resting state . . . . .	106
3.2.14	Results: between channel groups, $\beta_0$ , resting state . . . . .	106
3.2.15	Results: between 1 <sup>st</sup> PCs of channel groups, total, resting state . . . . .	107
3.2.16	Results: between 2 <sup>nd</sup> PCs of channel groups, total, resting state . . . . .	108
3.2.17	Results: between channel groups, total, resting state . . . . .	109
3.2.18	Results: between 1 <sup>st</sup> PCs of channel groups, $\delta$ , cognitive task . . . . .	110
3.2.19	Results: between 2 <sup>nd</sup> PCs of channel groups, $\delta$ , cognitive task . . . . .	111
3.2.20	Results: between channel groups, $\delta$ , cognitive task . . . . .	111
3.2.21	Results: between 1 <sup>st</sup> PCs of channel groups, $\theta$ , cognitive task . . . . .	112
3.2.22	Results: between 2 <sup>nd</sup> PCs of channel groups, $\theta$ , cognitive task . . . . .	113
3.2.23	Results: between channel groups, $\theta$ , cognitive task . . . . .	113
3.2.24	Results: between 1 <sup>st</sup> PCs of channel groups, $\alpha$ , cognitive task . . . . .	114
3.2.25	Results: between 2 <sup>nd</sup> PCs of channel groups, $\alpha$ , cognitive task . . . . .	114
3.2.26	Results: between channel groups, $\alpha$ , cognitive task . . . . .	115
3.2.27	Results: between 1 <sup>st</sup> PCs of channel groups, $\beta_0$ , cognitive task . . . . .	116
3.2.28	Results: between 2 <sup>nd</sup> PCs of channel groups, $\beta_0$ , cognitive task . . . . .	116
3.2.29	Results: between channel groups, $\beta_0$ , cognitive task . . . . .	117
3.2.30	Results: between 1 <sup>st</sup> PCs of channel groups, total, cognitive task . . . . .	118
3.2.31	Results: between 2 <sup>nd</sup> PCs of channel groups, total, cognitive task . . . . .	119
3.2.32	Results: between channel groups, total, cognitive task . . . . .	119
3.3.1	Significant changes within channel groups in resting state . . . . .	120
3.3.2	Significant changes within channel groups during the cognitive task . . . . .	121
3.3.3	Results: within channel groups, $\delta$ , resting state . . . . .	122
3.3.4	Results: within channel groups, $\theta$ , resting state . . . . .	122
3.3.5	Results: within channel groups, $\alpha$ , resting state . . . . .	123
3.3.6	Results: within channel groups, $\beta_0$ , resting state . . . . .	123
3.3.7	Results: within channel groups, total, resting state . . . . .	124



---

3.3.8	Results: within channel groups, $\delta$ , cognitive task . . . . .	125
3.3.9	Results: within channel groups, $\theta$ , cognitive task . . . . .	125
3.3.10	Results: within channel groups, $\alpha$ , cognitive task . . . . .	126
3.3.11	Results: within channel groups, $\beta_0$ , cognitive task . . . . .	126
3.3.12	Results: within channel groups, total, cognitive task . . . . .	127



# CHAPTER 1

---

## Introduction

---

The purpose of this chapter is to introduce the reader to the topic of this work. It provides an overview of the issue of Alzheimer's disease, of the electroencephalogram (EEG) in clinical diagnosis, and of previous studies about changes in the EEG in the course of Alzheimer's disease. Afterwards, the research questions addressed in this study will be defined. Finally, an outline of the thesis structure will conclude the introduction.

### 1.1 Alzheimer's Disease

Dementia is a disorder of cognitive abilities that has increasing prevalence with age. Among the causes of dementia, the most frequently occurring are vascular dementia, frontotemporal dementia, dementia with Lewy bodies, and – the most common cause – *Alzheimer's disease* (AD). AD is estimated to account for 60-80% of dementia cases; hybrid forms with other dementia types occur frequently [1], [2]. AD is a progressive brain disorder that is associated with neuronal cell loss and the development of neurofibrillary tangles and cortical amyloid plaques, e.g. in the hippocampus [3]. Additionally, alterations in transmitter-specific markers including forebrain cholinergic systems are prevalent in AD [4]. Cognitive deficits include impairment of learning and memory, semantic difficulties, deficits in judgement, abstract or logical reasoning, planning and organizing, and, in the late stage of AD, impaired motor functions including chewing and swallowing. As from AD diagnosis, the average survival time ranges from 5 to 8 years [5], [6]. Figure 1.1.1 illustrates the structural changes in the brain that occur in advanced AD.

In 2010, 112,600 individuals with any form of dementia were estimated to live in Austria. This number was projected to increase to 262,300 by 2050. The number of AD-caused dementia cases was estimated to increase from 74,300 to 182,700 over the same time period [1]. In Europe, 8.456 million individuals suffered from any form of dementia in 2010. Among them, there were approximately 4.662 million AD cases. These incidence rates were estimated to increase to

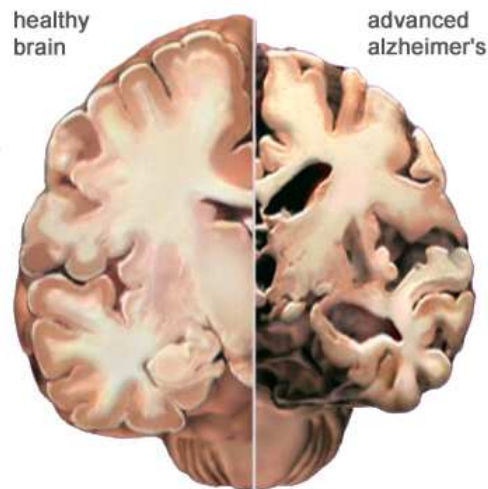


**Figure 1.1.1:** Cerebral slice of a healthy brain vs a brain in advanced AD: in AD, shrinkage is especially severe in the hippocampus; ventricles (fluid-filled spaces within the brain) grow larger. This image was taken from the site of the Alzheimer's Association <http://www.alz.org>, accessed 2 Sept. 2013.

16.242 million and 11.184 million respectively by 2050 [7]. On a global scale, the *World Health Organization* and the organization *Alzheimer's Disease International* projected the number of dementia cases to increase from 35.56 million in 2010 to 115.38 million by 2050 [8], [9]. Assuming a prevalence rate of 70% of AD-caused dementia, the incidence rate of AD would increase from 24.890 million in 2010 to approximately 81 million by 2050. The projected progress of the numbers of dementia and AD cases is illustrated in Figures 1.1.2a, 1.1.2b, and 1.1.2c.

Cognitive decline caused by AD entails both severe social and economic consequences [8], [9]. An early diagnosis of the disease is the basis for medical treatment, caregiving, and consultation [1], [10]. Up to this moment, there is no definite *in vivo* diagnosis of AD; the disease is classified either as *possible* or *probable* AD according to well-defined criteria [4]. In clinical practice, obligatory screening for AD includes the assessment of the neurological, internistic and psychiatric status, neuropsychological tests, a complete blood count, and cerebral magnetic resonance imaging (MRI). Additionally, clinical studies suggest genotyping, liquor analysis, serology, imaging procedures such as positron emission tomography (PET) and functional MRI, and, finally, the EEG as diagnostic supplements [1]. The advantage of the EEG is that it is non-invasive, low-priced, and easier accessible than procedures such as PET and functional MRI.

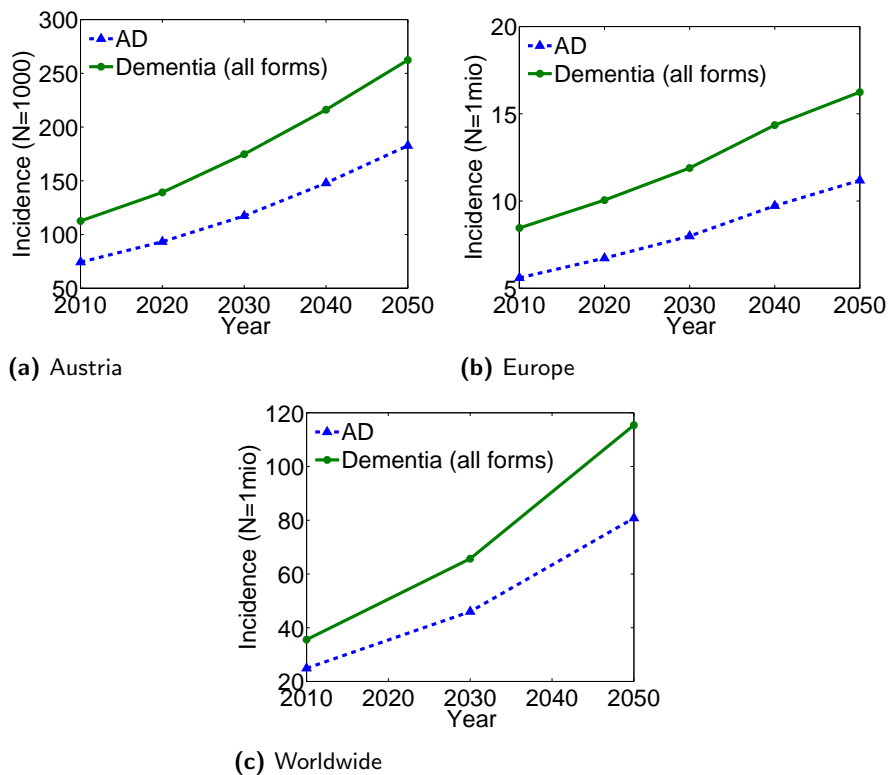


**Figure 1.1.2:** Projected incidence rates of dementia (all forms) and of AD in Austria (top left) [1], Europe (top right) [7], and worldwide (bottom) [8], [9].

## 1.2 Changes in the EEG of AD Patients

The EEG measures, usually with scalp electrodes, neuronal electrical activity. There is a variety of clinical EEG applications including the detection of epileptic seizures, monitoring of coma patients, and the study of sleep disorders. In AD-related clinical practice, the EEG is – if at all – analyzed visually by medical experts. However, several studies about changes in the EEG of AD patients and the automated quantification of these changes have been published. Three major alterations have been reported: EEG slowing, reduced EEG complexity, and – the focus of this work – perturbations of EEG synchrony (cf. [5], [11] for recent reviews).

Several studies have analyzed group differences of resting state EEG synchrony between AD patients, subjects with mild cognitive impairment (MCI), and normal elderly controls (NOLD): Pearson correlation coefficients were analyzed in [11], coherences in [12], [13], [14], [15], [16]<sup>1</sup>, [17], [18], [19], [11], partial coherences in

<sup>1</sup>Here, the control group consists of patients suffering from depression.

[11], Granger causalities and directed transfer functions in [11], [20], information-theoretic measures such as mutual information in [21], [22], [11], phase synchrony measures in [23], [24], [25], [26], [27], [28], [29], [11], and stochastic event synchrony in [30], [11]. Most of these studies have suggested a decrease of resting state EEG synchrony for AD patients as compared to the controls. Additionally, some studies have investigated group differences of EEG synchrony during cognitive tasks (coherences in [31], [32], [33], [34], [17], [35], and synchronization likelihood in [24]) or during photic stimulation (coherences in [13], [36], [37]). Especially during working memory tasks, increased EEG synchronies have been reported for MCI subjects (and in few cases also for AD patients) as compared to the controls (cf. e.g. [32], [33]). This phenomenon is often attributed to compensatory mechanisms of the brain [38].

However, there have been only few studies that correlate EEG synchrony measures with AD severity as measured by neuropsychological tests. Studies investigating coherences have reported no significant correlations with the neuropsychological test results, neither in resting state ([16], [36]) nor during a working memory task ([36]). There have been several studies finding significant correlations between neuropsychological test results and synchronization likelihood ([23], [24], [39]), and between test results and global field synchronization ([28]).

### 1.3 Research Questions

The *Austrian Alzheimer Society* conducts the multi-centric study *PRODEM-AUSTRIA*. Within the subproject "*Advanced*" *EEG in der Vorhersage des Verlaufs der Alzheimerdemenz* (project no. 827462) that is funded by the *Austrian Research Promotion Agency FFG* within the *BRIDGE* program, EEG samples of AD patients are being recorded. The recordings follow a predefined paradigm – including resting state with eyes closed and cognitive tasks – that has been developed by the clinical partners of the *BRIDGE* project. This thesis has been written in the course of the author's research activity at the *AIT Austrian Institute of Technology GmbH* within this *BRIDGE* project. The EEG recordings of 79 probable AD patients have been utilized.

The aim of this thesis is to examine whether changes of EEG synchrony correlate with AD severity as measured by the neuropsychological Mini Mental State Examination (MMSE) score [40]. Different measures for synchrony will be derived from the multivariate spectral density, i.e. only first and second moments will be considered. A major aspect will be the estimation procedure of the spectral density.

The main research hypotheses addressed in this thesis are the following:

- $H_0^1$ : Synchronies between single EEG channels change in the course of AD.
- $H_0^2$ : Synchronies between EEG channel groups change in the course of AD.

- $H_0^3$ : Synchronies within EEG channel groups change in the course of AD.

Although the applied methods originate from fields such as time series analysis and stochastic processes, this work is mainly clinically motivated. A thorough analysis of EEG synchrony may be valuable in clinical diagnosis and prediction of AD. However, it is not the author's intention to theorize about biophysical mechanisms behind the measurements.

## 1.4 Thesis Outline

This thesis has been organized in the following way: Chapter 2 is concerned with the materials and methods that were applied in this study. Hereby, the sample data, the necessity of EEG preprocessing, and consecutive preprocessing steps will be described. Then, stationary processes in both time and frequency domain, and measures for EEG synchrony based on the multivariate spectral density will be considered in a system theoretic framework. Statistical considerations of these concepts will follow. Chapter 3 provides the results of the analyses. According to the postulated null hypotheses, the findings will be divided into three categories: results between single channels, between groups of channels, and within groups of channels. Finally, Chapter 4 discusses the findings and provides concluding remarks.





### Materials and Methods

---

This chapter is concerned with the description of the sample data, preprocessing methods, time series and stochastic processes, the estimation of multivariate spectral densities, and measures for synchrony based on the multivariate spectral density. Both system theoretic and statistical considerations will be addressed. Hereby, the deliberations on stationary processes in Sections 2.3 and 2.4 have been inspired by [41]. Parts of the methods for analyzing changes in the EEG of AD patients have already been demonstrated in [42].

#### 2.1 Sample Data

In this study, EEG recordings from the *PRODEM-AUSTRIA*<sup>1</sup> database of the *Austrian Alzheimer Society* were used. More specifically, the EEG samples were recorded at the *Medical Universities of Graz, Innsbruck, Vienna*, and the *General Hospital Linz*, all complying with a homogeneous study protocol. The PRODEM participants were enrolled according to the following criteria:

- Diagnosis of AD according to NINCDS-ADRDA criteria [4]
- Minimum age 40 years
- Family caregiving provided
- Understanding and written informed consent of each participant and caregiver

The sample consists of EEG recordings from 79 subjects (50 female, 29 male) diagnosed with probable AD. The age of the subjects at recording date ranges from 52 to 88 years with mean 73.57 ( $\sigma = 9.22$ ). The duration of AD ranges from 2 to 120 months with mean 25.54 ( $\sigma = 22.08$ ). For each subject, the degree of education is classified on a scale from 1 to 6 with respect to the highest

---

<sup>1</sup><http://www.alzheimer.mcw-portal.com/index.php?id=27>

completed level of education; 1 stands for Volks/Hauptschule (primary school), 2 for Lehre (apprenticeship), 3 for AHS (grammar school), 4 for BHS (higher vocational school), 5 for Lehrerbildungsanstalt (teacher training school), and 6 for Hochschule (tertiary institution). On this scale, the mean degree of education is 2.37 ( $\sigma = 1.58$ ). The empirical distributions of sex, age, duration of AD, and degree of education are visualized as histogram plots in Figures 2.1.1a – 2.1.1d. The dotted lines represent the respective mean values.

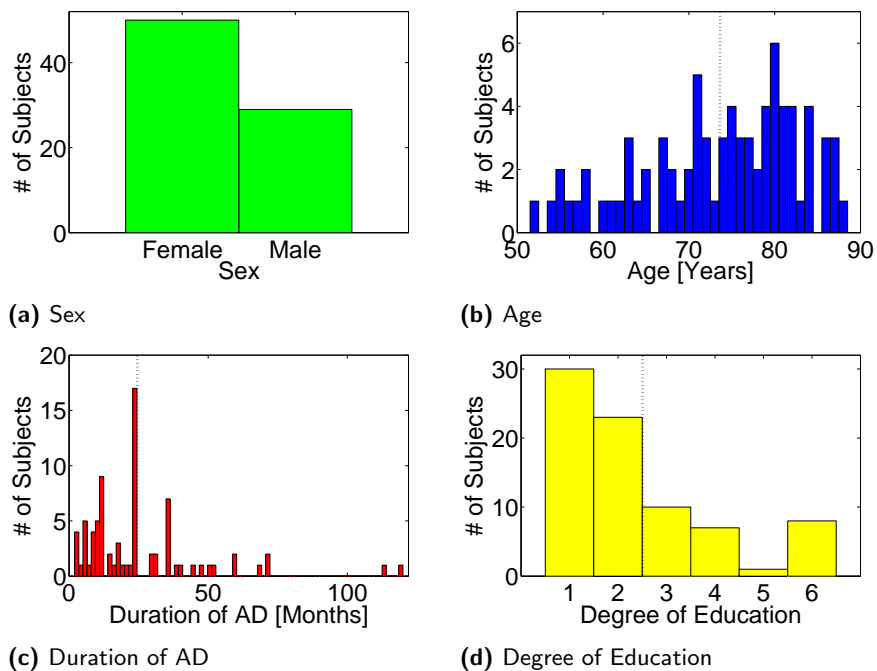


**Figure 2.1.1:** Empirical distribution of demographic variables: histogram plots of sex (top left), age (top right), duration of AD (bottom left), and degree of education (bottom right). Dotted lines represent the respective arithmetic mean.

All subjects underwent neuropsychological assessments including MMSE, Clinical Dementia Rating Scale (CDR) [43], Disability Assessment for Dementia (DAD) [44], Neuropsychiatric Inventory (NPI) [45], Geriatric Depression Scale (GDS) [46], and a neuropsychological test battery by the Consortium to Establish a Registry for AD (CERAD) [47], [48]. In this study, the AD severity is quantified by MMSE score, a clinically well-established evaluation criterion for cognitive impairment. MMSE scores range, on an ordinal scale, from 30 to 0, where lower scores indicate more severe cognitive impairment. The study subjects reached MMSE scores between 26 and 15 with an average score of 22 ( $\sigma = 3.16$ ). Figure 2.1.2 shows the empirical distribution of MMSE scores. The aforementioned characteristics age, sex, duration of AD, and degree of education will be applied as confounding variables for the statistical analyses.

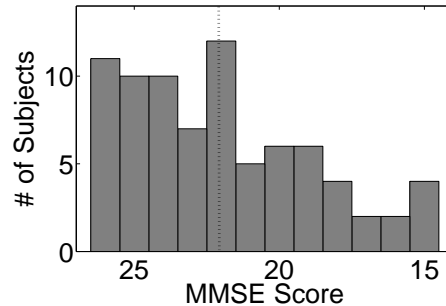


**Figure 2.1.2:** Empirical distribution of MMSE scores: histogram plot where high MMSE scores (left side of the abscissa) indicate less cognitive impairment, and low MMSE scores (right side of the abscissa) indicate more severe cognitive impairment. The dotted line represents the arithmetic mean.

There are various studies (e.g. [13]) on EEG dynamics of AD patients that exclude subjects receiving central nervous system active medication including antimentiva, antidepressants, and antipsychotics. The reason for that is the possibility of unknown influences of the medication on the EEG signals. However, in order to base this work on a clinically realistic scenario and to ensure a sufficient sample size, subjects receiving medication were not excluded, most of them being administered several drugs in different doses.

Within the PRODEM-AUSTRIA study, the EEG samples are recorded and digitalized using the *NeuroSpeed* software of the *alpha-trace digitalEEG System*<sup>2</sup> with sampling rate 256 Hz. EEG amplifiers have an analog band-pass filter in the range of 0.3–70 Hz, and a notch filter at 50 Hz. Nineteen gold cup electrodes are positioned on the subjects' scalps according to the *international 10-20 system* (cf. [49]). The channel names and positions are illustrated in Figure 2.1.3. Connected mastoids (i.e. parts of the temporal bones) are used as reference and the ground electrode is located between channels Fz and Cz. Additionally, both *horizontal* and *vertical electrooculogram* (EOG) channels and an *electrocardiogram* (ECG) channel (wrist clip electrodes) are recorded. Impedances are kept below 10 k $\Omega$ .

In order to ensure the comparability of the EEG recordings, all PRODEM-AUSTRIA data are conducted according to a clinically predefined paradigm. Initially, subjects are sitting in a resting but awake condition with eyes closed for 180 seconds. This is followed by a face-name encoding task with eyes opened. Subjects are asked to

1. memorize faces and corresponding names shown on a computer screen (50 seconds).

<sup>2</sup><http://www.alphatrace.at>

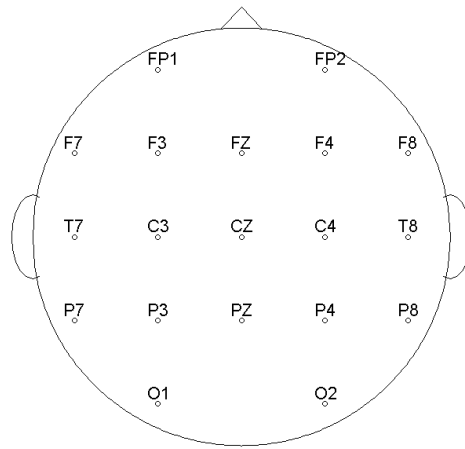


**Figure 2.1.3:** Electrode names and positions on the surface of the scalp as seen from above: 19 channels distributed according to the international 10-20 system.

2. recall the names while only the faces are presented.
3. memorize, once more, the faces and names shown on the screen (50 seconds).

These tasks have been selected for investigating AD-specific deficits including episodic memory and processing of complex stimuli. Throughout this work, the recording stages will be referred to as *resting state* and *cognitive task*.

## 2.2 EEG Preprocessing

EEG recordings are generally corrupted by electric signals other than brain signals. These interfering signals are commonly referred to as *artefacts*. Depending on their origin, artefacts are divided in two classes: those of physiological and those of technical origin. Physiological sources include eye movements and blinking, muscular activity, cardiac electric fields, and sweating. Technical interference is caused by poor electrode contacts, spurious noise from electronic devices, and induction from the mains supply at 50 Hz. Artefacts alter the EEG signals and distort the results of quantitative analyses. Hence, several preprocessing steps were applied in order to remove artefacts and to attain "pure" neuronal signals. A description of common artefacts will be provided in Section 2.2.1; the applied preprocessing methods will be presented in Sections 2.2.2 and 2.2.3.

### 2.2.1 Description of Artefacts

Electric fields induced by eye movements and blinking – so-called *eye artefacts* – corrupt the EEG signals in the frequency range below 10 Hz. Even with closed eyes, certain eye movements are present. The corruption is most notable on frontal

electrode positions but may affect central and even parietal electrodes as well. The current generated by eye movements and blinking is captured by the EOG. Figure 2.2.1 shows a 14 second segment of an EEG signal in resting state with eyes opened and the corresponding EOG and ECG signals at the bottom. From top to bottom, the EEG channels are sorted from frontal to occipital positions; even numbers (e.g. FP2, C4) correspond to the right brain hemisphere and odd numbers (e.g. T7, O1) correspond to the left (cf. Figure 2.1.3). In this example, three eye artefacts are visible at seconds 3, 7, and 12. The artefacts corrupt frontal and also central EEG channels.

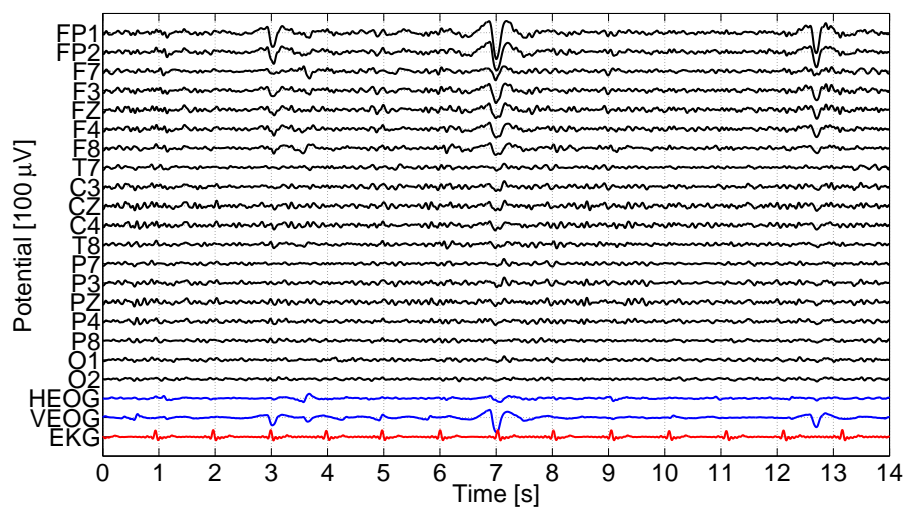


**Figure 2.2.1:** EEG segment (14 sec.) containing artefacts originating from blinking at seconds 3, 7 and 12: each signal represents a channel from top = frontal to bottom = occipital; in addition, at the very bottom, HEOG, VEOG and EKG channels are provided. Peaks in the VEOG channel are induced by blinking. In this example, artefacts occur simultaneously to these peaks and affect mostly frontal and EEG central channels.

Myogenic potentials from muscle activity corrupt EEG signals in frequency ranges above 15 Hz. They are present when a subject is clenching the jaw muscles, frowning, or talking. The EEG samples of this study are corrupted by muscle-induced artefacts mainly in the fronto-temporal, temporal, and parieto-temporal electrodes F7, F8, T7, T8, P7, and P8. Figure 2.2.2 shows high-frequency corruption originating from muscle tension on the EEG channels F8 and T8.

Cardiac electric fields that corrupt the EEG and EOG signals find expression in sharp near-periodic waves. For most subjects, the heartbeat rate ranges from 60 to 150 beats per minute; thus, the main frequency is between 1 and 2.5 Hz. However, the spiked form of the waves generates significant harmonics at integer multiples of the main frequency. In case of referential EEG montages, the cardiac artefacts, when being present, commonly occur in all EEG channels. In this study,

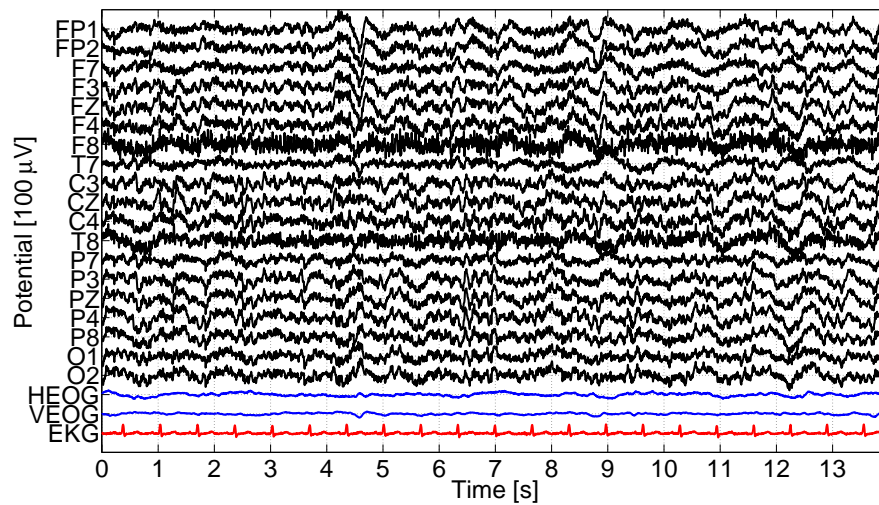


**Figure 2.2.2:** EEG segment (14 sec.) containing artefacts originating from muscle tension: each signal represents a channel from top = frontal to bottom = occipital; in addition, at the very bottom, HEOG, VEOG and EKG channels are provided. In this example, the artefacts manifest themselves as high-frequency signals that superimpose the EEG channels F8 and T8.

a parallel recorded ECG channel measuring the electric activity of the heart is available. The cardiac artefacts coincide with the so-called QRS complexes, i.e. the sharp peaks in the ECG signal. An example of cardiac artefacts corrupting all EEG channels is provided in Figure 2.2.3. The artefacts appear as spikes that occur synchronously in the EEG signals.

Electric fields originating from the activity of sweat glands on the scalp manifest themselves as high amplitude waves with frequency below 1.5 Hz. Figure 2.2.4 gives an example for this type of artefact.

Irregular signals due to poor electrode contact distinguish from the rest of the EEG signals either by sharp spikes or high amplitude waves due to abrupt impedance changes. These phenomena commonly occur only on single affected electrode channels and are thus easily detectable. In Figure 2.2.5, channel O1 is subject to poor electrode contact between seconds 1 and 4 resulting in a high-amplitude wave that differs in its morphology from the rest of the channel signals.

Spurious noise is generated by magnetic fields in the motor of electronic devices, e.g. medical equipment. Depending on the device, the corresponding artefacts vary in morphology, duration, and repetition rate. The best way to avoid these artefacts is to record the EEG in shielded rooms with no other electronic devices nearby.

Induction from the mains supply is characterized by a low amplitude and main

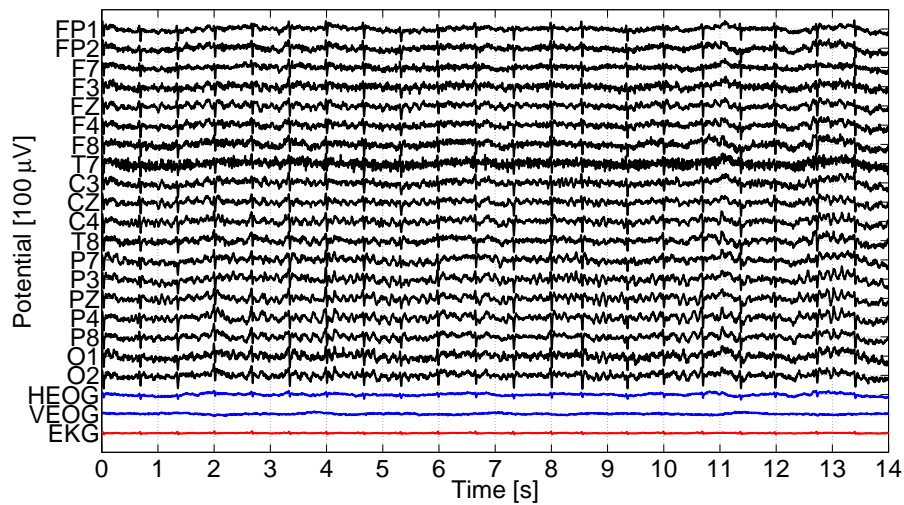


**Figure 2.2.3:** EEG segment (14 sec.) containing artefacts originating from cardiac activity: each signal represents a channel from top = frontal to bottom = occipital; in addition, at the very bottom, HEOG, VEOG and EKG channels are provided. In this example, artefacts manifest themselves as sharp periodic peaks affecting all EEG channels.

frequency of 50 Hz<sup>3</sup>. In this study, analog notch filtering at 50 Hz was performed during EEG recording.

## 2.2.2 Artefact Removal

At first, in order to remove artefacts from the EEG samples, a visual segment selection was performed. All EEG segments corrupted by artefacts that were not removable, e.g. artefacts from poor electrode contacts, were discarded from further analyses. Minimum length of remaining EEG segments was 4 seconds, i.e. 1024 sample points per channel. In order to make the visual selection objective and replicable, it was carried out according to predefined decision rules. Only segments meeting at least one of the following criteria were discarded:

- Segments where the EOG signals were disturbed and/or did not correspond to eye artefacts in the EEG signals
- Segments where the ECG signal was disturbed
- Segments corrupted by artefacts other than eye or cardiac artefacts in the frequency range of 2 – 15 Hz

All further processing was conducted using the software MATLAB<sup>®</sup> 7.11 (R2010b).

<sup>3</sup>In some countries the main frequency is 60 Hz, e.g. in North American countries, Brazil, Colombia, Peru, Venezuela, Saudi Arabia, and South Korea.

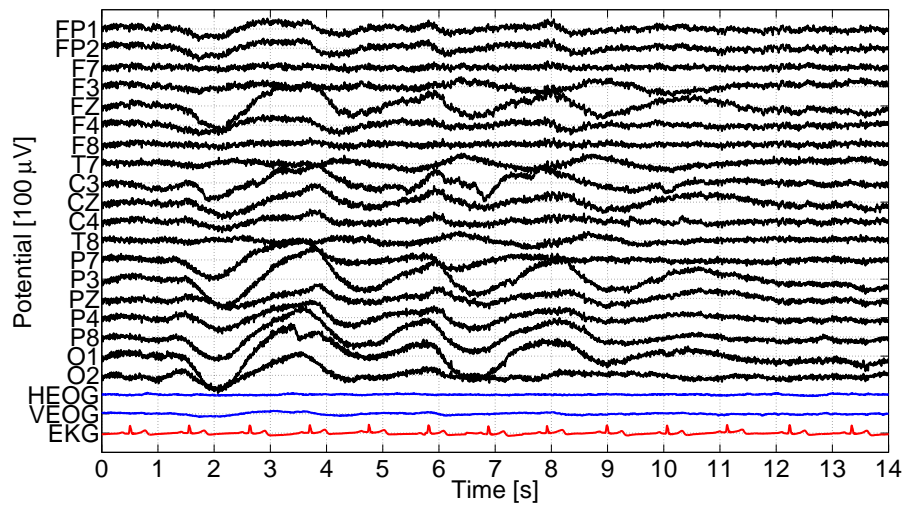


**Figure 2.2.4:** EEG segment (14 sec.) containing artefacts originating from sweat glands: each signal represents a channel from top = frontal to bottom = occipital; in addition, at the very bottom, HEOG, VEOG and EKG channels are provided. In this example, artefacts find expression as low-frequency waves superimposing most EEG channels.

For removing slow variations or trends, the EEG, ECG, and EOG signals were subject to digital high-pass filtering. A stable, direct-form finite impulse response (FIR) filter with linear phase and filter order 340 was used for high-pass filtering with border frequency 2 Hz. Thus, low-frequency artefacts, e.g. from sweating, were removed. Naturally, this procedure implied that no EEG signal portions with frequency below 2 Hz could be used for further analyses. Figures 2.2.6a and 2.2.6b show the gain and phase of the applied high-pass filter.

The resulting high-pass filtered EEG signals were tested for cardiac artefacts. The artefact detection was achieved both by visual inspection and by applying an automated detection algorithm, the so-called *energy interval histogram* (EIH) method (cf. [50] and [51]). This method relies on the assumptions that cardiac artefacts have the shape of sharp spikes, that they occur near-periodically, and that they are uncorrelated with the EEG signals. Each EEG segment was tagged as corrupted or non-corrupted by cardiac artefacts.

A robust method for the removal of cardiac artefacts was proposed in [52]. This method makes use of the ECG for identifying the position of the near-periodically occurring spikes. Cardiac artefacts in the EEG signals are assumed to be synchronous both in time and waveform to the ECG. By using this technique, the artefacts were removed without altering the rest of the EEG signals.

The vertical and horizontal EOG signals were used for removing eye-artefacts from the EEG. Since no dynamic relations between EOG and EEG were observed,



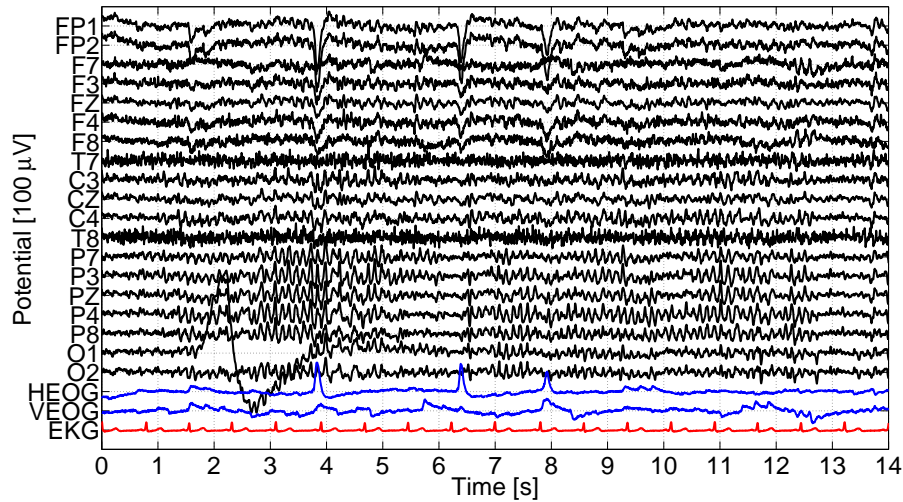


**Figure 2.2.5:** EEG segment (14 sec.) containing artefacts originating from poor electrode contact: each signal represents a channel from top = frontal to bottom = occipital; in addition, at the very bottom, HEOG, VEOG and EKG channels are provided. In this example, the contact disturbance affects the EEG channel O1 as high-amplitude wave from seconds 1.5 – 4.

static linear regression of each EEG signal on the EOG signals was applied. However, the EOG channels measure not only electric fields related to eye movements but also fields from neuronal activity. In order to eliminate these high-frequency signal components, the EOG signals were subject to prior low-pass filtering using a stable FIR filter with linear phase, order 340, and corner-frequency 12 Hz.

Finally, in order to remove high-frequency artefacts, e.g. from muscle tension, the EEG signals were subject to low-pass filtering at 15 Hz (linear, stable FIR filter with order 340). All further computations were carried out on the artefact-corrected and band-pass filtered (2–15 Hz) EEG segments.

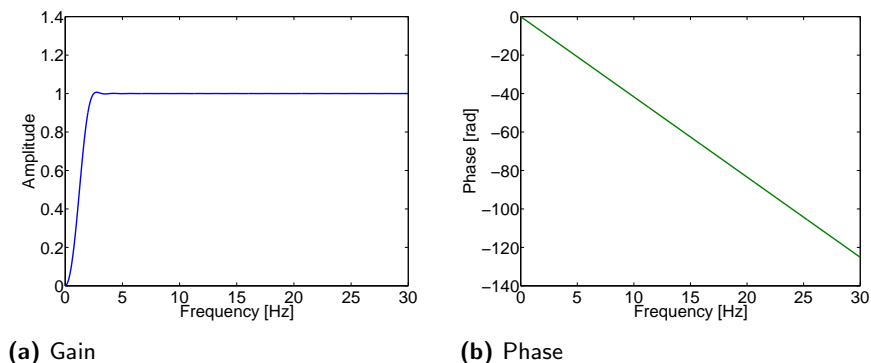


**Figure 2.2.6:** Gain and phase of high-pass FIR filter: stable, direct-form FIR filter with linear phase, filter order 340 and border frequency 2 Hz

The processing steps for artefact removal are illustrated in Figures 2.2.7 – 2.2.11. Figure 2.2.7 shows an EEG segment that is corrupted by several types of artefacts: low-frequency oscillations in frontal channels, cardiac artefacts in all channels, eye artefacts in the frontal and central channels, and high-frequency artefacts in frontal and occipital channels. In Figure 2.2.8, the high-pass filtered EEG segment is shown; trends and low-frequency artefacts are thus removed. The next preprocessing step is the removal of cardiac artefacts, the resulting EEG segment can be seen in Figure 2.2.9; the sharp spikes from the electric heart activity have disappeared. Figure 2.2.10 shows the EEG segment after removing eye artefacts. Finally, the EEG segment was subject to low-pass filtering at border frequency 15 Hz; the resulting signal is shown in Figure 2.2.11.

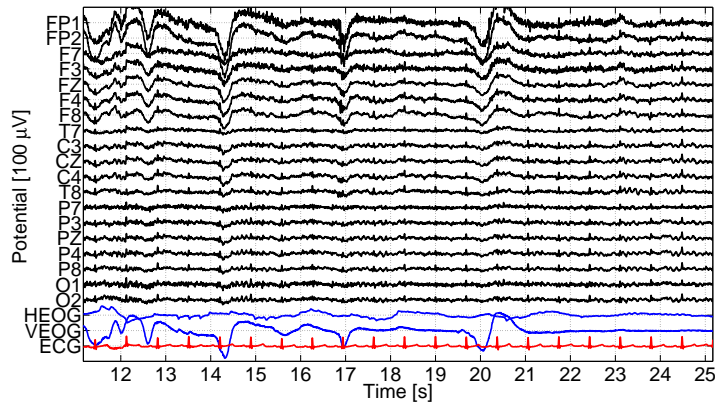


Figure 2.2.7: EEG preprocessing steps: original EEG segment

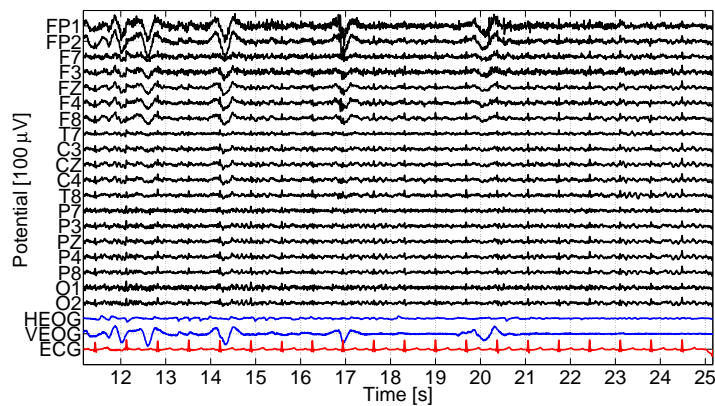


Figure 2.2.8: EEG preprocessing steps: high-pass filtering

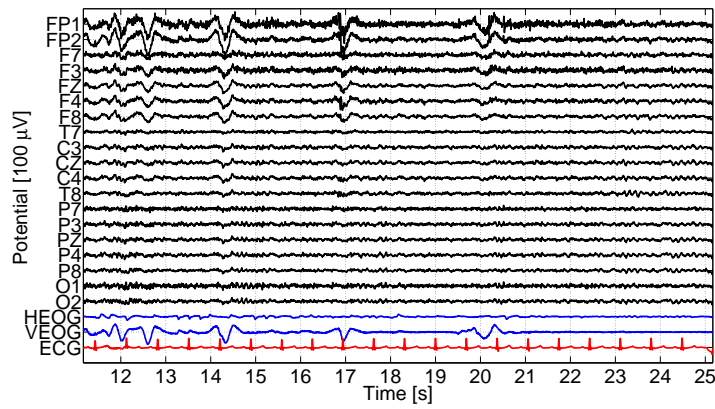


Figure 2.2.9: EEG preprocessing steps: removal of cardiac artefacts

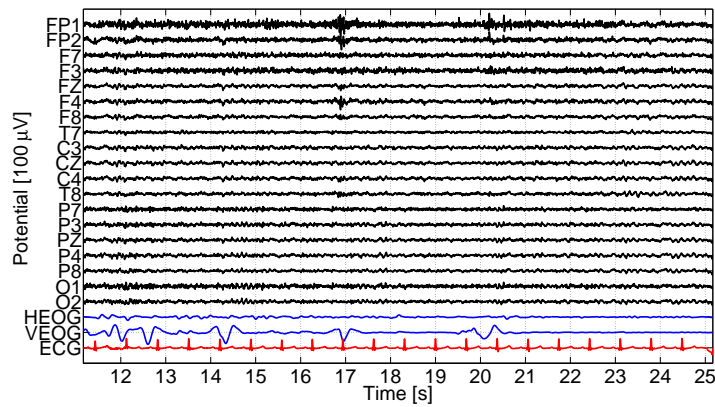


Figure 2.2.10: EEG preprocessing steps: removal of eye artefacts

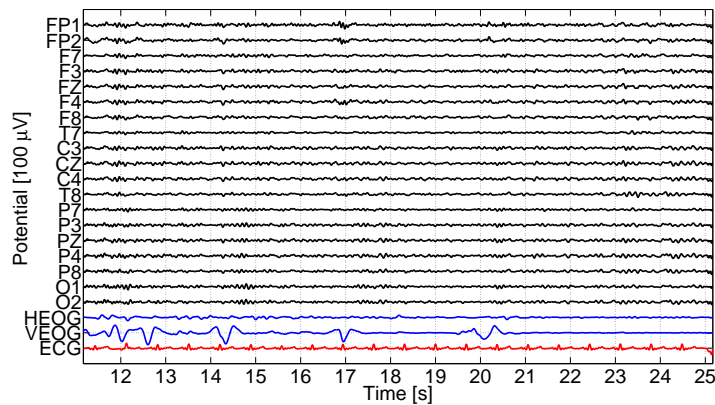


Figure 2.2.11: EEG preprocessing steps: low-pass filtering

### 2.2.3 Segmentation

The methods used in this work rely on a certain invariance of the first and second moments of the EEG signals with respect to time, the so-called wide-sense stationarity. A formal definition will follow in Section 2.3. However, brain dynamics and consequently the EEG are in general non-stationary (cf. e.g. [53]). In order to use methods that assume wide-sense stationarity, the EEG is divided in short "quasi-stationary" segments. In scientific literature, two approaches for EEG segmentation have been described: the first method is to search for structural breaks in the EEG and, according to these breaks, to divide the EEG in stationary intervals of different lengths (cf. e.g. [54], [55]). This approach is useful for finding changes in the cognitive state of a subject or for detecting drug effects on the EEG. In this work, the two different EEG stages – resting state and cognitive task – are a priori known. Within these stages, the first and second moments do not change abruptly but are rather subject to a drift with respect to time. Thus, the second segmentation approach was applied: dividing the EEG in segments with fixed duration of 4 seconds and overlap of 2 seconds. All further analyses were carried out on the resulting 4 second EEG segments.

## 2.3 Stationary Processes in Time Domain

This section will be concerned with stationary processes in time domain. Section 2.3.1 will provide basic definitions that are useful in this context. In Section 2.3.2, the concept of hilbert spaces will be described. Finally, Section 2.3.3 will be concerned with infinite autoregressive processes. Note that the concepts in the following sections are only those that are useful for the further understanding of this work; no claim to completeness is raised. For deeper insights about the analysis of stationary processes in time domain, the reader is referred to e.g. [56], [57], [58], and [59].

### 2.3.1 Foundations

For the remainder of this work, an EEG segment will be interpreted as an  $r$ -vector-valued time series

$$\mathbf{x}(t) = \begin{pmatrix} x_1(t) \\ \vdots \\ x_r(t) \end{pmatrix} \in \mathbb{R}^{r \times 1}, \quad t = 1, \dots, T \quad (2.3.1)$$

where the component  $x_i(t)$ ,  $i = 1, \dots, r$  represents the  $i^{\text{th}}$  electrode channel at sampling time  $t$ . All considerations will be carried out only for real-valued time series.

In this work, a time series is assumed to be generated by an underlying stochastic model called *stochastic process*.

**Definition 2.3.1** (Stochastic Process). *Starting from a probability space  $(\Omega, \mathfrak{A}, P)$ , consider random variables, i.e. measurable functions,  $\mathbf{x}(t, \omega) : \Omega \rightarrow \mathbb{R}^{r \times 1}$  with  $\omega \in \Omega$  and  $t \in \mathbb{Z}^4$ . A stochastic process is defined as a family of random variables  $(\mathbf{x}(t, \omega) | t \in \mathbb{Z}, \omega \in \Omega)$  on  $(\Omega, \mathfrak{A}, P)$ .*

The time series  $\mathbf{x}(t)$  is interpreted as a realization of  $(\mathbf{x}(t, \omega) | t \in \mathbb{Z}, \omega \in \Omega)$  for fixed  $\omega$ . As the parameter  $\omega$  has no relevance for this work and  $t \in \mathbb{Z}$  will always be assumed, from now on the notation  $(\mathbf{x}(t))$  will be used instead of  $(\mathbf{x}(t, \omega) | t \in \mathbb{Z}, \omega \in \Omega)$ .

The first two moments of  $(\mathbf{x}(t))$  are the *mean*  $\boldsymbol{\mu}(t)$  and *autocovariance function*  $\gamma(s, t)$ .

**Definition 2.3.2** (Mean). *Let  $(\mathbf{x}(t))$  be a stochastic process with component-wise expected absolute values  $\mathbb{E}[|x_i(t)|] < \infty \forall i = 1, \dots, r$ , then the mean of the process is defined as*

$$\boldsymbol{\mu}(t) = \mathbb{E}[\mathbf{x}(t)] = \begin{pmatrix} \mathbb{E}[x_1(t)] \\ \vdots \\ \mathbb{E}[x_r(t)] \end{pmatrix} = \begin{pmatrix} \mu_1(t) \\ \vdots \\ \mu_r(t) \end{pmatrix} \in \mathbb{R}^{r \times 1}, \quad t \in \mathbb{Z}. \quad (2.3.2)$$

The element  $\mu_i$  characterizes the level of the subprocess  $x_i(t)$ . In this work, zero mean is assumed, i.e.

$$\mu_i(t) = 0 \quad \forall i = 1, \dots, r, \quad t \in \mathbb{Z}. \quad (2.3.3)$$

This is no restriction for further analyses, as every stochastic process  $(\mathbf{x}(t))$  can easily be replaced by its centered process  $(\mathbf{x}(t) - \boldsymbol{\mu}(t))$ .

**Definition 2.3.3** (Autocovariance Function). *Let  $(\mathbf{x}(t))$  be a centered process with  $\mathbb{E}[\mathbf{x}(t)^\top \mathbf{x}(t)] < \infty$ , then the autocovariance function is defined as*

$$\begin{aligned} \gamma(s, t) = \mathbb{E}[\mathbf{x}(s)\mathbf{x}(t)^\top] &= \begin{pmatrix} \mathbb{E}[x_1(s)x_1(t)] & \cdots & \mathbb{E}[x_1(s)x_r(t)] \\ \vdots & \ddots & \vdots \\ \mathbb{E}[x_r(s)x_1(t)] & \cdots & \mathbb{E}[x_r(s)x_r(t)] \end{pmatrix} \\ &= \begin{pmatrix} \gamma_{11}(s, t) & \cdots & \gamma_{1r}(s, t) \\ \vdots & \ddots & \vdots \\ \gamma_{r1}(s, t) & \cdots & \gamma_{rr}(s, t) \end{pmatrix} \in \mathbb{R}^{r \times r}, \quad s, t \in \mathbb{Z}. \end{aligned} \quad (2.3.4)$$

The element  $\gamma_{ij}(s, t)$  describes the linear dependence between  $x_i(s)$  and  $x_j(t)$ . For  $s = t$ , the  $i^{\text{th}}$  diagonal element  $\gamma_{ii}(t, t)$  is the variance of  $x_i(t)$  and will be denoted by  $\text{Var}[x_i(t)]$ .

---

<sup>4</sup>Here, only the discrete-time case with equidistant time points will be considered.

Consider the class of stochastic processes with invariant first and second moments with respect to time. As mentioned in Section 2.2.3, this property is called *wide-sense stationarity*.

**Definition 2.3.4** (Wide-Sense Stationary Process). *An  $r$ -vector real valued stochastic process  $(\mathbf{x}(t))$  is wide-sense stationary if*

1.  $\mathbb{E}[\mathbf{x}(t)^\top \mathbf{x}(t)] < \infty \forall t \in \mathbb{Z}$
2.  $\boldsymbol{\mu}(t) = \boldsymbol{\mu}$  const.  $\forall t \in \mathbb{Z}$
3.  $\gamma(u, 0) = \gamma(t + u, t) \forall t, u \in \mathbb{Z}$

As the autocovariance function of a stationary process only depends on the time lag  $u$ , from now on it will be denoted by  $\gamma(u)$  instead of  $\gamma(u, 0) = \gamma(t + u, t)$ . Note that, for real-valued processes,  $\gamma(u)^\top = \gamma(-u)$  and  $\gamma(0) \geq 0$ . Although other types of stationarity exist, this work is concerned with wide-sense stationarity only; thus, the "wide-sense" will be skipped from now on.

When addressing stationary processes, two types of stochastic convergence will prove to be useful: *convergence in mean square* and *almost sure convergence*.

**Definition 2.3.5** (Convergence in Mean Square). *Consider the  $r$  vector-valued random variables*

$$\mathbf{x}(n) = \begin{pmatrix} x_1(n) \\ \vdots \\ x_r(n) \end{pmatrix}, \quad \mathbf{x} = \begin{pmatrix} x_1 \\ \vdots \\ x_r \end{pmatrix} \in \mathbb{R}^{r \times 1}, \quad n \in \mathbb{N} \quad (2.3.5)$$

on a probability space  $(\Omega, \mathfrak{A}, P)$ . *The sequence  $(\mathbf{x}(n)|n \in \mathbb{N})$  converges to  $\mathbf{x}$  with  $\mathbb{E}[|x_i|^2] < \infty \forall i = 1, \dots, r$  in mean square if*

$$\lim_{n \rightarrow \infty} \mathbb{E}[|(x_i(n) - x_i)|^2] = 0 \quad \forall i = 1, \dots, r \quad (2.3.6)$$

In this work, unless stated differently, the limit of a sequence of random variables is referring to the limit in mean square and is denoted by

$$\text{l.i.m.}_{n \rightarrow \infty} \mathbf{x}(n) = \mathbf{x} \quad (2.3.7)$$

**Definition 2.3.6** (Almost Sure Convergence). *The sequence  $(\mathbf{x}(n)|n \in \mathbb{N})$  converges to  $\mathbf{x}$  (cf. Definition 2.3.5) almost surely if*

$$P(\lim_{n \rightarrow \infty} x_i(n) = x_i) = 1 \quad \forall i = 1, \dots, r. \quad (2.3.8)$$

The almost sure convergence will be denoted by

$$\lim_{n \rightarrow \infty} \mathbf{x}(n) = \mathbf{x} \text{ a.s.} \quad (2.3.9)$$

### 2.3.2 Hilbert Space

Stationary processes have an elegant geometric interpretation in *Hilbert space*. In order to define Hilbert spaces, the concept of *inner products* is useful:

**Definition 2.3.7** (Inner Product). *Let  $\mathbb{H}$  be a linear space, then the mapping  $\langle \cdot, \cdot \rangle : \mathbb{H} \times \mathbb{H} \rightarrow \mathbb{C}$  is an inner product if*

1.  $\langle a_1x_1 + a_2x_2, y \rangle = a_1 \langle x_1, y \rangle + a_2 \langle x_2, y \rangle \quad \forall a_1, a_2 \in \mathbb{C}, x_1, x_2, y \in \mathbb{H}$
2.  $\langle x, y \rangle = \overline{\langle y, x \rangle} \quad \forall x, y \in \mathbb{H}$
3.  $\langle x, x \rangle \geq 0$  and  $\langle x, x \rangle = 0 \Leftrightarrow x = 0$ .

By using inner products, it is possible to define geometrical concepts such as length or angle.

**Definition 2.3.8** (Hilbert Space). *A linear space  $\mathbb{H}$  with inner product is called a Hilbert space if all sequences  $x(n) \in \mathbb{H}$  satisfying  $\lim_{m, n \rightarrow \infty} \|x(n) - x(m)\| = 0$  converge to some element  $x \in \mathbb{H}$  in the norm defined by  $\|x\| := \sqrt{\langle x, x \rangle}$ .*

Let  $\mathbb{M}$  be a subspace of the Hilbert space  $\mathbb{H}$  that contains all its limits in mean squares;  $\mathbb{M}$  is then called a *closed subspace* of  $\mathbb{H}$ . The *orthogonal complement* of  $\mathbb{M}$ , denoted by  $\mathbb{M}^\perp$ , is defined as the set of elements  $x \in \mathbb{H}$  with  $\langle x, y \rangle = 0 \quad \forall y \in \mathbb{M}$ .  $\mathbb{M}^\perp$  is a closed subspace of  $\mathbb{H}$  on its own [56]. Using this terminology, the *projection theorem* (cf. e.g. [56]) will be useful in the course of this work.

**Theorem 2.3.1** (Projection Theorem). *Let  $\mathbb{M}$  be a closed subspace of a Hilbert space  $\mathbb{H}$  with its orthogonal complement  $\mathbb{M}^\perp$ . For every  $x \in \mathbb{H}$*

1. *there exists a unique element  $\hat{x} \in \mathbb{M}$  satisfying  $\|x - \hat{x}\| = \min_{y \in \mathbb{M}} \|x - y\|$*

and

2.  $\|x - \hat{x}\| = \min_{y \in \mathbb{M}} \|x - y\| \Leftrightarrow (x - \hat{x}) \in \mathbb{M}^\perp$ .

$\hat{x}$  is called *orthogonal projection of  $x$  onto  $\mathbb{M}$* .

Let  $L_2(\Omega, \mathfrak{A}, P)$  denote the space of square-integrable random variables  $x : \Omega \rightarrow \mathbb{R}$ , i.e.  $\mathbb{E}[\|x\|^2] < \infty$ . The set of equivalence classes  $x = y$  a.s. for variables  $x, y \in L_2$  is denoted by  $\mathbb{L}_2(\Omega, \mathfrak{A}, P)$ .  $\mathbb{L}_2$  together with the inner product  $\langle x, y \rangle = \mathbb{E}[x^\top y]$  is a Hilbert space. The closed subspace  $\mathbb{H}_x \subset \mathbb{L}_2$  spanned by the scalar process  $(x(t))$  is a Hilbert space on its own and is called *time domain* of the process. Its elements are all linear combinations of the  $x(t)$  and their limits in mean square. In  $\mathbb{H}_x$ , a scalar stationary process  $(x(t))$  is represented by vectors  $x(t)$  of equal length. The angle between  $x(t)$  and  $x(t - u)$  for fixed  $u \in \mathbb{Z}$  is constant  $\forall t \in \mathbb{Z}$ .

On  $\mathbb{H}_x$ , the scalar stationary process  $(x(t))$  is associated with an *unitary operator*  $z$ .

**Definition 2.3.9** (Unitary Operator). *A bounded linear operator  $z : \mathbb{H}_x \rightarrow \mathbb{H}_x$  is called unitary if it is surjective and preserves the inner product*

$$\langle zx(t), zy(t) \rangle = \langle x(t), y(t) \rangle \quad \forall x(t), y(t) \in \mathbb{H}_x. \quad (2.3.10)$$

There exists a unique unitary operator  $z : \mathbb{H}_x \rightarrow \mathbb{H}_x$  such that (cf. e.g. [56])

$$z^k x(t) = x(t - k) \quad \text{for } k, t \in \mathbb{Z}. \quad (2.3.11)$$

Commonly, the operator  $z$  is referred to as *backshift operator*. The whole process  $(x(t))$  is generated by  $z$ :

$$x(t) = z^{-t} x(0). \quad (2.3.12)$$

The backshift operator  $z$  will turn out to be useful in the Sections 2.3.3 and 2.4.2.

### 2.3.3 Autoregressive Processes

A class of stochastic processes that is important for this work are *infinite autoregressive processes*, here denoted by *AR( $\infty$ )-processes*. Consider the linear system

$$\sum_{j=0}^{\infty} A(j) \mathbf{x}(t - j) = \boldsymbol{\epsilon}(t) \quad (2.3.13)$$

where  $A(j) \in \mathbb{R}^{r \times r}$  with  $\sum_{j=0}^{\infty} \|A(j)\| < \infty$  and  $\boldsymbol{\epsilon}(t)$  is  $r$ -dimensional *white noise*, i.e.  $\mathbb{E}[\boldsymbol{\epsilon}(t)] = 0$  and  $\mathbb{E}[\boldsymbol{\epsilon}(s)\boldsymbol{\epsilon}(t)^*] = \delta_{st}\Sigma - \delta_{st}$  being the Kronecker delta – for  $s, t \in \mathbb{Z}$ .  $\boldsymbol{\epsilon}(t)$  is orthogonal on the past  $\mathbf{x}(t - j), j > 0$ . A linear system satisfying Equation (2.3.13) is called *AR( $\infty$ )-system*. Using the notation  $z$  for both the backshift operator as defined in (2.3.10) and a complex variable, Equation (2.3.13) can be restated as

$$a(z) \mathbf{x}(t) = \boldsymbol{\epsilon}(t) \quad (2.3.14)$$

where  $a(z) = \sum_{j=0}^{\infty} A(j)z^j$  exists in the usual sense inside and on the unit circle [57]. If the *stability condition*

$$\det a(z) \neq 0 \quad \text{for } |z| \leq 1 \quad (2.3.15)$$

holds,  $a^{-1}(z)$  can be expanded into a power series that converges inside a disc containing the unit circle

$$a^{-1}(z) = \sum_{j=0}^{\infty} K(j)z^j \quad (2.3.16)$$

where  $K(j) \in \mathbb{R}^{r \times r}$  with  $\sum_{j=0}^{\infty} \|K(j)\| < \infty$  (cf. [58]). An *AR( $\infty$ )-process* is the unique stationary solution of the *AR( $\infty$ )-system* (2.3.13) and is given as

$$\mathbf{x}(t) = k(z)\boldsymbol{\epsilon}(t) \quad (2.3.17)$$

with  $k(z) = a^{-1}(z)$  [60]. From (2.3.17), it is clear that every *AR( $\infty$ )-process* has mean zero.



## 2.4 Stationary Processes in Frequency Domain

Whereas Section 2.3 was concerned with stationary processes in time domain, the focus of this section will be on the analysis of stationary processes in frequency domain. First, the discrete time Fourier transform will be discussed in Section 2.4.1. Section 2.4.2 will then provide the spectral representation of a stationary process. Finally, Section 2.4.3 will be concerned with the central concept of this work, the multivariate spectral density. Further insights on stationary processes in the frequency domain can be found in e.g. [56] and [60].

### 2.4.1 Discrete Time Fourier Transform

A central tool in the context of spectral representation is the *discrete time Fourier transform* (DFT). Consider a matrix-valued sequence  $(a(k) \in \mathbb{R}^{m \times n} | k \in \mathbb{Z})$ . The DFT of  $(a(k) | k \in \mathbb{Z})$  is defined as

$$A(\lambda) = \sum_{k=-\infty}^{\infty} e^{-i\lambda k} a(k), \quad \lambda \in \mathbb{R} \quad (2.4.1)$$

where  $i$  is the imaginary unit and  $\lambda$  is the frequency. Under the assumption

$$\sum_{k=-\infty}^{\infty} \|a(k)\| < \infty \quad (2.4.2)$$

where  $\|\cdot\|$  is a matrix norm, the partial sum

$$A^{(N)}(\lambda) = \sum_{k=-N}^N e^{-i\lambda k} a(k), \quad \lambda \in \mathbb{R}, \quad N \in \mathbb{N} \quad (2.4.3)$$

converges pointwise and uniformly

$$\begin{aligned} \|A(\lambda) - A^{(N)}(\lambda)\| &= \left\| \sum_{|k|>N} e^{-i\lambda k} a(k) \right\| \leq \\ &\leq \sum_{|k|>N} \|e^{-i\lambda k} a(k)\| \leq \\ &\leq \sum_{|k|>N} \|a(k)\| \rightarrow 0 \text{ for } N \rightarrow \infty, \quad \lambda \in \mathbb{R} \end{aligned} \quad (2.4.4)$$

and the sum in Equation (2.4.1) exists in the usual sense. The last inequality in (2.4.4) holds because  $\|e^{-i\lambda k}\| = 1$ ,  $\forall \lambda \in \mathbb{R}$ ,  $\forall k \in \mathbb{Z}$ . As  $e^{-i\lambda k} = \cos(\lambda k) - i \sin(\lambda k)$  is a  $2\pi$ -periodic function, i.e.  $e^{-i\lambda k} = e^{-i(\lambda+2\pi)k}$ , it suffices to consider the discrete time Fourier transform on  $[-\pi, \pi]$ .

The *inverse discrete time Fourier transform* (IDFT) is defined as

$$a(k) = \frac{1}{2\pi} \int_{-\pi}^{\pi} e^{i\lambda k} A(\lambda) d\lambda, \quad k \in \mathbb{Z}. \quad (2.4.5)$$

## 2.4.2 Spectral Representation of Stationary Processes

This section is concerned with the spectral representation of a stationary process. Therefore, the concept of *stochastic integration* with respect to a *process of orthogonal increments* is introduced.

**Definition 2.4.1** (Process of Orthogonal Increments). *Given a probability space  $(\Omega, \mathfrak{A}, P)$ , let  $(z(\lambda)|\lambda \in [-\pi, \pi])$  with  $z(\lambda) : \Omega \rightarrow \mathbb{C}^{r \times 1}$  be an  $r$ -vector valued stochastic process satisfying*

1.  $\mathbb{E}[z(\lambda)^* z(\lambda)] < \infty \quad \forall \lambda \in [-\pi, \pi]$
2.  $\mathbb{E}[z_i(\lambda)] = 0 \quad \forall \lambda \in [-\pi, \pi], i = 1, \dots, r$
3.  $\mathbb{E}[(z(\lambda_4) - z(\lambda_3))(z(\lambda_2) - z(\lambda_1))^*] = 0 \quad \forall \lambda_1 < \lambda_2 \leq \lambda_3 < \lambda_4$

*then  $(z(\lambda)|\lambda \in [-\pi, \pi])$  is called a process of orthogonal increments. Additionally, if  $(z(\lambda)|\lambda \in [-\pi, \pi])$  satisfies*

4.  $\text{l.i.m.}_{\epsilon \downarrow 0} z(\lambda + \epsilon) = z(\lambda)$

*it is a right-continuous process of orthogonal increments.*

Now, consider a square-integrable deterministic function  $g : [-\pi, \pi] \rightarrow \mathbb{C}$ . The sum

$$I_n(g) = \sum_{i=0}^{n-1} g(\lambda_i)(z(\lambda_{i+1}) - z(\lambda_i)) \quad (2.4.6)$$

with  $-\pi = \lambda_0 < \dots < \lambda_n = \pi$

weights  $g(\lambda_i)$  with the increment of the process  $(z(\lambda)|\lambda \in [-\pi, \pi])$  and is thus an extension of a Riemann sum. The stochastic integral  $I(g)$  is defined as the limit in mean squares of  $I_n(g)$

$$I(g) = \int_{-\pi}^{\pi} g(\lambda) dz(\lambda) = \text{l.i.m.}_{n \rightarrow \infty} I_n(g) \quad (2.4.7)$$

$I(g)$  is a random variable. As can be shown, its first and second moments are defined as (cf. e.g. [56])

$$\begin{aligned} \mathbb{E}[I(g)] &= \int_{-\pi}^{\pi} g(\lambda) d\mathbb{E}[z(\lambda)] \\ \mathbb{E}[I(g)I(h)^*] &= \int_{-\pi}^{\pi} g(\lambda) \overline{h(\lambda)} d\mathbb{E}[z(\lambda)z(\lambda)^*]. \end{aligned} \quad (2.4.8)$$

With these definitions, the spectral representation of a stationary process is given by the following theorem (cf. e.g. [56]).

**Theorem 2.4.1** (Spectral Representation Theorem). *Given a stationary process  $(\mathbf{x}(t))$ , there exists a right-continuous orthogonal increment process  $(z(\lambda)|\lambda \in [-\pi, \pi])$  with*

$$\mathbf{x}(t) = \int_{-\pi}^{\pi} e^{it\lambda} dz(\lambda) \text{ a.s.} \quad (2.4.9)$$

Theorem 2.4.1 states that every stationary process  $(\mathbf{x}(t))$  can be approximated (in mean squares) by a sum of harmonic oscillations. The process  $(z(\lambda)|\lambda \in [-\pi, \pi])$  defines a right-continuous, monotonically non-decreasing function  $\mathbf{F} : [-\pi, \pi] \rightarrow \mathbb{C}^{r \times r}$  by

$$\mathbf{F}(\lambda) = \mathbb{E}[z(\lambda)z(\lambda)^*]. \quad (2.4.10)$$

$\mathbf{F}$  is called the *spectral distribution function* of  $(\mathbf{x}(t))$ . For a centered stationary process, the spectral distribution function is in close relation to the autocovariance function

$$\gamma(u) = \int_{-\pi}^{\pi} e^{iu\lambda} d\mathbf{F}(\lambda) \quad \forall u \in \mathbb{Z} \quad (2.4.11)$$

### 2.4.3 Multivariate Spectral Density

This section is concerned with the central concept of this work, the *multivariate spectral density*. Let  $(\mathbf{x}(t))$  be an  $r$ -vector valued stationary process with mean zero and spectral distribution function  $\mathbf{F}$ . A function  $\mathbf{f} : [-\pi, \pi] \rightarrow \mathbb{C}^{r \times r}$  satisfying

$$\mathbf{F}(\lambda) = \int_{-\pi}^{\lambda} \mathbf{f}(\mu) d\mu \text{ for } \lambda \in [-\pi, \pi] \quad (2.4.12)$$

is called multivariate spectral density. Assuming that the process memory is fading, i.e.

$$\sum_{u=-\infty}^{\infty} \|\gamma(u)\| < \infty, \quad (2.4.13)$$

$\mathbf{F}$  is absolutely continuous and  $\mathbf{f}$  exists and is given by (cf. e.g. [60])

$$\mathbf{f}(\lambda) = \frac{1}{2\pi} \sum_{u=-\infty}^{\infty} \gamma(u) e^{-i\lambda u} \text{ for } \lambda \in [-\pi, \pi]. \quad (2.4.14)$$

The inverse relation is given by

$$\gamma(u) = \int_{-\pi}^{\pi} e^{iu\lambda} \mathbf{f}(\lambda) d\lambda \text{ for } u \in \mathbb{Z}. \quad (2.4.15)$$

From Equations (2.4.14) and (2.4.15),  $\mathbf{f}$  and  $\gamma$  are in a one-to-one relation via DFT and IDFT.

The multivariate spectral density  $\mathbf{f}$  is matrix-valued and can thus be written as

$$\mathbf{f}(\lambda) = \begin{pmatrix} f_{11}(\lambda) & \cdots & f_{1r}(\lambda) \\ \vdots & \ddots & \vdots \\ f_{r1}(\lambda) & \cdots & f_{rr}(\lambda) \end{pmatrix} \text{ for } \lambda \in [-\pi, \pi] \quad (2.4.16)$$

where  $f_{ii}(\lambda)$  is the auto-spectral density of  $x_i(t)$ , and  $f_{ij}(\lambda)$  is the cross-spectral density of  $x_i(t)$  with  $x_j(t)$  at frequency  $\lambda$ .  $\mathbf{f}$  is Hermitian and non-negative definite; this implies that the auto-spectral density is real and non-negative<sup>5</sup> [60]. As for real-valued processes  $\mathbf{f}(\lambda) = \mathbf{f}^\top(-\lambda)$  holds, the spectral density will only be considered on  $[0, \pi]$ .

For the interpretation of the multivariate spectral density, consider Equation (2.4.15) for the case  $u = 0$

$$\gamma(0) = \int_{-\pi}^{\pi} \mathbf{f}(\lambda) d\lambda. \quad (2.4.17)$$

In  $[\lambda_1, \lambda_2]$ , the area under  $\mathbf{f}$  may thus be interpreted as the contribution of the frequency-band  $[\lambda_1, \lambda_2]$  to the process  $(\mathbf{x}(t))$ . The frequency bands corresponding to the most important oscillations of the process are visible as peaks in  $\mathbf{f}$ .

## 2.5 Dependence Measures Derived from the Multivariate Spectral Density

This section will be concerned with measures for dependence based on the multivariate spectral density  $\mathbf{f}$ .

### 2.5.1 Framework

For the remainder of this work, only real-valued AR( $\infty$ )-processes (2.3.13) with full rank  $\Sigma$  and stability condition (2.3.15) will be considered. By imposing the additional requirement

$$\sum_{j=0}^{\infty} j^{\frac{1}{2}} \|A(j)\| < \infty, \quad (2.5.1)$$

the spectral density satisfies

$$\underline{c}I_r \leq \mathbf{f}(\lambda) \leq \bar{c}I_r \quad (2.5.2)$$

where  $\underline{c}$  and  $\bar{c}$  with  $0 < \underline{c} \leq \bar{c} < \infty$  are finite positive constants, and  $I_r$  is the  $(r \times r)$ -dimensional unity matrix [58]. Under the imposed conditions, the multivariate spectral density exists and has constant rank  $\forall \lambda$ .  $\mathbf{f}(\lambda)$  can be factorized as

$$\mathbf{f}(\lambda) = \mathbf{k}(e^{-i\lambda}) \Sigma \mathbf{k}^*(e^{-i\lambda}) \quad (2.5.3)$$

<sup>5</sup>These properties will be important for the spectral density estimators in Section 2.7.

where  $k(e^{-i\lambda}) = a(e^{-i\lambda})^{-1}$  as defined in Section 2.3.3 [59].

### 2.5.2 Coherence

The first measure for dependence derived from the cross-spectral density is the (*squared*) *coherence*.

Consider the univariate subprocesses  $(x_i(t))$  and  $(x_j(t))$  with corresponding auto-spectral densities  $f_{ii}$  and  $f_{jj}$  and cross-spectral density  $f_{ij}$ . Let  $(z_i(\lambda)|\lambda \in [-\pi, \pi])$  and  $(z_j(\lambda)|\lambda \in [-\pi, \pi])$  be the corresponding univariate processes of orthogonal increments. The cross-spectral density in  $[\lambda_1, \lambda_2]$  with  $-\pi \leq \lambda_1 \leq \lambda_2 \leq \pi$  is

$$\int_{\lambda_1}^{\lambda_2} f_{ij}(\lambda) d\lambda = \mathbb{E} \left[ (z_i(\lambda_2) - z_i(\lambda_1)) \overline{(z_j(\lambda_2) - z_j(\lambda_1))} \right]. \quad (2.5.4)$$

In imprecise terms, this may be written as

$$f_{ij}(\lambda) d\lambda = \mathbb{E} \left[ dz_i(\lambda) \overline{dz_j(\lambda)} \right]. \quad (2.5.5)$$

Accordingly,  $f_{ij}(\lambda)$  is interpreted as measure for the linear dependence of  $dz_i$  and  $dz_j$  at frequency  $\lambda$ . With this, the coherence  $C_{ij}^2$  between  $(x_i(t))$  and  $(x_j(t))$  at frequency  $\lambda \in [-\pi, \pi]$  is defined as

$$C_{ij}^2(\lambda) = \frac{|\mathbb{E} [dz_i(\lambda) \overline{dz_j(\lambda)}]|^2}{\mathbb{E} [|dz_i(\lambda)|^2] \mathbb{E} [|dz_j(\lambda)|^2]} = \frac{|f_{ij}(\lambda)|^2}{f_{ii}(\lambda) f_{jj}(\lambda)}. \quad (2.5.6)$$

$C_{ij}^2$  is a symmetric measure satisfying

$$0 \leq C_{ij}^2(\lambda) \leq 1 \quad (2.5.7)$$

where  $C_{ij}^2(\lambda)$  near 1 indicates strong linear dependence between  $dz_i$  and  $dz_j$  at frequency  $\lambda$  [56]. Due to the symmetry of  $C_{ij}^2$ , no direction of dependence can be determined by this measure.

### 2.5.3 Partial Coherence

The coherence is defined by the matrix-entries  $f_{ii}$ ,  $f_{jj}$  and  $f_{ij}$  of  $\mathbf{f}$ ; in this sense, it is a bivariate measure that does not distinguish between direct and indirect linear dependences. For measuring only direct linear dependences, the (*squared*) *partial coherence* was used.

One way to define this measure is by making use of the Projection Theorem (cf. Section 2.3.2). Let  $(\mathbf{x}_I(t))$  with  $I = \{1, \dots, r\} \setminus \{i, j\}$  denote all subprocesses of  $(\mathbf{x}(t))$  but  $(x_i(t))$  and  $(x_j(t))$ . The components of  $\mathbf{x}_I(t)$  span a closed

subspace  $\mathbb{M} \subset \mathbb{H}_x$ . By the Projection Theorem, the residuals  $\epsilon_i(t)$  and  $\epsilon_j(t)$  of the orthogonal projections of  $x_i(t)$  and  $x_j(t)$  on  $\mathbb{M}$  are defined in a unique way. The respective auto-spectral density of  $\epsilon_i$  and  $\epsilon_j$  will be denoted by  $f_{\epsilon_i\epsilon_i}$  and  $f_{\epsilon_j\epsilon_j}$ , and the cross-spectral density between  $\epsilon_i$  and  $\epsilon_j$  by  $f_{\epsilon_i\epsilon_j}$ .  $f_{\epsilon_i\epsilon_j}(\lambda)$  measures the linear dependence between  $x_i$  and  $x_j$  at frequency  $\lambda$  after removing the influence of  $x_I$  [61]. Analogously to the coherence, the partial coherence between  $x_i$  and  $x_j$  at frequency  $\lambda$  given  $x_I$  is defined as [60]

$$R_{ij|I}^2(\lambda) = \frac{|f_{\epsilon_i\epsilon_j}(\lambda)|^2}{f_{\epsilon_i\epsilon_i}(\lambda)f_{\epsilon_j\epsilon_j}(\lambda)}. \quad (2.5.8)$$

There is another representation of  $R_{ij|I}^2$  that may be obtained given  $\mathbf{f}$ . As  $\mathbf{f}(\lambda)$  has full rank, its inverse  $\mathbf{g}(\lambda) = \mathbf{f}^{-1}(\lambda)$  exists and  $R_{ij|I}^2$  has the representation [61]

$$R_{ij|I}^2(\lambda) = \frac{|g_{ij}(\lambda)|^2}{g_{ii}(\lambda)g_{jj}(\lambda)}. \quad (2.5.9)$$

The partial coherence takes values between 0 and 1 as well.

#### 2.5.4 Bivariate Granger Causality

Coherences and partial coherences are symmetric measures; however, not only linear dependence but also the direction of dependence is a point of interest in this work. Granger introduced an asymmetric measure called *Granger causality* in [62].

Consider the bivariate AR( $\infty$ )-process

$$\mathbf{x}(t) = \begin{pmatrix} x_1(t) \\ x_2(t) \end{pmatrix} \in \mathbb{R}^{2 \times 1} \quad (2.5.10)$$

with coefficients  $A(k) \in \mathbb{R}^{2 \times 2}$ ,  $k \in \mathbb{N}$ . If knowledge of the past ( $x_2(t-u)|u \in \mathbb{N}$ ) improves the prediction of  $x_1(t)$ , then  $x_2$  is said to be Granger causal for  $x_1$ . In order to define this concept more precisely, some additional notation needs to be introduced: Let  $\mathbb{M}_{\{1\}}$  be the space spanned by  $(x_1(t-u)|u \in \mathbb{N})$  and  $\mathbb{M}_{\{12\}}$  be the space spanned by  $(x_1(t-u)|u \in \mathbb{N})$  and  $(x_2(t-u)|u \in \mathbb{N})$ . Denote the residual of the orthogonal projection of  $x_1(t)$  on  $\mathbb{M}_{\{1\}}$  ( $\mathbb{M}_{\{12\}}$ ) by  $\epsilon_1(t|\mathbb{M}_{\{1\}})$  ( $\epsilon_1(t|\mathbb{M}_{\{12\}})$ ) and the residual variance by  $\sigma_1^2(t|\mathbb{M}_{\{1\}})$  ( $\sigma_1^2(t|\mathbb{M}_{\{12\}})$ ). Using this notation,  $x_2$  is *Granger causal* for  $x_1$  if the past ( $x_2(t-u)|u \in \mathbb{N}$ ) improve the prediction, i.e. the variances of the respective prediction errors satisfy [63]

$$\sigma_1^2(t|\mathbb{M}_{\{12\}}) < \sigma_1^2(t|\mathbb{M}_{\{1\}}). \quad (2.5.11)$$

If equality holds,  $x_2$  is said to be *Granger noncausal* for  $x_1$ . This is equivalent to [64]

$$A_{12}(k) = 0 \quad \forall k = 1, \dots, \infty. \quad (2.5.12)$$

In this way, Granger (non-)causality is defined as asymmetric measure for dependence that can be derived from the AR( $\infty$ )-representation of  $(\mathbf{x}(t))$ .

### 2.5.5 Conditional Granger Causality

Granger (non-)causality is a bivariate approach that only takes two univariate subprocesses into account. Extending this approach to  $r$  vector valued processes leads to the *conditional Granger causality* [63].

Let  $(\mathbf{x}(t))$  be an  $r$  vector valued  $\text{AR}(\infty)$ -process with coefficients  $A(l) \in \mathbb{R}^{r \times r}, l \in \mathbb{N}$ . Denote all subprocesses but  $(x_j(t))$  and  $(x_k(t))$  by  $(\mathbf{x}_I(t))$  with index set  $I = \{1, \dots, r\} \setminus \{j, k\}$ . Analogously to the bivariate case, let  $\mathbb{M}_{I \cup \{j, k\}}$  be the space spanned by  $(x_i(t-u)|u \in \mathbb{N})$  with  $i \in I \cup \{j, k\}$  and  $\mathbb{M}_{I \cup \{j\}}$  be the space spanned by  $(x_i(t-u)|u \in \mathbb{N})$  with  $i \in I \cup \{j\}$ . The prediction error  $\epsilon_j(t|\mathbb{M}_{I \cup \{j, k\}})$  ( $\epsilon_j(t|\mathbb{M}_{I \cup \{j\}})$ ) resulting from the orthogonal projection of the space spanned by  $x_j(t)$  on  $\mathbb{M}_{I \cup \{j, k\}}$  ( $\mathbb{M}_{I \cup \{j\}}$ ) has variance  $\sigma_j^2(t|\mathbb{M}_{I \cup \{j, k\}})$  ( $\sigma_j^2(t|\mathbb{M}_{I \cup \{j\}})$ ). With this,  $x_k$  is *conditionally Granger causal* for  $x_j$  given  $x_I$  if

$$\sigma_j^2(t|\mathbb{M}_{I \cup \{j, k\}}) < \sigma_j^2(t|\mathbb{M}_{I \cup \{j\}}). \quad (2.5.13)$$

Equality of the variances defines *conditional Granger non-causality* of  $x_k$  for  $x_j$  given  $x_I$ . This is equivalent to [64]

$$A_{jk}(l) = 0 \quad \forall l = 1, \dots, \infty. \quad (2.5.14)$$

In this way, conditional Granger (non-)causality is an asymmetric measure for direct dependence that can be derived from the  $\text{AR}(\infty)$ -representation of  $(\mathbf{x}(t))$ .

### 2.5.6 Static Canonical Correlation Analysis

For the analysis of time static dependence between two multivariate time series, Hotelling introduced the concept of *static canonical correlation analysis* in [65].

Take an  $(r+s)$  vector valued  $\text{AR}(\infty)$ -process  $(\mathbf{x}(t))$  of the form

$$\mathbf{x}(t) = \begin{pmatrix} \mathbf{y}(t) \\ \mathbf{z}(t) \end{pmatrix} \in \mathbb{R}^{(r+s) \times 1} \quad (2.5.15)$$

with  $(\mathbf{y}(t))$  and  $(\mathbf{z}(t))$  being  $r$ - and  $s$ -vector valued subprocesses. For better readability, the time index will be skipped:  $\mathbf{x} := \mathbf{x}(t)$ ,  $\mathbf{y} := \mathbf{y}(t)$ , and  $\mathbf{z} := \mathbf{z}(t)$ . The  $((r+s) \times (r+s))$  covariance matrix of  $\mathbf{x}$  will be denoted by

$$\gamma_{xx} = \begin{pmatrix} \gamma_{yy} & \gamma_{yz} \\ \gamma_{zy} & \gamma_{zz} \end{pmatrix} \quad (2.5.16)$$

where  $\gamma_{yy} = \mathbb{E}[yy^\top]$ ,  $\gamma_{zz} = \mathbb{E}[zz^\top]$ , and  $\gamma_{yz} = \gamma_{zy}^\top = \mathbb{E}[yz^\top]$ . Consider the problem of determining matrices  $D \in \mathbb{R}^{q \times r}$  and  $E \in \mathbb{R}^{q \times s}$ ,  $q = \min(r, s)$  such that

$$\mathbb{E}[(Ez - Dy)^\top(Ez - Dy)] \longrightarrow \min \quad (2.5.17)$$

with the normalization constraints  $E\gamma_{zz}E^\top = I$  and  $D\gamma_{yy}D^\top = I$ . The  $D$  and  $E$  satisfying (2.5.17) are

$$D = \begin{pmatrix} U_1^\top \\ \vdots \\ U_q^\top \end{pmatrix} \gamma_{yy}^{-\frac{1}{2}}, E = \begin{pmatrix} V_1^\top \\ \vdots \\ V_q^\top \end{pmatrix} \gamma_{zz}^{-\frac{1}{2}} \quad (2.5.18)$$

where  $U_i$  and  $V_i$  denote the respective  $i^{\text{th}}$  – according to size of the corresponding eigenvalue – eigenvector of (cf. [60])

$$\gamma_{yy}^{-\frac{1}{2}} \gamma_{yz} \gamma_{zz}^{-1} \gamma_{zy} \gamma_{yy}^{-\frac{1}{2}} \text{ and } \gamma_{zz}^{-\frac{1}{2}} \gamma_{zy} \gamma_{yy}^{-1} \gamma_{yz} \gamma_{zz}^{-\frac{1}{2}}. \quad (2.5.19)$$

By setting

$$\begin{aligned} a_i &= \gamma_{yy}^{-\frac{1}{2}} U_i \\ b_i &= \gamma_{zz}^{-\frac{1}{2}} V_i \end{aligned} \quad (2.5.20)$$

the  $i^{\text{th}}$  *static canonical correlation coefficient*  $\rho_i$  is defined as correlation coefficient between  $a_i^\top y$  and  $b_i^\top z$

$$\rho_i = \frac{a_i^\top \gamma_{yz} b_i}{((a_i^\top \gamma_{yy} a_i)(b_i^\top \gamma_{zz} b_i))^{\frac{1}{2}}} \quad (2.5.21)$$

with  $\rho_i = 0$  for  $i > q$ . Here,  $\rho_1^2 \geq \dots \geq \rho_q^2$  are the  $q$  greatest eigenvalues of both terms in (2.5.19) and correspond to the eigenvectors  $U_i$  and  $V_i$  [60]. The Euklidian norm of the  $q$  greatest canonical correlation coefficients  $\rho_i$  was used as symmetric measure for time static linear dependence between  $\mathbf{y}(t)$  and  $\mathbf{z}(t)$  as defined in (2.5.15).

## 2.5.7 Dynamic Canonical Correlation Analysis

For the investigation of time dynamic dependence between two multivariate time series, Brillinger introduced the concept of *dynamic canonical correlation analysis* in [60].

Consider the  $(r+s)$ -vector valued AR( $\infty$ )-process  $(\mathbf{x}(t))$  with  $r$ - and  $s$ -vector valued subprocesses  $(\mathbf{y}(t))$  and  $(\mathbf{z}(t))$ . The multivariate spectral density of  $(\mathbf{x}(t))$  can be written as

$$\mathbf{f}_{xx}(\lambda) = \begin{pmatrix} \mathbf{f}_{yy}(\lambda) & \mathbf{f}_{yz}(\lambda) \\ \mathbf{f}_{zy}(\lambda) & \mathbf{f}_{zz}(\lambda) \end{pmatrix} \in \mathbb{C}^{(r+s) \times (r+s)} \quad (2.5.22)$$

where  $\mathbf{f}_{yy}(\lambda)$  and  $\mathbf{f}_{zz}(\lambda)$  are the respective auto-spectral densities and  $\mathbf{f}_{yz}(\lambda) = \mathbf{f}_{zy}(\lambda)^*$  is the cross-spectral density of  $(\mathbf{y}(t))$  and  $(\mathbf{z}(t))$  at frequency  $\lambda$ . Now,



consider the problem of determining a series of  $(q \times r)$  matrices  $(b(u))$  and a series of  $(q \times s)$  matrices  $(c(u))$ ,  $u \in \mathbb{Z}$ ,  $q = \min(r, s)$  that minimize

$$\mathbb{E} \left[ \left( \sum_u c(t-u)z - \sum_u b(t-u)y \right)^\top \left( \sum_u c(t-u)z - \sum_u b(t-u)y \right) \right]. \quad (2.5.23)$$

Brillinger shows that Equation (2.5.23) is minimized by

$$\begin{aligned} b(u) &= \frac{1}{2\pi} \int_{-\pi}^{\pi} B(\lambda) e^{iu\lambda} d\lambda \\ c(u) &= \frac{1}{2\pi} \int_{-\pi}^{\pi} C(\lambda) e^{iu\lambda} d\lambda \end{aligned} \quad (2.5.24)$$

where  $B(\lambda)$  and  $C(\lambda)$  are given as

$$B(\lambda) = \begin{pmatrix} U_1^*(\lambda) \\ \vdots \\ U_q^*(\lambda) \end{pmatrix} \mathbf{f}_{yy}^{-\frac{1}{2}}(\lambda), C(\lambda) = \begin{pmatrix} V_1^*(\lambda) \\ \vdots \\ V_q^*(\lambda) \end{pmatrix} \mathbf{f}_{zz}^{-\frac{1}{2}}(\lambda). \quad (2.5.25)$$

Here,  $U_i(\lambda)$  and  $V_i(\lambda)$  denote the respective  $i^{\text{th}}$  eigenvector of

$$\mathbf{f}_{yy}^{-\frac{1}{2}}(\lambda) \mathbf{f}_{yz}(\lambda) \mathbf{f}_{zz}^{-1}(\lambda) \mathbf{f}_{zy}(\lambda) \mathbf{f}_{yy}^{-\frac{1}{2}}(\lambda) \quad (2.5.26)$$

and

$$\mathbf{f}_{zz}^{-\frac{1}{2}}(\lambda) \mathbf{f}_{zy}(\lambda) \mathbf{f}_{yy}^{-1}(\lambda) \mathbf{f}_{yz}(\lambda) \mathbf{f}_{zz}^{-\frac{1}{2}}(\lambda). \quad (2.5.27)$$

The root of the corresponding  $i^{\text{th}}$  eigenvalue  $\rho_i(\lambda)$  is then called the  $i^{\text{th}}$  *dynamic canonical correlation coefficient*<sup>6</sup>. The Euklidean norm of  $(\rho_1(\lambda), \dots, \rho_q(\lambda))$  was used as a time dynamic (frequency-wise) symmetric measure for linear dependence between  $\mathbf{y}(t)$  and  $\mathbf{z}(t)$ .

### 2.5.8 Static Principal Component Analysis

For analyzing time static dependences within a multivariate time series, Pearson and Hotelling introduced – independently from each other – the *static principal component analysis* (PCA) in [66] and [67].

Let  $(\mathbf{x}(t))$  be an  $r$ -vector valued  $\text{AR}(\infty)$ -process with covariance matrix  $\gamma$ . The time index will be skipped here:  $\mathbf{x} := \mathbf{x}(t)$ . Consider the problem of finding matrices  $B \in \mathbb{R}^{q \times r}$  and  $C \in \mathbb{R}^{r \times q}$  that minimize

$$\mathbb{E} [(\mathbf{x} - CB\mathbf{x})^\top (\mathbf{x} - CB\mathbf{x})] \quad (2.5.28)$$

with the constraint

$$B_i C_i = 1 \quad (2.5.29)$$

<sup>6</sup>Sometimes also referred to as  $i^{\text{th}}$  *canonical coherence*.

where  $B_i$  is the  $i^{\text{th}}$  row of  $B$  and  $C_i$  is the  $i^{\text{th}}$  column of  $C$ . The  $B$  and  $C$  satisfying (2.5.28) are

$$B = \begin{pmatrix} V_1^\top \\ \vdots \\ V_q^\top \end{pmatrix}, C = (V_1, \dots, V_q) = B^\top \quad (2.5.30)$$

where  $V_i$  denotes the  $i^{\text{th}}$  eigenvector of  $\gamma$  with corresponding eigenvalue  $\mu_i$ . The  $i^{\text{th}}$  principal component (PC) of  $\mathbf{x}$  is defined as

$$\zeta_i = V_i^\top \mathbf{x} \quad (2.5.31)$$

where the  $\zeta_i$  satisfy

$$\mathbb{E}[\zeta_i^\top \zeta_j] = \begin{cases} 0, & i \neq j \\ \mu_i, & i = j. \end{cases} \quad (2.5.32)$$

Thus, the PCs represent uncorrelated linear combinations of  $\mathbf{x}$ ;  $\mu_i$  is the variance of the  $i^{\text{th}}$  PC. The sum of all  $\mu_i$  equals the variance of  $x$  and, thus, the term

$$p_i = \frac{\mu_i}{\sum_j \mu_j} \quad (2.5.33)$$

gives the percentage of variance that is described by  $\zeta_i$ . When the subprocesses of  $\mathbf{x}$  show a rather homogeneous behavior, only few PCs suffice to describe most of the process information. Here,  $p_1$  was used as measure for time static homogeneity.

### 2.5.9 Dynamic Principal Component Analysis

For the investigation of time dynamic dependences within a multivariate time series, Brillinger introduced the *dynamic PCA* in [60].

Let  $(\mathbf{x}(t))$  be an  $r$ -vector valued AR( $\infty$ )-process with multivariate spectral density  $\mathbf{f}$ . Consider the problem of finding series of  $(q \times r)$  matrices  $(b(u))$  and  $(r \times q)$  matrices  $(c(u))$ ,  $u \in \mathbb{Z}$  that minimize

$$\mathbb{E} \left[ \left( \mathbf{x}(t) - \sum_u c(t-u)\zeta(u) \right)^\top \left( \mathbf{x}(t) - \sum_u c(t-u)\zeta(u) \right) \right] \quad (2.5.34)$$

where

$$\zeta(t) = \sum_u b(t-u)\mathbf{x}(u). \quad (2.5.35)$$

The term (2.5.34) is minimal for

$$b(u) = \frac{1}{2\pi} \int_{-\pi}^{\pi} B(\lambda) e^{iu\lambda} d\lambda \quad (2.5.36)$$

$$c(u) = \frac{1}{2\pi} \int_{-\pi}^{\pi} C(\lambda) e^{iu\lambda} d\lambda \quad (2.5.37)$$

where

$$B(\lambda) = \begin{pmatrix} V_1^*(\lambda) \\ \vdots \\ V_q^*(\lambda) \end{pmatrix}, C(\lambda) = (V_1(\lambda), \dots, V_q(\lambda)) = B^*. \quad (2.5.38)$$

where  $V_i(\lambda)$  is the  $i^{\text{th}}$  eigenvector of  $f(\lambda)$  with corresponding eigenvalue  $\mu_i(\lambda)$ . The  $i^{\text{th}}$  component of  $\zeta(t)$  (cf. Equation (2.5.35)) has the representation

$$\zeta_i(t) = \int_{-\pi}^{\pi} V_i(\lambda)^* e^{i\lambda t} d\mathbf{z}(\lambda) \quad (2.5.39)$$

where  $(\mathbf{z}(\lambda)|\lambda \in [-\pi, \pi])$  is the corresponding process of orthogonal increments.  $\zeta_i(t)$  is called the  $i^{\text{th}}$  PC series of  $\mathbf{x}(t)$  and has multivariate spectral density

$$\begin{pmatrix} \mu_1(\lambda) & & 0 \\ & \ddots & \\ 0 & & \mu_q(\lambda) \end{pmatrix} \text{ for } \lambda \in [-\pi, \pi]. \quad (2.5.40)$$

Analogously to the time static case, the term

$$p_i(\lambda) = \frac{\mu_i(\lambda)}{\sum_j \mu_j(\lambda)} \quad (2.5.41)$$

gives the percentage of variance that is described by the  $i^{\text{th}}$  PC at frequency  $\lambda$ . Here,  $p_1$  was used as measure for time dynamic homogeneity.

## 2.6 Estimating the First and Second Moments

Whereas the previous Sections 2.3, 2.4 and 2.5 were concerned with structure theoretic considerations, the focus of the following Sections 2.6, 2.7 and 2.8 will be on statistical considerations. The data will be assumed to be a realization of an  $\text{AR}(\infty)$ -process that satisfies the conditions listed in Section 2.5.1. At first, estimates for the mean  $\boldsymbol{\mu}$  and autocovariance function  $\boldsymbol{\gamma}$  will be considered.

### 2.6.1 Mean

Consider a scalar process  $(x(t))$  with realization  $x(0), \dots, x(T-1)$ . The mean of the process was estimated by the sample mean

$$\bar{x}(T) = \frac{1}{T} \sum_{t=0}^{T-1} x(t). \quad (2.6.1)$$

$\bar{x}(T)$  is an *unbiased* estimate since

$$\mathbb{E}[\bar{x}(T)] = \mathbb{E}\left[\left(\frac{1}{T} \sum_{t=0}^{T-1} x(t)\right)\right] = \frac{1}{T} \sum_{t=0}^{T-1} \mathbb{E}[x(t)] = 0. \quad (2.6.2)$$

Note that, for an  $r$ -vector valued process, the estimation is done component-wise; thus the employment of the scalar case is reasonable.

Under the conditions of this work,  $\bar{x}(T)$  satisfies both (cf. e.g. [56])

$$\lim_{T \rightarrow \infty} \mathbb{E} \left[ |(\bar{x}(T))|^2 \right] = 0 \quad (2.6.3)$$

$$\lim_{T \rightarrow \infty} T \mathbb{E} \left[ |(\bar{x}(T))|^2 \right] = \sum_{u=-\infty}^{\infty} \gamma(u). \quad (2.6.4)$$

The first part states that the estimate  $\bar{x}(T)$  converges in mean square to  $\mu = 0$  and is thus *weakly consistent*. From the second part, the spectral density holds

$$f(0) = \frac{1}{2\pi} \sum_{u=-\infty}^{\infty} \gamma(u) = \frac{1}{2\pi} \lim_{T \rightarrow \infty} T \mathbb{E} \left[ |(\bar{x}(T))|^2 \right]. \quad (2.6.5)$$

Thus,  $f(0)$  is a measure of the quality of the estimate  $\bar{x}(T)$ .

## 2.6.2 Autocovariance Function

Consider the  $r$ -vector valued process  $(\mathbf{x}(t))$  with realization  $\mathbf{x}(0), \dots, \mathbf{x}(T-1)$ . In this study, the autocovariance function  $\gamma$  was estimated by the sample covariance

$$\hat{\gamma}(u, T) = \begin{cases} \frac{1}{T} \sum_{t=0}^{T-u-1} (\mathbf{x}(t+u) - \bar{\mathbf{x}}(T)) (\mathbf{x}(t) - \bar{\mathbf{x}}(T))^{\top} & \text{for } T > u \geq 0 \\ \hat{\gamma}^{\top}(-u, T) & \text{for } -T < u < 0 \\ 0 & \text{else} \end{cases} \quad (2.6.6)$$

where  $\bar{\mathbf{x}}(T)$  is the vector of sample means of univariate subprocesses.  $\hat{\gamma}$  is a biased estimate for  $\gamma$ . However, since  $\bar{\mathbf{x}}(T)$  converges component-wise in mean square to 0,  $\hat{\gamma}$  is *asymptotically unbiased*

$$\lim_{T \rightarrow \infty} \mathbb{E} [\hat{\gamma}(u, T)] = \gamma(u). \quad (2.6.7)$$

Consistency of  $\hat{\gamma}(u, T)$  may be investigated by introducing an artificial stationary process  $(\mathbf{y}(t))$  where

$$\mathbf{y}(t) = \mathbf{x}(t+s)\mathbf{x}(t)^{\top}. \quad (2.6.8)$$

If

$$\sum_{u=-\infty}^{\infty} |\mathbb{E} [(\mathbf{y}(u) - \mathbb{E} [\mathbf{y}(u)]) (\mathbf{y}(0) - \mathbb{E} [\mathbf{y}(0)])]| < \infty \quad (2.6.9)$$

holds, then  $\lim_{T \rightarrow \infty} \hat{\gamma}(u, T) = \gamma(u)$  a.s. Thus,  $\hat{\gamma}(u, T)$  is a *consistent* estimate provided that the fourth moments of  $(\mathbf{x}(t))$  exist and are stationary.

Additionally, the matrix with the sample covariances as block entries

$$\hat{\mathbf{\Gamma}}(T) = \begin{pmatrix} \hat{\gamma}(0, T) & \cdots & \hat{\gamma}(-T+1, T) \\ \vdots & \ddots & \vdots \\ \hat{\gamma}(T-1, T) & \cdots & \hat{\gamma}(0, T) \end{pmatrix} \text{ for } T \geq 1 \quad (2.6.10)$$

is non-negative definite<sup>7</sup> [56]. Note that, for large  $u$ , the sum in (2.6.6) has only few summands. In this case,  $\hat{\gamma}(u, T)$  does not necessarily have full rank and is, for large  $u$ , not a proper estimate for  $\gamma(u)$ .

## 2.7 Estimating the Multivariate Spectral Density

This section will be concerned with non-parametric estimates for the multivariate spectral density  $\mathbf{f}$ . Several types of estimates, both their finite-sample and asymptotic properties, and their implementation will be considered. An estimate  $\hat{\mathbf{f}}$  qualifies as "good" if it is – at least asymptotically – unbiased and consistent, and if it preserves the properties of being Hermitian, positive semi-definite, and of full rank. The last property is important for the calculation of the partial coherence and the dynamic canonical correlation analysis via the inverse spectral density (cf. Sections 2.5.3 and 2.5.7). For literature on spectral estimation, the reader is referred to [60], [56], and [68], where the latter offers an approach that is mathematically less precise but rather descriptive.

### 2.7.1 Periodogram

At this point, recall the definition of the multivariate spectral density from Section 2.4.3

$$\mathbf{f}(\lambda) = \frac{1}{2\pi} \sum_{u=-\infty}^{\infty} \boldsymbol{\gamma}(u) e^{-i\lambda u} \text{ for } \lambda \in [-\pi, \pi]. \quad (2.7.1)$$

As a first estimate, the *periodogram* – originally introduced by Schuster in 1898 (cf. [69]) – will be considered. Let  $(\mathbf{x}(t))$  be an  $r$ -vector valued AR( $\infty$ )-process with a realization  $\mathbf{x}(0), \dots, \mathbf{x}(T-1)$ . For  $\lambda \not\equiv 0 \pmod{2\pi}$ , the periodogram is defined as

$$\mathbf{I}(\lambda, T) = \frac{1}{2\pi T} \left( \sum_{t=0}^{T-1} \mathbf{x}(t) e^{-i\lambda t} \right) \left( \sum_{t=0}^{T-1} \mathbf{x}(t) e^{-i\lambda t} \right)^*. \quad (2.7.2)$$

For  $\lambda \equiv 0 \pmod{2\pi}$ , the periodogram is given as

$$\mathbf{I}(\lambda, T) = \frac{T}{2\pi} \bar{\mathbf{x}}(T) \bar{\mathbf{x}}^T(T). \quad (2.7.3)$$

<sup>7</sup>This is not the case when the factor  $\frac{1}{T}$  in (2.6.6) is replaced by e.g.  $\frac{1}{T-s}$

For Fourier frequencies  $\lambda_j = \frac{2\pi j}{T} \not\equiv 0 \pmod{2\pi}$ , the periodogram takes the form

$$\mathbf{I}(\lambda_j, T) = \frac{1}{2\pi} \sum_{|u| < T} \hat{\gamma}(u, T) e^{-i\lambda_j u} \quad (2.7.4)$$

where  $\hat{\gamma}(u, T)$  is the estimate for the autocovariance function as defined in Equation (2.6.6). The restriction to Fourier frequencies simplifies the computation of  $\mathbf{I}(\lambda, T)$  as the vectors  $\frac{1}{\sqrt{T}} (e^{i\lambda_j 0}, \dots, e^{i\lambda_j(T-1)})^\top$  form an orthonormal basis of  $\mathbb{C}^T$ . For  $T \rightarrow \infty$ , every frequency  $\lambda$  may be approximated arbitrary close by a Fourier frequency. By comparing Equations (2.7.1) and (2.7.4), the periodogram seems to be a reasonable estimate for  $\mathbf{f}$ .

The expected value of the periodogram at Fourier frequency  $\lambda \not\equiv 0 \pmod{2\pi}$  is

$$\begin{aligned} \mathbb{E}[\mathbf{I}(\lambda, T)] &= \frac{1}{2\pi} \sum_{|u| < T} \left(1 - \frac{|u|}{T}\right) \gamma(u) e^{-i\lambda u} \\ &= \int_{-\pi}^{\pi} \mathbf{f}(\omega) g^F(\lambda - \omega, T) d\omega \end{aligned} \quad (2.7.5)$$

where

$$g^F(\omega, T) = \begin{cases} \frac{T}{2\pi} & \text{for } \omega = 0 \\ \frac{1}{2\pi T} \left| \frac{1 - e^{i\omega T}}{1 - e^{i\omega}} \right|^2 & \text{else} \end{cases} \quad (2.7.6)$$

is called *Fejér kernel* [60].  $g^F(\omega, T)$  is a symmetric and non-negative function that is zero for Fourier frequencies  $\omega = \lambda \not\equiv 0 \pmod{2\pi}$ . Furthermore, the Fejér kernel satisfies

$$\int_{-\pi}^{\pi} g^F(\omega, T) d\omega = 1. \quad (2.7.7)$$

For  $\lambda \equiv 0 \pmod{2\pi}$ , the expected value of the periodogram is

$$\mathbb{E}[\mathbf{I}(\lambda, T)] = \frac{T}{2\pi} \mathbb{E}[\bar{\mathbf{x}}(T) \bar{\mathbf{x}}^\top(T)] \quad (2.7.8)$$

and, thus, depends on the variance of the sample mean (cf. also Equation (2.6.5)).

The periodogram is an *asymptotically unbiased* estimator for the spectral density (cf. [56])

$$\lim_{T \rightarrow \infty} \mathbb{E}[\mathbf{I}(\lambda, T)] = \mathbf{f}(\lambda). \quad (2.7.9)$$

Alternatively, the asymptotic unbiasedness can be confirmed by considering the asymptotic behavior of the Fejér kernel:  $g^F(\omega, T)$ ,  $\omega \neq 0$  tends to 0 as  $T \rightarrow \infty$ . Given the additional assumption

$$\sum_{u=-\infty}^{\infty} |u| \|\gamma(u)\| < \infty, \quad (2.7.10)$$

the bias of the periodogram is of order  $O(T^{-1})$  (uniform in  $\lambda$ ) [60].

Now, let us turn to the second moments of the periodogram. Let  $\lambda_j$  and  $\lambda_k$  be Fourier frequencies, then (cf. [56])

$$\begin{aligned} \mathbb{E} [\mathbf{I}(\lambda_j, T) \mathbf{I}^*(\lambda_k, T)] &= & (2.7.11) \\ &= \begin{cases} \mathbf{f}(\lambda_j) \mathbf{f}^*(\lambda_j) + \mathbf{f}^*(\lambda_j) \mathbf{f}(\lambda_j) + O(T^{-\frac{1}{2}}) & \text{for } \lambda_j = \lambda_k \equiv 0 \pmod{2\pi} \\ \mathbf{f}(\lambda_j) \mathbf{f}^*(\lambda_j) + O(T^{-\frac{1}{2}}) & \text{for } \lambda_j = \lambda_k \not\equiv 0 \pmod{2\pi} \\ O(T^{-1}) & \text{for } \lambda_j \neq \lambda_k. \end{cases} \end{aligned}$$

Thus, the periodogram is not a consistent estimator with standard deviation of the same magnitude as the spectral density. The inconsistency arises from  $\hat{\gamma}(u, T)$  being a poor estimate for  $\gamma(u)$  when  $u$  is close to  $T$  as, in this case,  $\hat{\gamma}(u, T)$  is determined by only few summands. Additionally, the periodogram ordinates are, for Fourier frequencies  $\lambda_j \neq \lambda_k$ , asymptotically independent [56]. These properties result in the periodogram being a highly "irregular" function even when the spectral density is rather smooth [60].

### 2.7.2 Direct Spectral Estimates

Despite the non-consistency of the periodogram, it can serve as basis for the construction of consistent estimates. Due to the asymptotically uncorrelated periodogram ordinates, averaging over neighboring frequencies cf.ms to be a reasonable measure for lowering the variance of the estimate. This approach is referred to as *direct spectral estimation* [68].

Formally, a direct spectral estimate is defined by

$$\hat{\mathbf{f}}(\lambda, T) = \sum_{u=-m(T)}^{m(T)} w(u, T) \mathbf{I}(\lambda - \frac{2\pi u}{T}, T) \quad (2.7.12)$$

where  $m(T)$  is an integer defining the number of periodogram values used for smoothing and  $w(u, T)$  are filter weights satisfying

$$w(u, T) = w(-u, T) \quad (2.7.13)$$

$$w(u, T) \geq 0. \quad (2.7.14)$$

By the non-negativity of  $w(u, T)$ ,  $\hat{\mathbf{f}}(\lambda, T)$  is positive semi-definite. For the computation of the marginal values of  $\hat{\mathbf{f}}(\lambda, T)$ , the periodogram is periodically extended outside the interval  $(-\pi, \pi]$ .

The expected value of  $\hat{\mathbf{f}}(\lambda, T)$  is

$$\mathbb{E} [\hat{\mathbf{f}}(\lambda, T)] = \int_{-\pi}^{\pi} \mathbf{f}(\omega) g(\lambda - \omega, T) d\omega \quad (2.7.15)$$

where

$$g(\omega, T) = \sum_{u=-m(T)}^{m(T)} w(u, T) g^F\left(\omega - \frac{2\pi u}{T}, T\right) \quad (2.7.16)$$

with  $g^F(\omega)$  being the Fejér kernel (cf. Equation (2.7.6)) [56]. The functions  $g(\omega, T)$  are called *spectral windows*<sup>8</sup>.

Using Equation (2.7.12), the expected value of  $\hat{f}(\lambda, T)$  has the representation

$$\mathbb{E} \left[ \hat{f}(\lambda, T) \right] = \sum_{u=-m(T)}^{m(T)} w(u, T) \mathbb{E} \left[ \mathbf{I}\left(\lambda - \frac{2\pi u}{T}, T\right) \right] \quad (2.7.17)$$

and, as the periodogram is asymptotically unbiased,

$$\lim_{T \rightarrow \infty} \mathbb{E} \left[ \hat{f}(\lambda, T) \right] = \sum_{u=-m(T)}^{m(T)} w(u, T) \mathbf{f}(\lambda) \quad (2.7.18)$$

holds. By imposing the conditions

$$\sum_{u=-m(T)}^{m(T)} w(u, T) = 1 \quad (2.7.19)$$

$$\lim_{T \rightarrow \infty} \frac{m(T)}{T} = 0, \quad (2.7.20)$$

$\hat{f}(\lambda, T)$  is an asymptotically unbiased estimate for the spectral density.

The second moments of  $\hat{f}(\lambda, T)$  depend on the filter weights  $w(u, T)$  as well. Let  $\lambda_j$  and  $\lambda_k$  be Fourier frequencies, then

$$\begin{aligned} \lim_{T \rightarrow \infty} \frac{\mathbb{E} \left[ \hat{f}(\lambda_j, T) \hat{f}(\lambda_k, T)^* \right]}{\sum_{u=-m(T)}^{m(T)} w^2(u, T)} &= \\ &= \begin{cases} \mathbf{f}(\lambda_j) \mathbf{f}^*(\lambda_j) + \mathbf{f}^*(\lambda_j) \mathbf{f}(\lambda_j) & \text{for } \lambda_j = \lambda_k \equiv 0 \pmod{2\pi} \\ \mathbf{f}(\lambda_j) \mathbf{f}^*(\lambda_j) & \text{for } \lambda_j = \lambda_k \not\equiv 0 \pmod{2\pi} \\ 0 & \text{for } \lambda_j \neq \lambda_k \end{cases} \quad (2.7.21) \end{aligned}$$

holds. Thus, under the condition

$$\sum_{u=-m(T)}^{m(T)} w^2(u, T) \rightarrow 0 \quad \text{for } T, m(T) \rightarrow \infty \quad (2.7.22)$$

the smoothed periodogram is a consistent estimate for the spectral density [56].

<sup>8</sup>Note, that the Fejér kernel is a spectral window itself.



### 2.7.3 Indirect Spectral Estimates

The one-to-one relation between spectral density and autocovariance function suggests that a tapering of the autocovariance may lead to a consistent estimate as well. Hereby,  $\hat{\gamma}(u, T)$  is down-weighted for large  $u$  in order to reduce the variance of the estimate. This approach is called *indirect spectral estimation* [68].

Formally, an indirect spectral estimate is defined as

$$\tilde{\mathbf{f}}(\lambda, T) = \frac{1}{2\pi} \sum_{u=-n(T)}^{n(T)} l(u, T) \hat{\gamma}(u, T) e^{-i\lambda u} \quad (2.7.23)$$

where  $l(u, T)$  is a weight-function called *lagwindow* that satisfies

$$l(u, T) = l(-u, T) \quad (2.7.24)$$

$$l(u, T) \geq 0 \text{ for } |u| < n(T) \leq T \quad (2.7.25)$$

$$l(u, T) = 0 \text{ for } |u| \geq n(T). \quad (2.7.26)$$

The parameter  $n(T)$  is called *truncation point* and defines the number of lags included in the spectral estimate. Alternatively,  $\tilde{\mathbf{f}}(\lambda, T)$  may be written as

$$\tilde{\mathbf{f}}(\lambda, T) = \int_{-\pi}^{\pi} \mathbf{I}(\lambda - \omega, T) L(\omega, T) d\omega \quad (2.7.27)$$

with

$$L(\omega, T) = \frac{1}{2\pi} \sum_{|u| < T} l(u, T) e^{-i\omega u}. \quad (2.7.28)$$

The expected value of the estimate is

$$\mathbb{E} [\tilde{\mathbf{f}}(\lambda, T)] = \int_{-\pi}^{\pi} \mathbf{f}(\omega) g(\lambda - \omega, T) d\omega + O\left(\frac{\ln T}{T}\right) \quad (2.7.29)$$

with spectral window

$$g(\lambda, T) = \int_{-\pi}^{\pi} g^F(\omega, T) L(\lambda - \omega, T) d\omega \quad (2.7.30)$$

where  $g^F(\omega)$  is the *Fejér kernel* [68].

With  $T$  tending towards  $\infty$ ,

$$\mathbb{E} [\tilde{\mathbf{f}}(\lambda, T)] \rightarrow \mathbf{f}(\lambda) \int_{-\pi}^{\pi} L(\omega, T) d\omega. \quad (2.7.31)$$

Thus, by imposing the condition

$$\int_{-\pi}^{\pi} L(\omega, T) d\omega = 1, \quad (2.7.32)$$

or, equivalently,

$$l(0, T) = 1 \quad (2.7.33)$$

the indirect estimate is asymptotically unbiased.

The second moments of  $\tilde{\mathbf{f}}(\lambda, T)$  depend on  $L(\omega, T)$ . Let  $\lambda_j$  and  $\lambda_k$  be Fourier frequencies, then

$$\begin{aligned} & \lim_{T \rightarrow \infty} \frac{\mathbb{E} \left[ \tilde{\mathbf{f}}(\lambda_j, T) \tilde{\mathbf{f}}(\lambda_k, T)^* \right]}{\int_{-\pi}^{\pi} L^2(\omega, T) d\omega} = \\ & = \begin{cases} \mathbf{f}(\lambda_j) \mathbf{f}^*(\lambda_j) + \mathbf{f}^*(\lambda_j) \mathbf{f}(\lambda_j) & \text{for } \lambda_j = \lambda_k \equiv 0 \pmod{2\pi} \\ \mathbf{f}(\lambda_j) \mathbf{f}^*(\lambda_j) & \text{for } \lambda_j = \lambda_k \not\equiv 0 \pmod{2\pi} \\ 0 & \text{for } \lambda_j \neq \lambda_k \end{cases} \quad (2.7.34) \end{aligned}$$

holds. By imposing the condition

$$\int_{-\pi}^{\pi} L^2(\omega, T) d\omega \rightarrow 0 \quad \text{for } T \rightarrow \infty, \quad (2.7.35)$$

the indirect spectral estimate is a consistent estimate for the spectral density.

## 2.7.4 Implementation

The focus of this section will be on the implementation of the spectral estimates on real (EEG) data. Several issues of spectral estimation procedures will be addressed.

### Resolution (Narrow Band Bias)

From Equations (2.7.15) and (2.7.29), two sources for the finite sample bias of the presented estimation procedures become apparent. The first source affects the *frequency resolution* of the estimates and is referred to as *narrow band bias*. For the understanding of this type of bias, consider the shape of spectral windows as defined in Equations (2.7.16) and (2.7.30). These spectral windows have a main lobe and several declining side lobes. The width of the main lobe is measured by the respective bandwidth

$$B_d = \frac{1}{T \sum_u w^2(u, T)} \quad (2.7.36)$$

for direct spectral estimates, and

$$B_i = \frac{1}{\int_{-\pi}^{\pi} L^2(\omega, T) d\omega} \quad (2.7.37)$$

for indirect spectral estimates. Two peaks in the spectral density with frequency-distance smaller than  $B$  cannot be distinguished from each other. For this reason,

a small bandwidth would be desirable; however, by decreasing the bandwidth, the variance of the estimate increases (cf. Equations (2.7.21) and (2.7.34)). This issue is called the *uncertainty relation* of spectral estimation.

### Leakage (Broad Band Bias)

The second source of finite sample bias originates from the sidelobes of the spectral windows. Peaks in the spectral density coinciding with a sidelobe of the spectral window distort the estimate on other frequencies and, thus, increase the bias of the estimate. This phenomenon is known as *leakage effect*. The origin of the leakage effect is the finite length of the sample data. A finite realization can be treated as the element-wise multiplication of an infinite realization with a rectangular data window

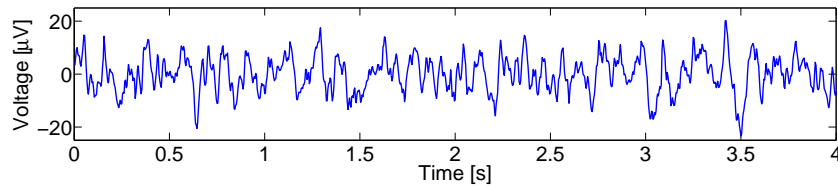
$$h(t) = \begin{cases} 1 & \text{for } t = 0, \dots, T - 1 \\ 0 & \text{else} \end{cases} \quad (2.7.38)$$

By choosing another data window with lower sidelobes of the corresponding spectral window, the leakage effect can be reduced. This procedure is referred to as *data tapering* and was originally described by Tukey in [70]. Examples for taper functions will be provided in Section 2.7.4.

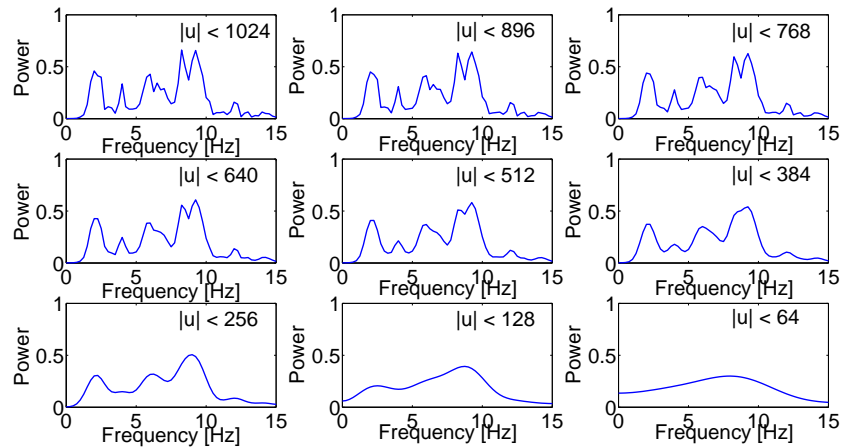
Another way to reduce the leakage is to *prewhiten* the data. Thereby, a linear transformation is applied on the data with the aim of simulating a realization of a white noise process. In this way, the spectral density has no significant peaks and the leakage effect can be reduced. The estimated spectral density is then *recolored*, i.e. retransformed to correspond to the original data. This approach is preferable in (semi-) parametric estimation procedures and will not be considered any further in this work.

### Window Closing

For both direct and indirect spectral estimation, the desired smoothness of the estimate has to be defined. This is done by choosing  $m(T)$  (cf. Section 2.7.2) or  $n(T)$  (cf. Section 2.7.3). As the chosen values have an impact on the bandwidth – and therefore on the narrow band bias – and on the second moments of the estimates, a proper choice is crucial for the quality of the estimation. A common procedure is *window closing*: different values for the respective  $m(T)$  or  $n(T)$  are applied in order to study the behavior of the estimate. Values causing a high bandwidth provide information about the basic trend of the estimate, whereas those causing a low bandwidth are used for the identification and localization of spectral peaks. Figure 2.7.1 illustrates the window closing for a 4 second (1024 sample points) EEG segment in resting state on channel CZ. The EEG signal is shown in Figure 2.7.1a. Indirect spectral estimation was performed with truncation points 1024, 896, 768, 640, 512, 384, 256, 128 and 64. The corresponding spectral estimates are shown in Figure 2.7.1b.



(a) EEG signal, 4 sec., resting state, Channel CZ



(b) Indirect spectral estimates with different truncation points

Figure 2.7.1: Window closing

### Window/Taper Functions

There is a broad range of functions that are designed for data tapering to reduce the leakage effect of spectral estimation and as window functions for direct and indirect spectral estimation to construct consistent estimates. Although the same functions may be applied for both tapering and windowing, the functions have to meet different requirements for the respective application. In case of tapering, a small bandwidth and low, rapidly decreasing sidelobes are desirable. For windowing, on the other hand, additional restrictions are required in order to design consistent estimates and to preserve properties such as the positive semi-definiteness of the estimate. Here, several examples for these functions are provided. For the sake of readability, the functions will be referred to as *window* functions although they are used for tapering as well. A selection of commonly used window functions can be found in the *Signal Processing Toolbox* in MATLAB. The MATLAB functions `wintool` and `wvtool` provide means for the design, analysis and visualization of window functions both in time and frequency domain.

Applying no window function is equivalent to applying the *rectangular window*  $h(t)$  as defined in Equation (2.7.38). As pointed out earlier, this window is not ideal in terms of both bandwidth and height of sidelobes of the corresponding

spectral window. Figure 2.7.2a shows the rectangular window and Figure 2.7.2b shows the corresponding spectral window for  $T = 1024$ . The MATLAB function used for generating this window is `rectwin`.

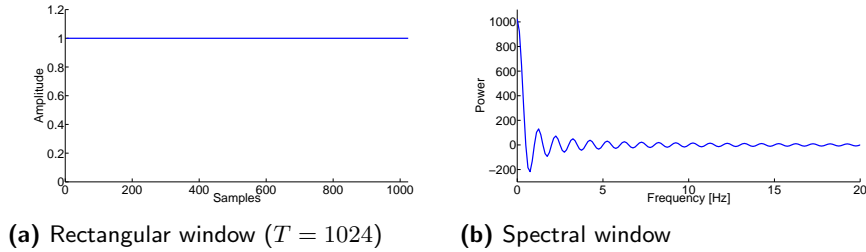


**Figure 2.7.2:** Rectangular window and corresponding spectral window

For  $T$  odd, the *triangular window* is defined as

$$h(t) = \begin{cases} \frac{2t}{T+1} & \text{for } 0 \leq t \leq \frac{T-1}{2} \\ 2 - \frac{2t}{T+1} & \text{for } \frac{T+1}{2} \leq t \leq T-1 \end{cases} \quad (2.7.39)$$

and, for  $T$  even

$$h(t) = \begin{cases} \frac{2t+1}{T} & \text{for } 0 \leq t \leq \frac{T}{2} - 1 \\ 2 - \frac{2t+1}{T} & \text{for } \frac{T}{2} \leq t \leq T-1. \end{cases} \quad (2.7.40)$$

Figures 2.7.3a and 2.7.3b show the triangular window and the corresponding spectral window for  $T = 1024$ . The MATLAB function used for generating this window is `triang`.

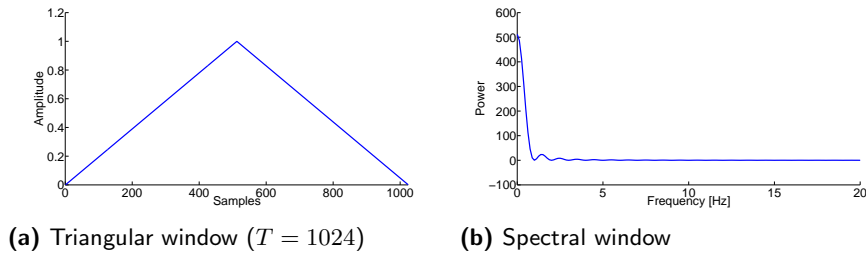


**Figure 2.7.3:** Triangular window and corresponding spectral window

A widely used window function is the *Hann window* that is named after the Austrian meteorologist J. von Hann (cf. [71]). It is defined as

$$h(t) = \frac{1}{2} - \frac{1}{2} \cos\left(\frac{2\pi t}{T-1}\right). \quad (2.7.41)$$

The Hann window is designed to have strongly decreasing sidelobes. Figures 2.7.4a and 2.7.4b show the Hann window and the corresponding spectral window for  $T = 1024$ . The MATLAB function used for generating this window is `hann`.

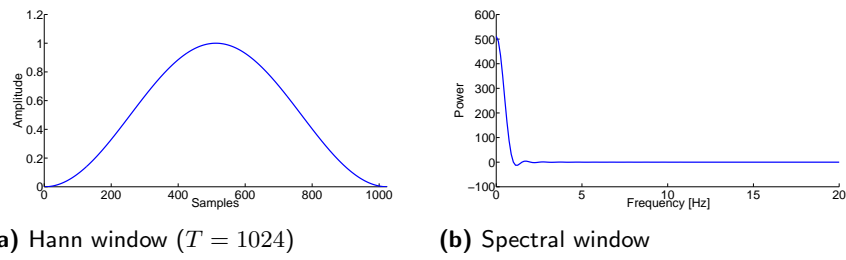


**Figure 2.7.4:** Hann window and corresponding spectral window

In order to minimize the sidelobes closest to the main lobe, the US mathematician R. W. Hamming proposed the *Hamming window* (cf. [71])

$$h(t) = 0.54 - 0.46 \cos\left(\frac{2\pi t}{T-1}\right). \quad (2.7.42)$$

It is similar to the Hann window but with slightly modified parameters 0.54 and 0.46 instead of two times 0.5. This modification leads to lower first sidelobes, but the decrease of height is slower than for the Hann window. Figures 2.7.5a and 2.7.5b show the Hamming window and the corresponding spectral window for  $T = 1024$ . The MATLAB function used for generating this window is `hamming`.

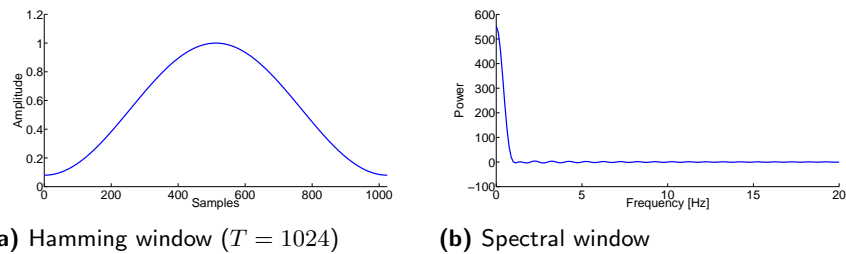


**Figure 2.7.5:** Hamming window and corresponding spectral window

Finally, the *Parzen window* – named after the US statistician E. Parzen – is defined as (cf. [72])

$$h(t) = \begin{cases} 1 - 6\left|\frac{2t}{T}\right|^2 + 6\left|\frac{2t}{T}\right|^3 & 0 \leq |t| \leq \frac{T}{4} \\ 2\left(1 - \left|\frac{2t}{T}\right|\right)^3 & \frac{T}{4} \leq |t| \leq \frac{T}{2}. \end{cases} \quad (2.7.43)$$

Although there are better window functions in terms of bandwidth and leakage reduction, the Parzen window preserves, in contrast to the Hann and Hamming window, the positive semi-definiteness of the estimate. It is a well-established window function, especially when used as lag window [68]. Figures 2.7.6a and 2.7.6b show the Parzen window and the corresponding spectral window for  $T = 1024$ . The MATLAB function used for generating this window is `parzenwin`.

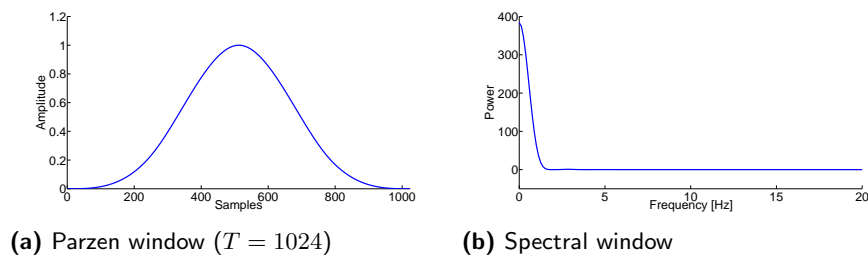


Figure 2.7.6: Parzen window and corresponding spectral window

### 2.7.5 Spectral Estimation in this Study

For the analyses of EEG synchrony in AD, an indirect spectral estimate was used for estimating the multivariate spectral density. As mentioned in Sections 2.1 and 2.2.3, analyses were carried out on 4 second EEG segments with an overlap of 2 seconds. At first, the mean of each channel was estimated according to Equation (2.6.1) with the MATLAB function `mean` and subtracted from each channel. Then, for reducing the leakage effect, the data were channelwise pre-tapered with a Hamming window by using the MATLAB function `hamming` (cf. Section 2.7.4). The autocovariance function was then estimated according to Equation (2.6.6) with the MATLAB function `xcov`. The Parzen window was applied as lag window. By window closing, the truncation point  $n(T) = 255$  corresponding to 1 second was determined. Higher lags and the corresponding inaccuracy of estimation were avoided and a satisfying degree of smoothness of the spectral estimate was achieved. The DFT was applied on the windowed autocovariance function by making use of the MATLAB functions `fft` and `ifft`. The resulting estimate is Hermitian, positive semi-definite, and has full rank.

The most important lines of MATLAB source code for this estimation procedure are the following:

---

```

1 % Zero mean EEG segment X with dimensions samples x channels
2 [nX,r] = size(X);
3
4 % Sampling rate
5 fs = 256;
6
7 % Taper the data with a Hamming window for leakage reduction
8 taper = hamming(nX)*ones(1,r);
9 X = X.*taper;
10
11 % Autocovariance function of X
12 C = xcov(X);
13 [nC,m] = size(C);
14
15 % Apply lag window with truncation point 256 samples (maximum lag 255)

```

---

```

16 u = -255:255;
17 nLags = length(u);
18 lagwin = parzenwin(nLags);
19 lagwin = [zeros((nC-nLags)/2,1); lagwin; zeros((nC-nLags)/2,1)];
20 lagwin = lagwin*ones(1,m);
21 C = C.*lagwin;
22
23 % Calculate DFT of windowed autocovariance function
24 S1 = fft(C(nX:end,:));
25 S2 = nX*ifft(C(nX:-1:1,:))-ones(nX,1)*C(nX,:);
26 S = S1 + S2;
27 S(:,1:r+1:end) = 2*real(S1(:,1:r+1:end))-ones(nX,1)*C(nX,1:r+1:end);
28 S = S/(2*pi*nX*fs);
29
30 % Spectral density in [0,pi]
31 S = S(1:nX/2+1,:);
32
33 % Reshape spectral density S
34 tmpS = cell(length(f),1);
35 for k = 1:length(f)
36     tmpS(k,1) = {reshape(S(k,:),r,r)'};
37 end
38 S = tmpS;
39
40 % Corresponding vector of positive Fourier frequencies
41 f = linspace(0,fs/2,nX/2+1);

```

---

## 2.8 Implementation of the Dependence Measures

This section will be concerned with the implementation of the dependence measures defined in Section 2.5. Starting point is a 4 second EEG segment with corresponding estimates for the mean  $\bar{x}(T)$ , autocovariance function  $\hat{\gamma}(u, T)$ , and multivariate spectral density  $\tilde{f}(\lambda, T)$  as described in the previous sections.

### 2.8.1 Coherence

An estimate for the coherence (cf. Equation (2.5.6)) between the univariate samples  $x_i(0), \dots, x_i(T-1)$  and  $x_j(0), \dots, x_j(T-1)$  was derived by

$$\hat{C}_{ij}^2(\lambda, T) = \frac{|\tilde{f}_{ij}(\lambda, T)|^2}{\tilde{f}_{ii}(\lambda, T)\tilde{f}_{jj}(\lambda, T)}. \quad (2.8.1)$$

Hence, the estimation is straightforward. For a discussion of the asymptotic properties of the empirical coherence  $\hat{C}_{ij}^2$ , the reader is referred to [60] and [56].



Given the MATLAB source code for the spectral estimation, the most relevant code lines for the calculation of the empirical coherence between channel  $i$  and  $j$  at frequency  $\lambda$  are as follows:

---

```

1 % Find index of Fourier frequency lambda
2 [~,fIdx] = max(f==lambda);
3
4 % Calculate coherence between channels i and j at lambda
5 Cij = S{fIdx}(i,j) / sqrt(S{fIdx}(i,i)*S{fIdx}(j,j));
6 Cij = abs(Cij)^2;

```

---

### 2.8.2 Partial Coherence

The empirical partial coherence was estimated by

$$\hat{R}_{ij}^2(\lambda, T) = \frac{|\hat{g}_{ij}(\lambda, T)|^2}{\hat{g}_{ii}(\lambda, T)\hat{g}_{jj}(\lambda, T)}. \quad (2.8.2)$$

where  $\hat{g}_{ij}(\lambda, T)$  is the  $(i, j)$ -element of  $\hat{\mathbf{g}}(\lambda, T) = \tilde{\mathbf{f}}^{-1}(\lambda, T)$  at frequency  $\lambda$ . As  $\tilde{\mathbf{f}}^{-1}$  has full rank, its inverse  $\hat{\mathbf{g}}$  exists. The estimate is the finite sample analog of the corresponding population definition (2.5.9) [60]. Dahlhaus describes the distribution of  $\hat{R}_{ij}^2$  in [73] and applies the estimate on air pollution data in [61]; Brillinger addresses the bias and asymptotic properties of  $\hat{R}_{ij}^2$  in [60].

Given the MATLAB source code for the spectral estimation, the crucial code lines for the calculation of the empirical partial coherence are the following:

---

```

1 % Find index of Fourier frequency lambda
2 [~,fIdx] = max(f==lambda);
3
4 % Invert spectral density at lambda
5 iS{fIdx} = S{fIdx}\eye(r);
6
7 % Calculate partial coherence between channels i and j at lambda
8 Rij = iS{fIdx}(i,j) / sqrt(iS{fIdx}(i,i)*iS{fIdx}(j,j));
9 Rij = abs(Rij)^2;

```

---

### 2.8.3 Bivariate Granger Causality

For the calculation of the empirical bivariate Granger causality, a bivariate autoregressive model was estimated at first. This was done by using the empirical autocovariance function  $\hat{\gamma}(u, T)$  and the Yule-Walker equations that connect  $\hat{\gamma}(u, T)$  with the AR model coefficients  $\hat{A}(k) \in \mathbb{R}^{2 \times 2}$ ,  $k = 1, \dots, p$  by least squares estimation

$$\hat{A}_p = \hat{\Gamma}_p^{-1} \hat{\gamma}_p \quad (2.8.3)$$

with

$$\hat{\Gamma}_p = \begin{pmatrix} \hat{\gamma}(0,p) & \cdots & \hat{\gamma}(-p+1,p) \\ \vdots & \ddots & \vdots \\ \hat{\gamma}(p-1,p) & \cdots & \hat{\gamma}(0,p) \end{pmatrix}, \quad \hat{\gamma}_p = \begin{pmatrix} \hat{\gamma}(1,p) \\ \vdots \\ \hat{\gamma}(p,p) \end{pmatrix}, \quad \hat{A}_p = \begin{pmatrix} \hat{A}(1) \\ \vdots \\ \hat{A}(p) \end{pmatrix}. \quad (2.8.4)$$

The model order  $p$  was decided by Akaike's AIC criterion (cf. [74]). Analogously to Equation (2.5.12), Granger non-causality of the univariate sample  $x_2(0), \dots, x_2(T-1)$  for the univariate  $x_1(0), \dots, x_1(T-1)$  was defined by

$$\hat{A}_{12}(k) = 0 \quad \forall k = 1, \dots, p. \quad (2.8.5)$$

In order to compare the "degree" of Granger (non-)causality, the Euklidian norm of the elements  $\hat{A}_{12}(k)$  for  $k = 1, \dots, p$  was used as measure of synchrony. A value close to 0 indicates a low degree of Granger causality, whereas high values – this measure has no upper bound – indicate a high degree of Granger causality. Eichler describes test statistics for bivariate Granger non-causality in [64].

The MATLAB source code for the AR model and the calculation of the degree of bivariate Granger causality – with auxiliary MATLAB functions `MARyulewalker` and `MARpolynomcoeffnorm` – is as follows:

---

```

1 % Zero mean EEG segment X with dimensions samples x channels
2 [nX,r] = size(X);
3
4 % Multivariate AR model using AIC criterion and Yule-Walker equations
5 m_vec = ones(1,nX);
6 idx = 0;
7 min_trigger = 0;
8 while min_trigger == 0
9     idx = idx+1;
10    % Yule-Walker equations
11    [~, Sigma] = MARyulewalker(X,idx);
12    % AIC criterion
13    m_vec(idx) = 2*log(det(Sigma)) + 2*r^2*idx/nX;
14    if idx > 1 && m_vec(idx) > m_vec(idx-1)
15        min_trigger = 1;
16        m = idx-1;
17    end
18 end
19
20 % Calculate AR(m)-model coefficients
21 [ A, Sigma ] = MARyulewalker( X, m );
22
23 % Calculate Euklidian norm of AR(m)-model coefficients
24 [ PolyNorm ] = MARpolynomcoeffnorm( A, m );
25

```

```

26 % Granger causality between channel i and j
27 i = 1;
28 j = 2;
29 GCij = PolyNorm(j,i);
30
31
32 function [ A, Sigma ] = MARYulewalker( X, m )
33
34 % Zero mean EEG segment X with dimensions samples x channels
35 [nX,r] = size(X);
36
37 % Normalized autocovariance function with maximum lag m
38 C = xcov(X,m,'coeff');
39 g = reshape(C',nX,nX*(2*m+1))';
40
41 % Matrix of autocovariance functions with all lags
42 Gamma_m = zeros(m*nX,m*nX);
43 k = m*nX+1;
44 for ordIdx = 0:m-1
45     Gamma_m(:,ordIdx*nX+1:ordIdx*nX+nX) = g(k:k+m*nX-1,:);
46     k = k-nX;
47 end
48
49 % Vector of autocovariance functions with all lags
50 gam_m = g((m+1)*nX+1:end,:);
51
52 % Yule-Walker equations
53 invGamma_m = Gamma_m\eye(m*nX);
54 A = invGamma_m*gam_m;
55 Sigma = g(m*nX+1:m*nX+nX,:) - A'*gam_m;
56
57 end
58
59
60 function [ PolyNorm ] = MARpolynomcoeffnorm( A, m )
61
62 % Size of AR(m)-model coefficients
63 nA = size(A,2);
64
65 % Sum of squares of AR(m)-model coefficients
66 PolyNorm = zeros(nA);
67 for ordIdx = 1:m
68     PolyNorm = PolyNorm + abs(A((ordIdx-1)*nA+1:(ordIdx-1)*nA+nA,1:nA)).^2;
69 end
70
71 % Squareroot of sum of squares
72 PolyNorm = sqrt(PolyNorm);
73
74 end

```

### 2.8.4 Conditional Granger Causality

The empirical conditional Granger causality was constructed analogously to the bivariate case described in Section 2.8.3. A multivariate AR model was estimated by using the Yule-Walker equations and the AIC criterion. Here, the AR model coefficients  $\hat{A}(k), k = 1, \dots, p$  are elements of  $\mathbb{R}^{r \times r}$ . Granger non-causality of  $x_j(0), \dots, x_j(T-1)$  for  $x_i(0), \dots, x_i(T-1)$  was defined as

$$\hat{A}_{ij}(k) = 0 \quad \forall k = 1, \dots, p. \quad (2.8.6)$$

By using the Euklidean norm of the elements  $\hat{A}_{ij}(k)$ , a directed measure for synchrony between channels  $i$  and  $j$  given all other channels was derived.

The MATLAB source code for the calculation of the degree of conditional Granger causality was provided in Section 2.8.3, only with  $r=19$  being the number of channels instead of  $r=2$ .

### 2.8.5 Static Canonical Correlation Analysis

The estimate for the static canonical correlation between  $y(0), \dots, y(T-1) \in \mathbb{R}^{r \times 1}$  and  $z(0), \dots, z(T-1) \in \mathbb{R}^{s \times 1}$  is based on the empirical autocovariance function of  $x(t) = (y(t)^\top, z(t)^\top)^\top \in \mathbb{R}^{(r+s) \times 1}$ , i.e.

$$\hat{\gamma}_{xx}(0, T) = \begin{pmatrix} \hat{\gamma}_{yy}(0, T) & \hat{\gamma}_{yz}(0, T) \\ \hat{\gamma}_{zy}(0, T) & \hat{\gamma}_{zz}(0, T) \end{pmatrix} \quad (2.8.7)$$

where  $\hat{\gamma}_{yy}$  and  $\hat{\gamma}_{zz}$  are the respective empirical autocovariance functions of  $y(t)$  and  $z(t)$ , and  $\hat{\gamma}_{yz} = \hat{\gamma}_{zy}^\top$  is the empirical crosscovariance function between  $y(t)$  and  $z(t)$ . In accordance with Equations (2.5.18) - (2.5.21), the  $i^{th}$  empirical static canonical correlation coefficient was defined as

$$\hat{\rho}_i = \frac{\hat{a}_i^\top \hat{\gamma}_{yz} \hat{b}_i}{((\hat{a}_i^\top \hat{\gamma}_{yy} \hat{a}_i)(\hat{b}_i^\top \hat{\gamma}_{zz} \hat{b}_i))^{\frac{1}{2}}} \quad (2.8.8)$$

where

$$\begin{aligned} \hat{a}_i &= \hat{\gamma}_{yy}^{-\frac{1}{2}} \hat{U}_i \\ \hat{b}_i &= \hat{\gamma}_{zz}^{-\frac{1}{2}} \hat{V}_i \end{aligned} \quad (2.8.9)$$

with  $\hat{U}_i$  and  $\hat{V}_i$  denoting the respective  $i^{th}$  eigenvector of

$$\hat{\gamma}_{yy}^{-\frac{1}{2}} \hat{\gamma}_{yz} \hat{\gamma}_{zz}^{-1} \hat{\gamma}_{zy} \hat{\gamma}_{yy}^{-\frac{1}{2}} \quad \text{and} \quad \hat{\gamma}_{zz}^{-\frac{1}{2}} \hat{\gamma}_{zy} \hat{\gamma}_{yy}^{-1} \hat{\gamma}_{yz} \hat{\gamma}_{zz}^{-\frac{1}{2}}. \quad (2.8.10)$$

Brillinger gives a detailed description of the asymptotic properties of  $\hat{\rho}_i$  in chapter 10 of [60]. The Euklidean norm of the coefficients  $\hat{\rho}_i$  was used as measure for the dependence between the channel groups.

The MATLAB source code for the calculation of the empirical static canonical correlation coefficients is as follows:

---

```

1 % Zero mean channel groups Y and Z with dimensions (samples x channels)
2 [nY,r] = size(Y);
3 [nZ,s] = size(Z);
4
5 % Calculate Eukclidean norm of canonical correlation coefficients
6 [~,~,rho] = canoncorr(Y,Z);
7 CC = sqrt(sum(rho.^2));

```

---

## 2.8.6 Dynamic Canonical Correlation Analysis

The estimate for the dynamic canonical correlation coefficient between  $y(0), \dots, y(T-1) \in \mathbb{R}^{r \times 1}$  and  $z(0), \dots, z(T-1) \in \mathbb{R}^{s \times 1}$  is the finite sample analog of the corresponding population formulae (2.5.24) - (2.5.27). Following these equations, the estimation procedure is straightforward by applying the estimate  $\hat{f}(\lambda, T)$  for the multivariate spectral density. Brillinger describes the asymptotic distribution of the empirical dynamic canonical correlation coefficients in chapter 10 of [60].

The MATLAB source code for the calculation of the empirical dynamic canonical correlation coefficients between the two channel groups Y and Z at frequency  $\lambda$ , given the spectral density S and vector of Fourier frequencies  $\mathbf{f}$ , is as follows:

---

```

1 % Find index of Fourier frequency lambda
2 [~,fIdx] = max(f==lambda);
3
4 % Length of channel indices of Y and Z
5 nY = length(idxY);
6 nZ = length(idxZ);
7
8 % Auto- and cross-spectral densities of Y and Z
9 Syy = S{fIdx}(idxY,idxY);
10 Szz = S{fIdx}(idxZ,idxZ);
11 Syz = S{fIdx}(idxY,idxZ);
12 Szy = S{fIdx}(idxZ,idxY);
13
14 % Calculate dynamic canonical correlation coefficients
15 rho = real(sqrt(eig(sqrtm(Syy)\Syz/Szz*Szy/sqrtm(Syy))));
16 rho = sort(rho, 'descend');
17 rho = rho(1:min(nY,nZ));
18
19 % Calculate Eukclidean norm of canonical correlation coefficients
20 CC = sqrt(sum(rho.^2));

```

---

## 2.8.7 Static Principal Component Analysis

The empirical static PCs of a finite sample  $x(0), \dots, x(T-1) \in \mathbb{R}^{r \times 1}$  are defined – skipping the time index as in Section 2.5.8 – as

$$\hat{\zeta}_i = \hat{V}_i^T x \quad (2.8.11)$$

where  $\hat{V}_i$  denotes the  $i^{\text{th}}$  eigenvector of  $\hat{\gamma}$  with corresponding eigenvalue  $\hat{\mu}_i$ . The term

$$\hat{p}_1 = \frac{\hat{\mu}_1}{\sum_j \hat{\mu}_j} \quad (2.8.12)$$

gives the percentage of variance that is described by the first PC and is used as measure for homogeneity within the sample  $x(t)$ . The asymptotic properties of  $\hat{p}_1$  are discussed in chapter 9 of [60].

The MATLAB source code for the calculation of the empirical static PCs is as follows:

---

```

1 % Autocovariance function of X (samples x channels)
2 C = xcov(X);
3
4 % PCA
5 [~,~,p] = pcacov(C);
6
7 % Percentage of var described by first PC
8 p(1) = p(1)./100;

```

---

## 2.8.8 Dynamic Principal Component Analysis

Following Equations (2.5.36) - (2.5.41), the calculation of the empirical dynamic PCs is straightforward with the estimate  $\tilde{f}$  being on hand. For the frequency  $\lambda$ , the term

$$\hat{p}_1(\lambda) = \frac{\hat{\mu}_1(\lambda)}{\sum_j \hat{\mu}_j(\lambda)} \quad (2.8.13)$$

with  $\hat{\mu}_i(\lambda)$  being the  $i^{\text{th}}$  eigenvalue of  $\tilde{f}(\lambda, T)$  gives the percentage of variance that is described by the first PC.  $\hat{p}_1$  is used as frequency-wise measure for homogeneity within a realization  $x(t)$ . Brillinger explains the asymptotics of dynamic PCA in chapter 9 of [60].

Given the spectral density  $S$  and vector of Fourier frequencies  $\mathbf{f}$ , the MATLAB source code for the calculation of the empirical dynamic PCs at  $\lambda$  is as follows:

---

```

1 % Find index of Fourier frequency lambda
2 [~,fIdx] = max(f==lambda);
3
4 % PCA of spectral density at frequency lambda
5 [~,~,p] = pcacov(S{fIdx});
6
7 % Percentage of var described by first PC
8 p(1) = p(1)./100;

```

## 2.9 Analyzing EEG Synchrony

Coherences, partial coherences, dynamic canonical correlations and dynamic PCA were calculated frequency-wise and averaged within predefined frequency bands, the  $\delta$ -,  $\theta$ -,  $\alpha$ -,  $\beta_0$ -band, and for the whole band-pass filtered signal (here referred to as "total"). The applied border-frequencies are given in Table 2.9.1. Hereby, the respective lower frequency border was included in the frequency band, whereas the upper border was excluded from it.

**Table 2.9.1:** Frequency bands names and borders

Frequency Band	Frequency Borders
$\delta$ -band	2 - 4 Hz
$\theta$ -band	4 - 8 Hz
$\alpha$ -band	8 - 13 Hz
$\beta_0$ -band	13 - 15 Hz
total	2 - 15 Hz

Dividing the frequency domain in frequency bands is common practice in EEG analysis; however, frequency borders vary in literature and the transition frequencies between the four frequency bands may differ from the transition frequencies used here by  $\pm 1$  Hz. The lower frequency border of the  $\delta$ -band is often defined as 0 or 0.5 Hz. The upper  $\beta$ -border is usually defined in a range of 20 to 30 Hz; here, the border of 15 Hz was chosen in order to make sure that no artefacts deteriorate the analyses in the  $\beta$ -band (cf. Sections 2.2.1 and 2.2.2). Due to the comparatively low upper frequency border, the band is referred to as  $\beta_0$ -band instead of  $\beta$ -band. Bivariate and conditional Granger causalities, static canonical correlations, and static PCA were computed for the whole band-pass filtered (2-15 Hz) EEG signals.

Synchrony was investigated in three different ways: between single EEG channels, between groups of EEG channels, and within groups of EEG channels. For the investigation between channel pairs, ten *far intrahemispheric* (FP1-P3, FP2-P4, FP1-O1, FP2-O2, F3-P3, F4-P4, F3-O1, F4-O2, C3-O1, C4-O2), seven *far interhemispheric* (F3-F4, F7-F8, C3-C4, T7-T8, P3-P4, P7-P8, O1-O2), ten *local*

*anterior* (FP1-F7, FP1-F3, FP2-F4, FP2-F8, F7-T7, F7-C3, F3-C3, F4-C4, F8-C4, F8-T8), and ten *local posterior* channel pairs (C3-P7, C3-P3, C4-P4, C4-P8, P7-P3, P4-P8, P7-O1, P3-O1, P4-O2, P8-O2) were defined. These channel pairs are shown in Figures 2.9.1a - 2.9.1d. For these channel pairs, coherences, partial coherences, bivariate and conditional Granger causalities were calculated.

For the analysis of synchrony between and within EEG channel groups, the following two channel partitions were defined: the first partition consists of the channel groups (cf. also [38]) *Anterior* (FP1, FP2, F3, F4), *Central* (FZ, C3, CZ, C4, PZ), *Posterior* (P3, P4, O1, O2), *Temporal Left* (F7, T7, P7), and *Temporal Right* (F8, T8, P8). The second partition consists of the channel groups *Left* (FP1, F7, F3, T7, C3, P7, P3, O1) and *Right* (FP2, F4, F8, C4, T8, P4, P8, O2). The partitions are illustrated in Figures 2.9.2a and 2.9.2b. For each channel group, (static) PCA was performed. Between the respective first and second PCs of channel groups, coherences, partial coherences, bivariate and conditional Granger causalities were investigated. Static and dynamic canonical correlation analyses were performed both between the respective first and second PCs of the channel groups and – in a multivariate way – directly between the groups of EEG channels.

Finally, as a measure for the degree of local synchrony, the amount of variance explained by the first static and dynamic PCs in relation to the total variance was considered for each channel group.

For both resting state and during cognitive task, synchronies were analyzed versus MMSE via quadratic least squares regression. Quadratic regression was chosen in order to capture compensating mechanisms at the initial stage of AD. As covariables, the subjects' age, sex, degree of education, and the duration of AD were taken into account; hereby, age and duration of AD were introduced via both linear and quadratic terms. The statistical significance and the goodness of fit were evaluated by Fisher's F-test and by the coefficients of determination. The regression and regression diagnostics were implemented using the MATLAB function `regstats`.



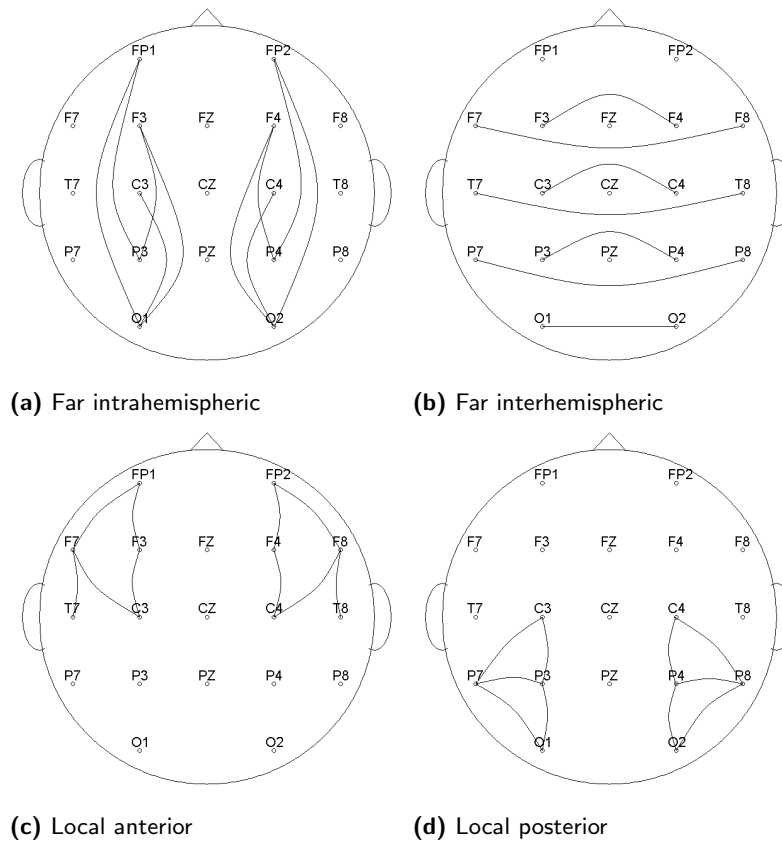


**Figure 2.9.1:** Electrode pairs: each channel pair connected with a line was investigated. Channel pairs were divided into far intrahemispheric, far interhemispheric, local anterior and local posterior pairs.

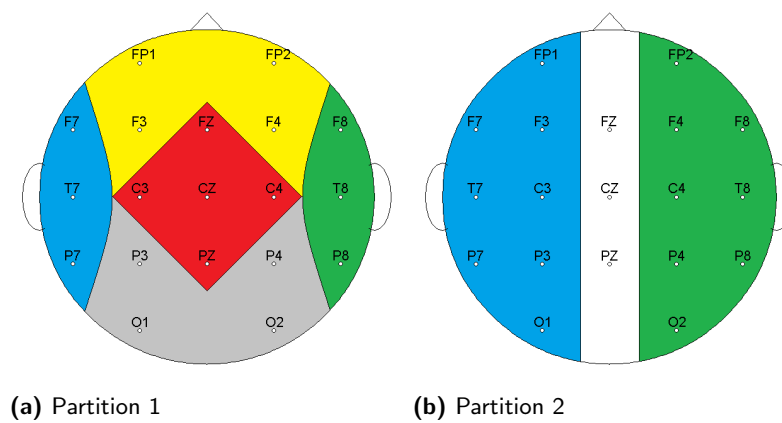


**Figure 2.9.2:** Division of channels into partition 1 (anterior (yellow), central (red), posterior (grey), temporal left (blue), temporal right (green)) and partition 2 (left (blue), right (green))



---

### Results

---

This chapter is concerned with the results of measuring EEG synchrony versus MMSE scores. First, let us recall the research hypotheses:

- $H_0^1$ : Synchronies between single EEG channels change in the course of AD.
- $H_0^2$ : Synchronies between EEG channel groups change in the course of AD.
- $H_0^3$ : Synchronies within EEG channel groups change in the course of AD.

In accordance with these hypotheses, the results will be divided into the three Section 3.1, 3.2, and 3.3. Due to the multitude of findings, the main results will be summarized at the respective beginning of each section. This will be followed by a detailed listing of all results, both in textual and tabular form. Provided that only the most significant results are matter of interest, the reader is free to skip these detailed listings and proceed to the main results of the next section. In the tables, the dependence measures will be abbreviated as follows: coherence (Coh), partial coherence (pCoh), bivariate Granger causality (bGC), conditional Granger causality (cGC), static canonical correlations (statCC), dynamic caonical correlations (dynCC), static PCA (statPCA), and dynamic PCA (dynPCA). Throughout this chapter, the terms *significant* and *highly significant* will be used for the F-test results of quadratic regression on the levels  $p = 0.05$  and  $p = 0.01$  respectively. In the tables, significance is indicated by "\*" and high significance by "\*\*". Besides, values of the coefficients of determination will be provided and the shape of the fitted quadratic regression will be addressed. For the Granger causality measures, the direction of dependence will be indicated by "→", e.g. P4 → FP2 and Central → Temporal Left.

### 3.1 Synchrony Between Single EEG Channels

In this section, the findings for synchrony between single EEG channels will be presented. Coherences and partial coherences were estimated in the  $\delta$ -,  $\theta$ -,  $\alpha$ - and  $\beta_0$ -frequency band. For the whole bandpass-filtered (2–15 Hz) signal, coherences,

partial coherences, bivariate and conditional Granger causalities were investigated. In Section 3.1.1, the main findings will be summarized, whereas Sections 3.1.2 and 3.1.3 will provide a detailed listing of the results for resting state and cognitive task.

### 3.1.1 Main Results

Resting state analyses revealed significant changes of coherences in 18 EEG channel pairs. However, for the majority (i.e. 14) of channel pairs, the changes were significant only in a single frequency band. Highly significant changes were observed at four channel pairs: C4-O2 in the  $\beta_0$ -frequency band ( $R^2 = 0.184$ ), FP2-F8 in the  $\delta$ -frequency band ( $R^2 = 0.161$ ), C4-P8 in the  $\beta_0$ -frequency band ( $R^2 = 0.166$ ), and P4-C4 in the  $\beta_0$ -frequency band ( $R^2 = 0.179$ ). For partial coherences, the most significant findings were obtained between F7-T7 in the  $\delta$ - ( $R^2 = 0.203$ ),  $\theta$ -frequency band ( $R^2 = 0.223$ ), and for the whole signal ( $R^2 = 0.166$ ), and between C3-P7 in the  $\delta$ - ( $R^2 = 0.236$ ),  $\theta$ -frequency band ( $R^2 = 0.229$ ), and for the whole signal ( $R^2 = 0.205$ ). In addition, highly significant changes were observed between FP1-O1 in  $\theta$  ( $R^2 = 0.204$ ) and  $\beta_0$  ( $R^2 = 0.222$ ), FP1-P3 in  $\delta$  ( $R^2 = 0.239$ ), F3-O1 in  $\theta$  ( $R^2 = 0.183$ ) and for the whole signal ( $R^2 = 0.181$ ), T7-T8 in  $\theta$  ( $R^2 = 0.236$ ), P7-P8 in  $\delta$  ( $R^2 = 0.187$ ) and  $\beta_0$  ( $R^2 = 0.147$ ), and O1-O2 in the  $\alpha$ -frequency band ( $R^2 = 0.155$ ). Figure 3.1.1 shows the estimated partial coherences between C3-P7 in the  $\delta$ -frequency band as scatterdiagram versus MMSE scores. The quadratic regression ( $p < 0.001$ ,  $R^2 = 0.236$ ) is characterized by an increase of partial coherences for MMSE scores between 26 and 19, and a decrease from 19 downwards.

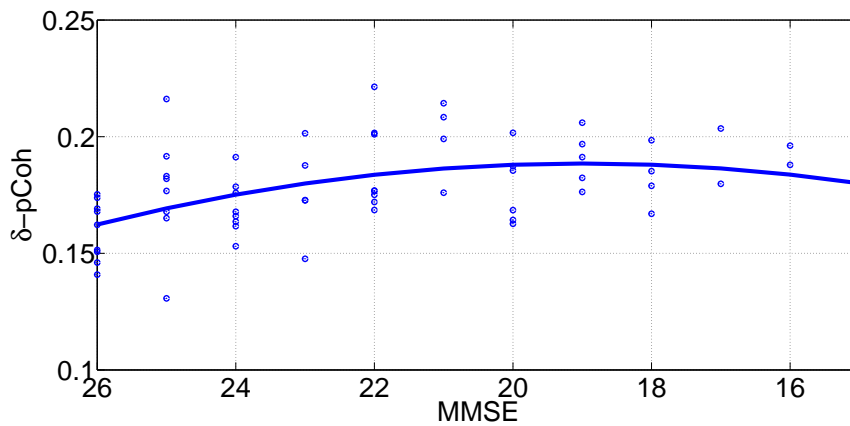


**Figure 3.1.1:** Example for synchrony changes between single channels in **resting state: partial coherences** between **C3-P7** in the  **$\delta$ -frequency band** versus MMSE scores. Low MMSE scores (right side of the abscissa) indicate a more severe severity of AD. A quadratic regression was fitted to the data with  $p < 0.001$  and  $R^2 = 0.236$ .

The bivariate Granger causality measure yielded highly significant findings

between P4  $\rightarrow$  FP2 ( $R^2 = 0.195$ ), FP1  $\rightarrow$  F3 ( $R^2 = 0.200$ ), and F7  $\rightarrow$  T7 ( $R^2 = 0.146$ ). Additionally, significant changes were observed in 5 channel pairs, all of them only in one direction. The analysis of the conditional Granger causality measure revealed no highly significant changes. Significance was observed in 5 channel pairs different from those of bivariate Granger causalities. Table 3.1.1 provides an overview of the significant test results for each measure, frequency band, and channel pair in resting state.



During the cognitive task, significant changes of coherences were observed mainly in local posterior channel pairs: P7-O1 in  $\beta_0$  ( $R^2 = 0.188$ ), C4-P8 in  $\delta$  ( $R^2 = 0.148$ ),  $\theta$  ( $R^2 = 0.225$ ) and for the whole signal ( $R^2 = 0.178$ ), P3-C3 in  $\theta$  ( $R^2 = 0.171$ ), P3-P7 in  $\delta$  ( $R^2 = 0.171$ ),  $\alpha$  ( $R^2 = 0.183$ ),  $\beta_0$  ( $R^2 = 0.215$ ) and for the whole signal ( $R^2 = 0.194$ ), and P4-P8 in  $\delta$  ( $R^2 = 0.149$ ),  $\theta$  ( $R^2 = 0.250$ ),  $\alpha$  ( $R^2 = 0.161$ ) and for the whole signal ( $R^2 = 0.161$ ). Besides, highly significant results in  $\beta_0$  ( $R^2 = 0.152$ ) were observed between the far interhemispheric channels O1-O2. Figure 3.1.2 shows the estimated coherences between P4-P8 in the  $\theta$ -frequency band as scatterdiagram versus MMSE scores. The quadratic regression ( $p < 0.001$ ,  $R^2 = 0.250$ ) is characterized by an increase of coherences for MMSE scores between 26 and 20, and a decrease from 20 downwards.

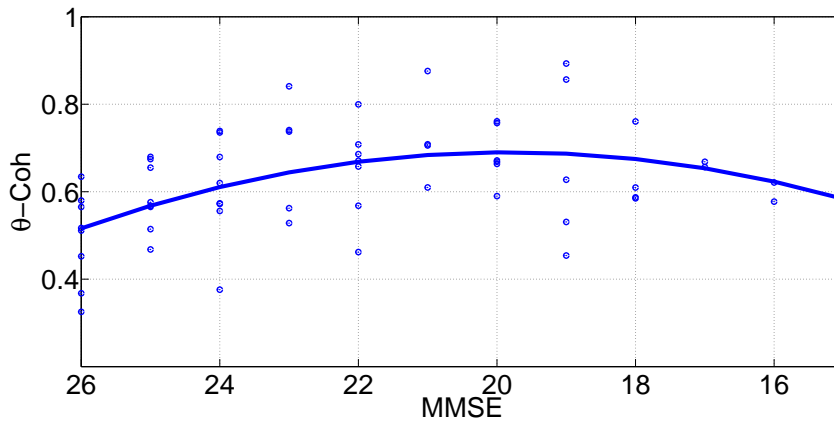


**Figure 3.1.2:** Example for synchrony changes between single channels during the **cognitive task**: **coherences** between **P4-P8** in the  **$\theta$ -frequency band** versus MMSE scores. Low MMSE scores (right side of the abscissa) indicate a higher degree of severity of AD. A quadratic regression was fitted to the data with  $p < 0.001$  and  $R^2 = 0.250$ .

For partial coherences, the most significant findings were observed between O1-O2 in  $\alpha$  ( $R^2 = 0.168$ ) and in  $\beta_0$  ( $R^2 = 0.203$ ), F7-T7 in  $\theta$  ( $R^2 = 0.199$ ) and for the whole signal ( $R^2 = 0.157$ ), and F8-T8 in  $\delta$  ( $R^2 = 0.149$ ),  $\alpha$  ( $R^2 = 0.155$ ) and for the whole signal ( $R^2 = 0.153$ ). In addition, highly significant test results were obtained between F3-P3 in  $\alpha$  ( $R^2 = 0.212$ ), F4-P4 in  $\theta$  ( $R^2 = 0.151$ ), and T7-T8 in  $\beta_0$  ( $R^2 = 0.147$ ). As opposed to coherences, no significant findings were observed for partial coherences in the local posterior channel pairs. The bivariate Granger causality measure yielded high significance between C3  $\rightarrow$  O1 ( $R^2 = 0.158$ ), and between both F7  $\rightarrow$  T7 ( $R^2 = 0.225$ ) and T7  $\rightarrow$  F7 ( $R^2 = 0.228$ ). In the latter channel pair, highly significant results were observed for the conditional Granger causality measure as well ( $R^2 = 0.168$ ). Furthermore, high significance was obtained between F7  $\rightarrow$  F8 ( $R^2 = 0.173$ ). Table 3.1.2 provides an overview of the significant test results for each measure, frequency band, and channel pair during the cognitive task.





### 3.1.2 Detailed Results: Resting State

In this section, all resting state results for synchrony between single EEG channels will be presented. The findings will be divided into far intrahemispheric, far inter-hemispheric, local anterior, and local posterior channel pairs (cf. Figures 2.9.1a - 2.9.1d).

#### Far Intrahemispheric

At first, let us consider the far intrahemispheric channel pairs (cf. Figure 2.9.1a). In the  $\delta$ -frequency band, coherences yielded statistically significant results only in C4-O2 ( $R^2 = 0.107$ ). For partial coherence, significant changes were observed between FP1-O1 ( $R^2 = 0.121$ ), and C4-O2 ( $R^2 = 0.094$ ). High significance was obtained between FP1-P3 ( $R^2 = 0.239$ ). The resting state findings for the far intrahemispheric channel pairs in the  $\delta$ -band are illustrated in Table 3.1.3.

**Table 3.1.3:** Significance  $p$  and coefficient of determination  $R^2$  as determined by Fisher's F-test for a least squares quadratic regression model: measures between far intrahemispheric channel pairs in the  $\delta$ -frequency band in resting state; "\*" and "\*\*" indicate  $p < 0.05$  and  $p < 0.01$  respectively

$\delta$ -band	Coh.		pCoh.	
	$p$	$R^2$	$p$	$R^2$
FP1-O1	0.904	0.003	0.020*	0.121
FP2-O2	0.169	0.057	0.402	0.029
FP1-P3	0.952	0.002	<0.001**	0.239
FP2-P4	0.911	0.003	0.447	0.026
F3-O1	0.223	0.048	0.083	0.078
F4-O2	0.102	0.072	0.055	0.091
F3-P3	0.532	0.020	0.099	0.073
F4-P4	0.543	0.020	0.098	0.073
C3-O1	0.191	0.053	0.063	0.087
C4-O2	0.031*	0.107	0.049*	0.094

In the  $\theta$ -frequency band, changes of coherence were significant only between FP1-O1 ( $R^2 = 0.132$ ). Analyzing partial coherence resulted in significant findings between F3-P3 ( $R^2 = 0.108$ ), and F4-P4 ( $R^2 = 0.121$ ); between FP1-O1 ( $R^2 = 0.204$ ) and F3-O1 ( $R^2 = 0.183$ ), high significance was observed. Table 3.1.4 provides the resting state results for the far intrahemispheric channel pairs in the  $\theta$ -frequency band.

In the  $\alpha$ -frequency band, coherences yielded significant results between F3-O1 ( $R^2 = 0.127$ ) and C4-O2 ( $R^2 = 0.110$ ). No significant results were found for

**Table 3.1.4:** Significance  $p$  and coefficient of determination  $R^2$  as determined by Fisher's F-test for a least squares quadratic regression model: measures between far intrahemispheric channel pairs in the  $\theta$ -frequency band in resting state; "\*" and "\*\*\*" indicate  $p < 0.05$  and  $p < 0.01$  respectively

$\theta$ -band	Coh.		pCoh.	
	p	$R^2$	p	$R^2$
FP1-O1	0.013*	0.132	0.001**	0.204
FP2-O2	0.163	0.058	0.856	0.005
FP1-P3	0.998	<0.001	0.186	0.054
FP2-P4	0.881	0.004	0.826	0.006
F3-O1	0.410	0.029	0.002**	0.183
F4-O2	0.402	0.029	0.164	0.058
F3-P3	0.624	0.015	0.030*	0.108
F4-P4	0.434	0.027	0.020*	0.121
C3-O1	0.361	0.033	0.130	0.065
C4-O2	0.132	0.064	0.746	0.010

partial coherences. In Table 3.1.5, the resting state findings for the far intrahemispheric channel pairs in the  $\alpha$ -frequency band are shown.

**Table 3.1.5:** Significance  $p$  and coefficient of determination  $R^2$  as determined by Fisher's F-test for a least squares quadratic regression model: measures between far intrahemispheric channel pairs in the  $\alpha$ -frequency band in resting state; "\*" and "\*\*\*" indicate  $p < 0.05$  and  $p < 0.01$  respectively

$\alpha$ -band	Coh.		pCoh.	
	p	$R^2$	p	$R^2$
FP1-O1	0.101	0.072	0.863	0.005
FP2-O2	0.367	0.032	0.143	0.062
FP1-P3	0.149	0.060	0.148	0.061
FP2-P4	0.212	0.050	0.434	0.027
F3-O1	0.016*	0.127	0.345	0.034
F4-O2	0.082	0.079	0.789	0.008
F3-P3	0.591	0.017	0.540	0.020
F4-P4	0.283	0.041	0.107	0.071
C3-O1	0.213	0.049	0.387	0.031
C4-O2	0.028*	0.110	0.644	0.014

In the  $\beta_0$ -frequency band, coherences yielded significant results between FP2-P4 ( $R^2 = 0.130$ ) and F4-P4 ( $R^2 = 0.103$ ). For channel pair C4-O2, high significance was observed ( $R^2 = 0.184$ ). Changes of partial coherences were significant between FP2-O2 ( $R^2 = 0.127$ ) and F4-O2 ( $R^2 = 0.107$ ). In addition, high sig-

nificance between FP1-O1 was observed ( $R^2 = 0.222$ ). Table 3.1.6 provides the resting state results for the far intrahemispheric channel pairs in the  $\beta_0$ -frequency band.

**Table 3.1.6:** Significance  $p$  and coefficient of determination  $R^2$  as determined by Fisher's F-test for a least squares quadratic regression model: measures between far intrahemispheric channel pairs in the  $\beta_0$ -frequency band in resting state; "\*" and "\*\*" indicate  $p < 0.05$  and  $p < 0.01$  respectively

$\beta_0$ -band	p	Coh.	$R^2$	p	pCoh.	$R^2$
FP1-O1	0.975		0.001	<0.001**		0.222
FP2-O2	0.598		0.017	0.016*		0.127
FP1-P3	0.771		0.008	0.084		0.078
FP2-P4	0.014*		0.130	0.158		0.059
F3-O1	0.755		0.009	0.848		0.005
F4-O2	0.166		0.057	0.032*		0.107
F3-P3	0.877		0.004	0.966		0.001
F4-P4	0.036*		0.103	0.093		0.075
C3-O1	0.372		0.032	0.088		0.077
C4-O2	0.002**		0.184	0.059		0.089

The analysis on the whole signal revealed significant changes of coherences between C4-O2 ( $R^2 = 0.129$ ), and of partial coherences between F4-P4 ( $R^2 = 0.108$ ). Partial coherences yielded high significance between F3-O1 ( $R^2 = 0.181$ ). The bivariate Granger causality yielded significant results between FP1  $\rightarrow$  P3 ( $R^2 = 0.095$ ), F3  $\rightarrow$  O1 ( $R^2 = 0.102$ ), and C4  $\rightarrow$  O2 ( $R^2 = 0.100$ ). For FP2  $\rightarrow$  P4, high significance was reached ( $R^2 = 0.195$ ). Changes of conditional Granger causalities were significant between C3  $\rightarrow$  O1 ( $R^2 = 0.117$ ). Table 3.1.7 provides the resting state results for the far intrahemispheric channel pairs on the whole signal.

**Table 3.1.7:** Significance  $p$  and coefficient of determination  $R^2$  as determined by Fisher's F-test for a least squares quadratic regression model: measures between far intrahemispheric channel pairs on the whole EEG signals in resting state; "\*" and "\*\*" indicate  $p < 0.05$  and  $p < 0.01$  respectively. For directed measures, the first line per channel pair indicates the first direction of dependence (e.g. from FP1  $\rightarrow$  O1), and the second line indicates the second direction of dependence (e.g. from O1  $\rightarrow$  FP1).

total	Coh.		pCoh.		bGC		cGC	
	p	R <sup>2</sup>	p	R <sup>2</sup>	p	R <sup>2</sup>	p	R <sup>2</sup>
FP1-O1	0.154	0.060	0.296	0.039	0.239	0.046	0.050	0.094
					0.626	0.015	0.739	0.010
FP2-O2	0.567	0.018	0.359	0.033	0.685	0.012	0.098	0.073
					0.554	0.019	0.190	0.053
FP1-P3	0.765	0.009	0.190	0.053	0.788	0.008	0.230	0.047
					0.048*	0.095	0.450	0.026
FP2-P4	0.578	0.018	0.848	0.005	0.323	0.036	0.074	0.082
					0.001**	0.195	0.559	0.019
F3-O1	0.070	0.084	0.002**	0.181	0.037*	0.102	0.101	0.072
					0.918	0.003	0.502	0.022
F4-O2	0.056	0.090	0.313	0.037	0.425	0.028	0.145	0.061
					0.861	0.005	0.221	0.048
F3-P3	0.662	0.013	0.143	0.062	0.532	0.021	0.244	0.045
					0.857	0.005	0.225	0.048
F4-P4	0.246	0.045	0.031*	0.108	0.315	0.037	0.113	0.069
					0.436	0.027	0.261	0.043
C3-O1	0.332	0.036	0.285	0.040	0.581	0.018	0.022*	0.117
					0.335	0.035	0.645	0.014
C4-O2	0.015*	0.129	0.923	0.003	0.041*	0.100	0.099	0.073
					0.154	0.060	0.124	0.066

### Far Interhemispheric

Now, let us consider the far interhemispheric channel pairs (cf. Figure 2.9.1b). P7-P8 showed significant results in the  $\delta$ -frequency band for coherences ( $R^2 = 0.139$ ), and highly significant results for partial coherences ( $R^2 = 0.187$ ). Coherences yielded no further significant findings, whereas partial coherences yielded significance between T7-T8 ( $R^2 = 0.107$ ), C3-C4 ( $R^2 = 0.141$ ), and P3-P4 ( $R^2 = 0.114$ ). Table 3.1.8 provides the resting state results for the far interhemispheric channel pairs in the  $\delta$ -frequency band.

**Table 3.1.8:** Significance  $p$  and coefficient of determination  $R^2$  as determined by Fisher's F-test for a least squares quadratic regression model: measures between far interhemispheric channel pairs in the  $\delta$ -frequency band in resting state; "\*" and "\*\*" indicate  $p < 0.05$  and  $p < 0.01$  respectively

$\delta$ -band	Coh.		pCoh.	
	$p$	$R^2$	$p$	$R^2$
F7-F8	0.051	0.093	0.100	0.073
F3-F4	0.550	0.019	0.368	0.032
T7-T8	0.514	0.022	0.031*	0.107
C3-C4	0.432	0.027	0.010*	0.141
P7-P8	0.010*	0.139	0.002**	0.187
P3-P4	0.053	0.092	0.025*	0.114
O1-O2	0.145	0.061	0.102	0.072

In the  $\theta$ -frequency band, changes of coherences were significant between F7-F8 ( $R^2 = 0.100$ ), and P3-P4 ( $R^2 = 0.108$ ). The estimated partial coherences showed significant findings between P7-P8 ( $R^2 = 0.126$ ), and O1-O2 ( $R^2 = 0.098$ ), and highly significant results between T7-T8 ( $R^2 = 0.236$ ). Table 3.1.9 provides the resting state results for the far interhemispheric channel pairs in the  $\theta$ -frequency band.

The analysis in the  $\alpha$ -frequency band revealed significant results for coherences between P3-P4 ( $R^2 = 0.107$ ), and O1-O2 ( $R^2 = 0.099$ ). For the latter channel pair, changes of partial coherences were highly significant ( $R^2 = 0.155$ ). Table 3.1.10 provides the resting state results for the far interhemispheric channel pairs in the  $\alpha$ -frequency band.

In the  $\beta_0$ -frequency band, the channel pair O1-O2 yielded significant results for both coherences ( $R^2 = 0.123$ ) and partial coherences ( $R^2 = 0.137$ ). Additionally, significance was obtained for partial coherences between C3-C4 ( $R^2 = 0.103$ ), and high significance between P7-P8 ( $R^2 = 0.147$ ). Table 3.1.11 provides the resting state results for the far interhemispheric channel pairs in the  $\beta_0$ -frequency band.

**Table 3.1.9:** Significance  $p$  and coefficient of determination  $R^2$  as determined by Fisher's F-test for a least squares quadratic regression model: measures between far interhemispheric channel pairs in the  $\theta$ -frequency band in resting state; "\*" and "\*\*\*" indicate  $p < 0.05$  and  $p < 0.01$  respectively

$\theta$ -band	Coh.		pCoh.	
	p	$R^2$	p	$R^2$
F7-F8	0.040*	0.100	0.089	0.076
F3-F4	0.896	0.004	0.460	0.025
T7-T8	0.356	0.033	<0.001**	0.236
C3-C4	0.488	0.023	0.111	0.070
P7-P8	0.794	0.008	0.017*	0.126
P3-P4	0.031*	0.108	0.094	0.075
O1-O2	0.101	0.072	0.043*	0.098

**Table 3.1.10:** Significance  $p$  and coefficient of determination  $R^2$  as determined by Fisher's F-test for a least squares quadratic regression model: measures between far interhemispheric channel pairs in the  $\alpha$ -frequency band in resting state; "\*" and "\*\*\*" indicate  $p < 0.05$  and  $p < 0.01$  respectively

$\alpha$ -band	Coh.		pCoh.	
	p	$R^2$	p	$R^2$
F7-F8	0.997	<0.001	0.209	0.050
F3-F4	0.513	0.022	0.176	0.055
T7-T8	0.166	0.057	0.255	0.044
C3-C4	0.276	0.041	0.292	0.040
P7-P8	0.121	0.067	0.313	0.037
P3-P4	0.031*	0.107	0.247	0.045
O1-O2	0.041*	0.099	0.006**	0.155

**Table 3.1.11:** Significance  $p$  and coefficient of determination  $R^2$  as determined by Fisher's F-test for a least squares quadratic regression model: measures between far interhemispheric channel pairs in the  $\beta_0$ -frequency band in resting state; "\*" and "\*\*\*" indicate  $p < 0.05$  and  $p < 0.01$  respectively

$\beta_0$ -band	Coh.		pCoh.	
	p	$R^2$	p	$R^2$
F7-F8	0.614	0.016	0.100	0.073
F3-F4	0.525	0.021	0.390	0.030
T7-T8	0.996	<0.001	0.114	0.069
C3-C4	0.669	0.013	0.036*	0.103
P7-P8	0.256	0.044	0.008**	0.147
P3-P4	0.149	0.060	0.293	0.039
O1-O2	0.018*	0.123	0.011*	0.137

The analysis of far interhemispheric channel pairs on the whole EEG signals showed significant changes of coherences between P3-P4 ( $R^2 = 0.120$ ), and O1-O2 ( $R^2 = 0.099$ ). Partial coherences yielded significant findings between T7-T8 ( $R^2 = 0.127$ ), C3-C4 ( $R^2 = 0.108$ ), and O1-O2 ( $R^2 = 0.104$ ). No high significance was observed. Bivariate Granger causalities yielded significant results between F4  $\rightarrow$  F3 ( $R^2 = 0.106$ ), and P4  $\rightarrow$  P3 ( $R^2 = 0.138$ ). None of the channel pairs showed significant changes in the reverse direction. For conditional Granger causalities, changes were significant between F7  $\rightarrow$  F8 ( $R^2 = 0.126$ ), and T7  $\rightarrow$  T8 ( $R^2 = 0.110$ ). Table 3.1.12 provides the resting state results for the far interhemispheric channel pairs on the whole EEG signals.

**Table 3.1.12:** Significance  $p$  and coefficient of determination  $R^2$  as determined by Fisher's F-test for a least squares quadratic regression model: measures between far interhemispheric channel pairs on the whole EEG signals in resting state; "\*" and "\*\*\*" indicate  $p < 0.05$  and  $p < 0.01$  respectively. For directed measures, the first line per channel pair indicates the first direction of dependence (e.g. from F7  $\rightarrow$  F8), and the second line indicates the second direction of dependence (e.g. from F8  $\rightarrow$  F7).

total	Coh.		pCoh.		bGC		cGC	
	p	R <sup>2</sup>	p	R <sup>2</sup>	p	R <sup>2</sup>	p	R <sup>2</sup>
F7-F8	0.396	0.030	0.105	0.071	0.213	0.049	0.017*	0.126
					0.942	0.002	0.515	0.022
F3-F4	0.883	0.004	0.245	0.045	0.201	0.051	0.191	0.053
					0.032*	0.106	0.229	0.047
T7-T8	0.252	0.044	0.016*	0.127	0.405	0.029	0.029*	0.110
					0.379	0.031	0.762	0.009
C3-C4	0.343	0.034	0.030*	0.108	0.547	0.020	0.050	0.094
					0.425	0.028	0.373	0.032
P7-P8	0.143	0.062	0.567	0.018	0.422	0.028	0.744	0.010
					0.370	0.032	0.059	0.089
P3-P4	0.020*	0.120	0.094	0.075	0.533	0.020	0.085	0.078
					0.011*	0.138	0.505	0.022
O1-O2	0.042*	0.099	0.035*	0.104	0.217	0.049	0.201	0.051
					0.086	0.077	0.068	0.084

### Local Anterior

Now, let us consider the local anterior channel pairs (cf. Figure 2.9.1c). The analysis of coherences in the  $\delta$ -frequency band yielded significant findings between FP1-F7 ( $R^2 = 0.100$ ), and FP1-F3 ( $R^2 = 0.115$ ), and highly significant findings between FP2-F8 ( $R^2 = 0.161$ ). For partial coherences, changes were highly significant between F7-T7 ( $R^2 = 0.203$ ). Table 3.1.13 provides the resting state results for the local anterior channel pairs in the  $\delta$ -frequency band.

**Table 3.1.13:** Significance  $p$  and coefficient of determination  $R^2$  as determined by Fisher's F-test for a least squares quadratic regression model: measures between local anterior channel pairs in the  $\delta$ -frequency band in resting state; "\*" and "\*\*\*" indicate  $p < 0.05$  and  $p < 0.01$  respectively

$\delta$ -band	Coh.		pCoh.	
	$p$	$R^2$	$p$	$R^2$
FP1-F7	0.040*	0.100	0.063	0.086
FP2-F8	0.005**	0.161	0.261	0.043
FP1-F3	0.024*	0.115	0.834	0.006
FP2-F4	0.155	0.059	0.342	0.035
F7-C3	0.244	0.045	0.446	0.026
F8-C4	0.388	0.031	0.940	0.002
F7-T7	0.594	0.017	0.001**	0.203
F8-T8	0.950	0.002	0.358	0.033
F3-C3	0.756	0.009	0.639	0.015
F4-C4	0.963	0.001	0.163	0.058

In the  $\theta$ -frequency band, no significant changes of coherences were observed. Partial coherences yielded highly significance between F7-T7 ( $R^2 = 0.223$ ). Table 3.1.14 provides the resting state results for the local anterior channel pairs in the  $\theta$ -frequency band.

In the  $\alpha$ -frequency band, no significant changes of coherences were observed. Partial coherences yielded significant findings between F7-T7 ( $R^2 = 0.104$ ). Table 3.1.15 provides the resting state results for the local anterior channel pairs in the  $\alpha$ -frequency band.

The analysis in the  $\beta_0$ -frequency band showed no significant findings for neither coherences nor partial coherences. Table 3.1.16 provides the resting state results for the local anterior channel pairs in the  $\beta_0$ -frequency band.

Coherences yielded no significant results between local anterior channels on the whole EEG signals. For F7-T7, changes of partial coherences were highly significant ( $R^2 = 0.166$ ). Also bivariate Granger causalities yielded high significance between  $F7 \rightarrow T7$  ( $R^2 = 0.146$ ). Additionally, changes of bivariate Granger



**Table 3.1.14:** Significance  $p$  and coefficient of determination  $R^2$  as determined by Fisher's F-test for a least squares quadratic regression model: measures between local anterior channel pairs in the  $\theta$ -frequency band in resting state; "\*" and "\*\*\*" indicate  $p < 0.05$  and  $p < 0.01$  respectively

$\theta$ -band	Coh.		pCoh.	
	p	$R^2$	p	$R^2$
FP1-F7	0.121	0.067	0.359	0.033
FP2-F8	0.053	0.092	0.813	0.007
FP1-F3	0.189	0.053	0.754	0.009
FP2-F4	0.386	0.031	0.110	0.070
F7-C3	0.829	0.006	0.917	0.003
F8-C4	0.467	0.025	0.525	0.021
F7-T7	0.638	0.015	<0.001**	0.223
F8-T8	0.714	0.011	0.313	0.037
F3-C3	0.816	0.007	0.876	0.004
F4-C4	0.915	0.003	0.151	0.060

**Table 3.1.15:** Significance  $p$  and coefficient of determination  $R^2$  as determined by Fisher's F-test for a least squares quadratic regression model: measures between local anterior channel pairs in the  $\alpha$ -frequency band in resting state; "\*" and "\*\*\*" indicate  $p < 0.05$  and  $p < 0.01$  respectively

$\alpha$ -band	Coh.		pCoh.	
	p	$R^2$	p	$R^2$
FP1-F7	0.927	0.002	0.263	0.043
FP2-F8	0.817	0.007	0.457	0.025
FP1-F3	0.589	0.017	0.649	0.014
FP2-F4	0.767	0.009	0.241	0.046
F7-C3	0.488	0.023	0.986	<0.001
F8-C4	0.488	0.023	0.338	0.035
F7-T7	0.328	0.036	0.035*	0.104
F8-T8	0.565	0.019	0.765	0.009
F3-C3	0.639	0.015	0.957	0.001
F4-C4	0.929	0.002	0.383	0.031

causalities were highly significant between  $FP1 \rightarrow F3$  ( $R^2 = 0.200$ ), and significant between  $F3 \rightarrow FP1$  ( $R^2 = 0.110$ ). Conditional Granger causalities yielded significant findings between  $FP2 \rightarrow F4$  ( $R^2 = 0.109$ ). Table 3.1.17 provides the resting state results for the local anterior channel pairs on the whole EEG signals.

**Table 3.1.16:** Significance  $p$  and coefficient of determination  $R^2$  as determined by Fisher's F-test for a least squares quadratic regression model: measures between local anterior channel pairs in the  $\beta_0$ -frequency band in resting state; "\*" and "\*\*\*" indicate  $p < 0.05$  and  $p < 0.01$  respectively

$\beta_0$ -band	Coh.		pCoh.	
	p	$R^2$	p	$R^2$
FP1-F7	0.938	0.002	0.484	0.024
FP2-F8	0.829	0.006	0.347	0.034
FP1-F3	0.688	0.012	0.344	0.034
FP2-F4	0.281	0.041	0.228	0.047
F7-C3	0.792	0.008	0.356	0.033
F8-C4	0.967	0.001	0.060	0.088
F7-T7	0.120	0.067	0.457	0.025
F8-T8	0.891	0.004	0.912	0.003
F3-C3	0.623	0.015	0.766	0.009
F4-C4	0.327	0.036	0.414	0.028

**Table 3.1.17:** Significance  $p$  and coefficient of determination  $R^2$  as determined by Fisher's F-test for a least squares quadratic regression model: measures between local anterior channel pairs in the total frequency band in resting state; "\*" and "\*\*\*" indicate  $p < 0.05$  and  $p < 0.01$  respectively. For directed measures, the first line per channel pair indicates the first direction of dependence (e.g. from FP7  $\rightarrow$  F7), and the second line indicates the second direction of dependence (e.g. from F7  $\rightarrow$  FP7).

total	Coh.		pCoh.		bGC		cGC	
	p	$R^2$	p	$R^2$	p	$R^2$	p	$R^2$
FP1-F7	0.461	0.025	0.224	0.048	0.475	0.024	0.147	0.061
					0.073	0.082	0.105	0.071
FP2-F8	0.340	0.035	0.455	0.025	0.717	0.011	0.096	0.074
					0.302	0.038	0.351	0.034
FP1-F3	0.322	0.036	0.688	0.012	0.001**	0.200	0.050	0.093
					0.028*	0.110	0.262	0.043
FP2-F4	0.421	0.028	0.223	0.048	0.873	0.004	0.030*	0.109
					0.853	0.005	0.244	0.045
F7-C3	0.583	0.018	0.921	0.003	0.678	0.013	0.089	0.076
					0.217	0.049	0.471	0.024
F8-C4	0.555	0.019	0.291	0.040	0.494	0.023	0.054	0.091
					0.942	0.002	0.122	0.067
F7-T7	0.301	0.039	0.004**	0.166	0.008**	0.146	0.114	0.069
					0.954	0.002	0.296	0.039
F8-T8	0.712	0.011	0.562	0.019	0.897	0.004	0.257	0.044
					0.922	0.003	0.144	0.062
F3-C3	0.733	0.010	0.962	0.001	0.995	<0.001	0.362	0.033
					0.319	0.037	0.123	0.066
F4-C4	0.841	0.006	0.275	0.041	0.751	0.009	0.112	0.069
					0.747	0.010	0.088	0.077

### Local Posterior

The resting state analysis of local posterior channel pairs (cf. Figure 2.9.1d) in the  $\delta$ -frequency band showed significant changes of coherences between C3-P7 ( $R^2 = 0.115$ ), C4-P8 ( $R^2 = 0.104$ ), and P3-P7 ( $R^2 = 0.118$ ). Partial coherences yielded significant results between C4-P8 ( $R^2 = 0.117$ ), P3-C3 ( $R^2 = 0.117$ ), and P4-P8 ( $R^2 = 0.140$ ), and highly significant results between C3-P7 ( $R^2 = 0.236$ ). Table 3.1.18 provides the resting state results for the local posterior channel pairs in the  $\delta$ -frequency band.

**Table 3.1.18:** Significance  $p$  and coefficient of determination  $R^2$  as determined by Fisher's F-test for a least squares quadratic regression model: measures between local posterior channel pairs in the  $\delta$ -frequency band in resting state; "\*" and "\*\*\*" indicate  $p < 0.05$  and  $p < 0.01$  respectively

$\delta$ -band	Coh.		pCoh.	
	$p$	$R^2$	$p$	$R^2$
P7-O1	0.069	0.084	0.266	0.042
P8-O2	0.751	0.009	0.296	0.039
P3-O1	0.602	0.016	0.645	0.014
P4-O2	0.113	0.069	0.774	0.008
C3-P7	0.024*	0.115	<0.001**	0.236
C4-P8	0.035*	0.104	0.022*	0.117
P3-C3	0.102	0.072	0.022*	0.117
P4-C4	0.077	0.081	0.072	0.083
P3-P7	0.022*	0.118	0.430	0.027
P4-P8	0.360	0.033	0.010*	0.140

In the  $\theta$ -frequency band, coherences yielded significant results only between C4-P8 ( $R^2 = 0.101$ ), whereas partial coherences yielded significance between P3-C3 ( $R^2 = 0.108$ ), and high significance between C3-P7 ( $R^2 = 0.229$ ). Table 3.1.19 provides the resting state results for the local posterior channel pairs in the  $\theta$ -frequency band.

In the  $\alpha$ -frequency band, changes of coherences were significant only between C4-P8 ( $R^2 = 0.102$ ). No significant changes of partial coherences were observed. Table 3.1.20 provides the resting state results for the local posterior channel pairs in the  $\alpha$ -frequency band.

In the  $\beta_0$ -frequency band, the analysis of coherences showed significant findings between P4-O2 ( $R^2 = 0.131$ ) and P4-P8 ( $R^2 = 0.123$ ), and in highly significant findings between C4-P8 ( $R^2 = 0.166$ ) and P4-C4 ( $R^2 = 0.179$ ). For partial coherences, the quadratic regression was significant between P3-P7 ( $R^2 = 0.120$ ). Table 3.1.21 provides the resting state results for the local posterior channel pairs

**Table 3.1.19:** Significance  $p$  and coefficient of determination  $R^2$  as determined by Fisher's F-test for a least squares quadratic regression model: measures between local posterior channel pairs in the  $\theta$ -frequency band in resting state; "\*" and "\*\*\*" indicate  $p < 0.05$  and  $p < 0.01$  respectively

$\theta$ -band	Coh.		pCoh.	
	$p$	$R^2$	$p$	$R^2$
P7-O1	0.143	0.062	0.339	0.035
P8-O2	0.450	0.026	0.314	0.037
P3-O1	0.408	0.029	0.964	0.001
P4-O2	0.155	0.059	0.783	0.008
C3-P7	0.150	0.060	<0.001**	0.229
C4-P8	0.039*	0.101	0.351	0.034
P3-C3	0.179	0.055	0.030*	0.108
P4-C4	0.354	0.033	0.212	0.050
P3-P7	0.062	0.087	0.333	0.035
P4-P8	0.094	0.075	0.118	0.068

**Table 3.1.20:** Significance  $p$  and coefficient of determination  $R^2$  as determined by Fisher's F-test for a least squares quadratic regression model: measures between local posterior channel pairs in the  $\alpha$ -frequency band in resting state; "\*" and "\*\*\*" indicate  $p < 0.05$  and  $p < 0.01$  respectively

$\alpha$ -band	Coh.		pCoh.	
	$p$	$R^2$	$p$	$R^2$
P7-O1	0.424	0.028	0.808	0.007
P8-O2	0.225	0.048	0.589	0.017
P3-O1	0.080	0.080	0.192	0.053
P4-O2	0.118	0.068	0.411	0.029
C3-P7	0.715	0.011	0.191	0.053
C4-P8	0.037*	0.102	0.084	0.078
P3-C3	0.641	0.014	0.467	0.025
P4-C4	0.170	0.057	0.460	0.025
P3-P7	0.429	0.027	0.082	0.079
P4-P8	0.144	0.061	0.212	0.050

in the  $\beta_0$ -frequency band.

On the whole EEG signals, both coherences and partial coherences yielded significant changes between C4-P8 ( $R^2 = 0.135$  and  $R^2 = 0.098$ ). Additionally, high significance was observed for partial coherences between C3-P7 ( $R^2 = 0.205$ ). The analysis of conditional Granger causalities revealed significant changes between P3  $\rightarrow$  O1 ( $R^2 = 0.102$ ). Table 3.1.22 provides the resting state results for the local posterior channel pairs on the whole EEG signals.

**Table 3.1.21:** Significance  $p$  and coefficient of determination  $R^2$  as determined by Fisher's F-test for a least squares quadratic regression model: measures between local posterior channel pairs in the  $\beta_0$ -frequency band in resting state; "\*" and "\*\*\*" indicate  $p < 0.05$  and  $p < 0.01$  respectively

$\beta_0$ -band	Coh.		pCoh.	
	p	$R^2$	p	$R^2$
P7-O1	0.779	0.008	0.748	0.009
P8-O2	0.146	0.061	0.545	0.020
P3-O1	0.230	0.047	0.080	0.080
P4-O2	0.014*	0.131	0.122	0.067
C3-P7	0.498	0.023	0.142	0.062
C4-P8	0.004**	0.166	0.241	0.046
P3-C3	0.125	0.066	0.334	0.035
P4-C4	0.002**	0.179	0.170	0.056
P3-P7	0.210	0.050	0.020*	0.120
P4-P8	0.018*	0.123	0.176	0.055

**Table 3.1.22:** Significance  $p$  and coefficient of determination  $R^2$  as determined by Fisher's F-test for a least squares quadratic regression model: measures between local posterior channel pairs in the total frequency band in resting state; "\*" and "\*\*\*" indicate  $p < 0.05$  and  $p < 0.01$  respectively. For directed measures, the first line per channel pair indicates the first direction of dependence (e.g. from P7  $\rightarrow$  O1), and the second line indicates the second direction of dependence (e.g. from O1  $\rightarrow$  P7).

total	Coh.		pCoh.		bGC		cGC	
	p	$R^2$	p	$R^2$	p	$R^2$	p	$R^2$
P7-O1	0.260	0.043	0.594	0.017	0.592	0.017	0.097	0.074
					0.635	0.015	0.264	0.043
P8-O2	0.327	0.036	0.486	0.023	0.733	0.010	0.108	0.070
					0.737	0.010	0.857	0.005
P3-O1	0.280	0.041	0.487	0.023	0.140	0.062	0.037*	0.102
					0.084	0.078	0.461	0.025
P4-O2	0.125	0.066	0.515	0.021	0.133	0.064	0.187	0.054
					0.909	0.003	0.135	0.064
C3-P7	0.274	0.042	0.001**	0.205	0.489	0.023	0.072	0.082
					0.150	0.060	0.603	0.016
C4-P8	0.012*	0.135	0.043*	0.098	0.166	0.057	0.394	0.030
					0.144	0.062	0.051	0.093
P3-C3	0.240	0.046	0.120	0.067	0.582	0.018	0.422	0.028
					0.611	0.016	0.061	0.088
P4-C4	0.103	0.072	0.257	0.044	0.424	0.028	0.124	0.066
					0.551	0.019	0.055	0.091
P3-P7	0.125	0.066	0.131	0.065	0.286	0.040	0.111	0.069
					0.169	0.057	0.256	0.044
P4-P8	0.072	0.083	0.124	0.066	0.877	0.004	0.901	0.003
					0.295	0.039	0.097	0.074

### 3.1.3 Detailed Results: Cognitive Task

This section will provide all findings of channel pair analyses during the cognitive task. As in the previous section, the results will be divided into far intrahemispheric, far interhemispheric, local anterior, and local posterior pairs (cf. Figures 2.9.1a - 2.9.1d).

#### Far Intrahemispheric

First, let us consider the far intrahemispheric channel pairs. In the  $\delta$ -frequency band, only coherences between C4-O2 ( $R^2 = 0.135$ ) showed significant test results. Table 3.1.23 provides the cognitive task results for all far intrahemispheric channel pairs in the  $\delta$ -frequency band.

**Table 3.1.23:** Significance  $p$  and coefficient of determination  $R^2$  as determined by Fisher's F-test for a least squares quadratic regression model: measures between far intrahemispheric channel pairs in the  $\delta$ -frequency band during the cognitive task; "\*" and "\*\*\*" indicate  $p < 0.05$  and  $p < 0.01$  respectively

$\delta$ -band	Coh.		pCoh.	
	p	$R^2$	p	$R^2$
FP1-O1	0.503	0.023	0.414	0.029
FP2-O2	0.578	0.018	0.824	0.007
FP1-P3	0.865	0.005	0.050	0.097
FP2-P4	0.755	0.009	0.106	0.073
F3-O1	0.607	0.017	0.051	0.096
F4-O2	0.054	0.094	0.372	0.033
F3-P3	0.760	0.009	0.158	0.061
F4-P4	0.192	0.054	0.052	0.095
C3-O1	0.108	0.073	0.704	0.012
C4-O2	0.014*	0.135	0.113	0.071

The analysis in the  $\theta$ -frequency band showed significant changes of coherences between C4-O2 ( $R^2 = 0.109$ ), and highly significant changes of partial coherences between F4-P4 ( $R^2 = 0.151$ ). Table 3.1.24 provides the cognitive task results for all far intrahemispheric channel pairs in the  $\theta$ -frequency band.

In the  $\alpha$ -frequency band, the quadratic regression model was significant for coherences between F4-O2 ( $R^2 = 0.105$ ), and C4-O2 ( $R^2 = 0.127$ ). For partial coherences, high significance was obtained between F3-P3 ( $R^2 = 0.212$ ). Table 3.1.25 provides the cognitive task results for all far intrahemispheric channel pairs in the  $\alpha$ -frequency band.

**Table 3.1.24:** Significance  $p$  and coefficient of determination  $R^2$  as determined by Fisher's F-test for a least squares quadratic regression model: measures between far intrahemispheric channel pairs in the  $\theta$ -frequency band during the cognitive task; "\*" and "\*\*\*" indicate  $p < 0.05$  and  $p < 0.01$  respectively

$\theta$ -band	Coh.		pCoh.	
	p	$R^2$	p	$R^2$
FP1-O1	0.618	0.016	0.838	0.006
FP2-O2	0.665	0.014	0.394	0.031
FP1-P3	0.264	0.044	0.068	0.087
FP2-P4	0.864	0.005	0.937	0.002
F3-O1	0.731	0.011	0.263	0.044
F4-O2	0.297	0.040	0.216	0.051
F3-P3	0.226	0.049	0.110	0.072
F4-P4	0.088	0.079	0.008**	0.151
C3-O1	0.175	0.057	0.560	0.019
C4-O2	0.033*	0.109	0.208	0.052

**Table 3.1.25:** Significance  $p$  and coefficient of determination  $R^2$  as determined by Fisher's F-test for a least squares quadratic regression model: measures between far intrahemispheric channel pairs in the  $\alpha$ -frequency band during the cognitive task; "\*" and "\*\*\*" indicate  $p < 0.05$  and  $p < 0.01$  respectively

$\alpha$ -band	Coh.		pCoh.	
	p	$R^2$	p	$R^2$
FP1-O1	0.515	0.022	0.293	0.041
FP2-O2	0.251	0.046	0.109	0.072
FP1-P3	0.768	0.009	0.613	0.016
FP2-P4	0.714	0.011	0.061	0.090
F3-O1	0.273	0.043	0.067	0.088
F4-O2	0.038*	0.105	0.821	0.007
F3-P3	0.562	0.019	0.001**	0.212
F4-P4	0.206	0.052	0.398	0.031
C3-O1	0.177	0.057	0.770	0.009
C4-O2	0.018*	0.127	0.761	0.009

Significant changes of coherences between C4-O2 ( $R^2 = 0.107$ ) were observed in the  $\beta_0$ -frequency band. None of the other channel pairs showed significant test results, neither for coherences nor for partial coherences. Table 3.1.26 provides the cognitive task results for all far intrahemispheric channel pairs in the  $\beta_0$ -frequency band.

On the whole EEG signals, significant changes of coherences were observed between C4-O2 ( $R^2 = 0.128$ ). Partial coherences yielded significant results between

**Table 3.1.26:** Significance  $p$  and coefficient of determination  $R^2$  as determined by Fisher's F-test for a least squares quadratic regression model: measures between far intrahemispheric channel pairs in the  $\beta_0$ -frequency band during the cognitive task; "\*" and "\*\*" indicate  $p < 0.05$  and  $p < 0.01$  respectively

$\beta_0$ -band	Coh.		pCoh.	
	p	$R^2$	p	$R^2$
FP1-O1	0.622	0.016	0.472	0.025
FP2-O2	0.291	0.041	0.115	0.071
FP1-P3	0.351	0.035	0.357	0.034
FP2-P4	0.249	0.046	0.345	0.035
F3-O1	0.217	0.050	0.918	0.003
F4-O2	0.185	0.056	0.896	0.004
F3-P3	0.715	0.011	0.434	0.028
F4-P4	0.052	0.095	0.917	0.003
C3-O1	0.125	0.068	0.833	0.006
C4-O2	0.035*	0.107	0.198	0.053

F3-O1 ( $R^2 = 0.117$ ), F3-P3 ( $R^2 = 0.146$ ), and F4-P4 ( $R^2 = 0.111$ ). Considering bivariate Granger causalities, the quadratic regression was significant between FP1  $\rightarrow$  P3 ( $R^2 = 0.098$ ) and P3  $\rightarrow$  F3 ( $R^2 = 0.107$ ), and highly significant between C3  $\rightarrow$  O1 ( $R^2 = 0.158$ ). Conditional Granger causalities yielded no significant findings. Table 3.1.27 provides the cognitive task results for all far intrahemispheric channel pairs on the whole EEG signals.



**Table 3.1.27:** Significance  $p$  and coefficient of determination  $R^2$  as determined by Fisher's F-test for a least squares quadratic regression model: measures between far intrahemispheric channel pairs on the whole EEG signals during the cognitive task; "\*" and "\*\*" indicate  $p < 0.05$  and  $p < 0.01$  respectively. For directed measures, the first line per channel pair indicates the first direction of dependence (e.g. from FP1  $\rightarrow$  O1), and the second line indicates the second direction of dependence (e.g. from O1  $\rightarrow$  FP1).

total	Coh.		pCoh.		bGC		cGC	
	p	R <sup>2</sup>	p	R <sup>2</sup>	p	R <sup>2</sup>	p	R <sup>2</sup>
FP1-O1	0.375	0.033	0.763	0.009	0.260	0.045	0.479	0.025
					0.724	0.011	0.800	0.008
FP2-O2	0.165	0.059	0.139	0.065	0.277	0.043	0.552	0.020
					0.265	0.044	0.592	0.018
FP1-P3	0.476	0.025	0.245	0.047	0.047*	0.098	0.914	0.003
					0.712	0.011	0.537	0.021
FP2-P4	0.833	0.006	0.204	0.053	0.754	0.010	0.542	0.021
					0.072	0.085	0.446	0.027
F3-O1	0.226	0.049	0.026*	0.117	0.406	0.030	0.301	0.040
					0.824	0.007	0.879	0.004
F4-O2	0.058	0.092	0.221	0.050	0.375	0.033	0.562	0.019
					0.202	0.053	0.234	0.048
F3-P3	0.546	0.020	0.010*	0.146	0.065	0.088	0.777	0.008
					0.036*	0.107	0.316	0.038
F4-P4	0.079	0.082	0.031*	0.111	0.952	0.002	0.919	0.003
					0.196	0.054	0.385	0.032
C3-O1	0.130	0.067	0.822	0.007	0.006**	0.158	0.138	0.065
					0.705	0.012	0.963	0.001
C4-O2	0.018*	0.128	0.316	0.038	0.238	0.047	0.516	0.022
					0.531	0.021	0.676	0.013

### Far Interhemispheric

Now, consider the far interhemispheric channel pairs (cf. Figure 2.9.1b). In the  $\delta$ -frequency band, no significant changes were observed. Table 3.1.28 provides the cognitive task results for all far interhemispheric channel pairs in the  $\delta$ -frequency band.

**Table 3.1.28:** Significance  $p$  and coefficient of determination  $R^2$  as determined by Fisher's F-test for a least squares quadratic regression model: measures between far interhemispheric channel pairs in the  $\delta$ -frequency band during the cognitive task; "\*" and "\*\*\*" indicate  $p < 0.05$  and  $p < 0.01$  respectively

$\delta$ -band	Coh.		pCoh.	
	$p$	$R^2$	$p$	$R^2$
F7-F8	0.533	0.021	0.042*	0.102
F3-F4	0.448	0.027	0.326	0.037
T7-T8	0.636	0.015	0.103	0.074
C3-C4	0.955	0.002	0.935	0.002
P7-P8	0.079	0.082	0.420	0.029
P3-P4	0.278	0.042	0.557	0.020
O1-O2	0.183	0.056	0.238	0.048

In the  $\theta$ -frequency band, coherences yielded significant findings between P3-P4 ( $R^2 = 0.141$ ), and O1-O2 ( $R^2 = 0.127$ ). The analysis of partial coherences showed significant results between T7-T8 ( $R^2 = 0.098$ ), and O1-O2 ( $R^2 = 0.106$ ). Table 3.1.29 provides the cognitive task results for all far interhemispheric channel pairs in the  $\theta$ -frequency band.

**Table 3.1.29:** Significance  $p$  and coefficient of determination  $R^2$  as determined by Fisher's F-test for a least squares quadratic regression model: measures between far interhemispheric channel pairs in the  $\theta$ -frequency band during the cognitive task; "\*" and "\*\*\*" indicate  $p < 0.05$  and  $p < 0.01$  respectively

$\theta$ -band	Coh.		pCoh.	
	$p$	$R^2$	$p$	$R^2$
F7-F8	0.229	0.049	0.287	0.041
F3-F4	0.862	0.005	0.694	0.012
T7-T8	0.921	0.003	0.048*	0.098
C3-C4	0.507	0.023	0.952	0.002
P7-P8	0.373	0.033	0.516	0.022
P3-P4	0.011*	0.141	0.333	0.037
O1-O2	0.018*	0.127	0.036*	0.106

In the  $\alpha$ -frequency band, significant changes of coherences ( $R^2 = 0.140$ )

and highly significant changes of partial coherences ( $R^2 = 0.168$ ) were observed between O1-O2. Table 3.1.30 provides the cognitive task results for all far interhemispheric channel pairs in the  $\alpha$ -frequency band.

**Table 3.1.30:** Significance  $p$  and coefficient of determination  $R^2$  as determined by Fisher's F-test for a least squares quadratic regression model: measures between far interhemispheric channel pairs in the  $\alpha$ -frequency band during the cognitive task; "\*" and "\*\*\*" indicate  $p < 0.05$  and  $p < 0.01$  respectively

$\alpha$ -band	$p$	Coh.	$R^2$	$p$	pCoh.	$R^2$
F7-F8	0.258		0.045	0.682		0.013
F3-F4	0.650		0.014	0.315		0.038
T7-T8	0.851		0.005	0.175		0.057
C3-C4	0.888		0.004	0.559		0.020
P7-P8	0.418		0.029	0.437		0.028
P3-P4	0.294		0.041	0.660		0.014
O1-O2	0.012*		0.140	0.004**		0.168

In the  $\beta_0$ -frequency band, both coherences and partial coherences yielded highly significant results between O1-O2 ( $R^2 = 0.152$  and  $R^2 = 0.203$ ). Additionally, highly significant changes of partial coherences were observed between T7-T8 ( $R^2 = 0.147$ ). Table 3.1.31 provides the cognitive task results for all far interhemispheric channel pairs in the  $\beta_0$ -frequency band.

**Table 3.1.31:** Significance  $p$  and coefficient of determination  $R^2$  as determined by Fisher's F-test for a least squares quadratic regression model: measures between far interhemispheric channel pairs in the  $\beta_0$ -frequency band during the cognitive task; "\*" and "\*\*\*" indicate  $p < 0.05$  and  $p < 0.01$  respectively

$\beta_0$ -band	$p$	Coh.	$R^2$	$p$	pCoh.	$R^2$
F7-F8	0.666		0.014	0.264		0.044
F3-F4	0.144		0.064	0.548		0.020
T7-T8	0.371		0.033	0.009**		0.147
C3-C4	0.897		0.004	0.291		0.041
P7-P8	0.584		0.018	0.253		0.045
P3-P4	0.323		0.038	0.121		0.069
O1-O2	0.008**		0.152	0.001**		0.203

On the whole EEG signals, significant changes of both coherences and partial coherences were observed between O1-O2 ( $R^2 = 0.142$  and  $R^2 = 0.139$ ). Whereas bivariate Granger causalities yielded no significant results, conditional

Granger causalities showed highly significant test results between F7 → F8 ( $R^2 = 0.173$ ), and significant results between C3 → C4 ( $R^2 = 0.100$ ). Table 3.1.32 provides the cognitive task results for all far interhemispheric channel pairs on the whole EEG signals.

**Table 3.1.32:** Significance  $p$  and coefficient of determination  $R^2$  as determined by Fisher's F-test for a least squares quadratic regression model: measures between far interhemispheric channel pairs on the whole EEG signals during the cognitive task; "\*" and "\*\*" indicate  $p < 0.05$  and  $p < 0.01$  respectively. For directed measures, the first line per channel pair indicates the first direction of dependence (e.g. from F7 → F8), and the second line indicates the second direction of dependence (e.g. from F8 → F7).

total	Coh.		pCoh.		bGC		cGC	
	p	R <sup>2</sup>	p	R <sup>2</sup>	p	R <sup>2</sup>	p	R <sup>2</sup>
F7-F8	0.256	0.045	0.287	0.041	0.774	0.009	0.004**	0.173
					0.857	0.005	0.604	0.017
F3-F4	0.741	0.010	0.752	0.010	0.639	0.015	0.113	0.071
					0.238	0.047	0.892	0.004
T7-T8	0.740	0.010	0.178	0.057	0.034	0.108	0.128	0.067
					0.262	0.044	0.416	0.029
C3-C4	0.904	0.003	0.996	<0.001	0.569	0.019	0.045*	0.100
					0.891	0.004	0.632	0.015
P7-P8	0.265	0.044	0.642	0.015	0.527	0.021	0.089	0.079
					0.691	0.012	0.170	0.058
P3-P4	0.091	0.078	0.619	0.016	0.066	0.088	0.459	0.026
					0.104	0.074	0.744	0.010
O1-O2	0.011*	0.142	0.012*	0.139	0.052	0.096	0.693	0.012
					0.687	0.013	0.605	0.017

### Local Anterior

Next, let us consider the local anterior channel pairs (cf. Figure 2.9.1c). In the  $\delta$ -frequency band, no significant changes of coherences were observed. Partial coherences yielded significance between F7-T7 ( $R^2 = 0.132$ ), and high significance between F8-T8 ( $R^2 = 0.149$ ). Table 3.1.33 provides the cognitive task results for all local anterior channel pairs in the  $\delta$ -frequency band.

**Table 3.1.33:** Significance  $p$  and coefficient of determination  $R^2$  as determined by Fisher's F-test for a least squares quadratic regression model: measures between local anterior channel pairs in the  $\delta$ -frequency band during the cognitive task; "\*" and "\*\*\*" indicate  $p < 0.05$  and  $p < 0.01$  respectively

$\delta$ -band	Coh.		pCoh.	
	p	$R^2$	p	$R^2$
FP1-F7	0.174	0.057	0.784	0.008
FP2-F8	0.947	0.002	0.653	0.014
FP1-F3	0.115	0.071	0.317	0.038
FP2-F4	0.381	0.032	0.155	0.061
F7-C3	0.143	0.064	0.820	0.007
F8-C4	0.074	0.084	0.321	0.038
F7-T7	0.692	0.012	0.016*	0.132
F8-T8	0.543	0.020	0.009**	0.149
F3-C3	0.545	0.020	0.532	0.021
F4-C4	0.420	0.029	0.066	0.088

In the  $\theta$ -frequency band, changes of coherences were significant between FP1-F7 ( $R^2 = 0.140$ ). Partial coherences yielded significant results between FP2-F4 ( $R^2 = 0.101$ ) and F8-T8 ( $R^2 = 0.128$ ), and highly significant results between F7-T7 ( $R^2 = 0.199$ ). Table 3.1.34 provides the cognitive task results for all local anterior channel pairs in the  $\theta$ -frequency band.

In the  $\alpha$ -frequency band, significant changes of coherences were found between FP1-F7 ( $R^2 = 0.102$ ). Partial coherences yielded significant results between FP2-F4 ( $R^2 = 0.098$ ) and F7-T7 ( $p = 0.019$ ,  $R^2 = 0.126$ ), and highly significant results between F8-T8 ( $R^2 = 0.155$ ). Table 3.1.35 provides the cognitive task results for all local anterior channel pairs in the  $\alpha$ -frequency band.

In the  $\beta_0$ -band, coherences yielded significant findings only between F4-C4 ( $R^2 = 0.106$ ). For partial coherences, no significant changes were observed. Table 3.1.36 provides the cognitive task results for all local anterior channel pairs in the  $\beta_0$ -frequency band.

On the whole EEG signals, coherences yielded significant results between FP1-

**Table 3.1.34:** Significance  $p$  and coefficient of determination  $R^2$  as determined by Fisher's F-test for a least squares quadratic regression model: measures between local anterior channel pairs in the  $\theta$ -frequency band during the cognitive task; "\*" and "\*\*\*" indicate  $p < 0.05$  and  $p < 0.01$  respectively

$\theta$ -band	Coh.		pCoh.	
	p	$R^2$	p	$R^2$
FP1-F7	0.012*	0.140	0.204	0.052
FP2-F8	0.734	0.010	0.851	0.005
FP1-F3	0.067	0.087	0.160	0.060
FP2-F4	0.634	0.015	0.043*	0.101
F7-C3	0.649	0.015	0.835	0.006
F8-C4	0.471	0.025	0.487	0.024
F7-T7	0.508	0.023	0.001**	0.199
F8-T8	0.734	0.010	0.018*	0.128
F3-C3	0.878	0.004	0.230	0.049
F4-C4	0.571	0.019	0.116	0.070

**Table 3.1.35:** Significance  $p$  and coefficient of determination  $R^2$  as determined by Fisher's F-test for a least squares quadratic regression model: measures between local anterior channel pairs in the  $\alpha$ -frequency band during the cognitive task; "\*" and "\*\*\*" indicate  $p < 0.05$  and  $p < 0.01$  respectively

$\alpha$ -band	Coh.		pCoh.	
	p	$R^2$	p	$R^2$
FP1-F7	0.043*	0.102	0.142	0.064
FP2-F8	0.703	0.012	0.572	0.019
FP1-F3	0.106	0.073	0.139	0.065
FP2-F4	0.766	0.009	0.048*	0.098
F7-C3	0.502	0.023	0.620	0.016
F8-C4	0.852	0.005	0.377	0.033
F7-T7	0.079	0.083	0.019*	0.126
F8-T8	0.085	0.080	0.007**	0.155
F3-C3	0.150	0.062	0.264	0.044
F4-C4	0.203	0.053	0.202	0.053

F7 ( $R^2 = 0.103$ ). Changes of partial coherences were significant between FP2-F4 ( $R^2 = 0.103$ ), and highly significant between F7-T7 ( $R^2 = 0.147$ ) and F8-T8 ( $R^2 = 0.153$ ). Bivariate Granger causalities yielded significant results between FP1  $\rightarrow$  F7 ( $R^2 = 0.111$ ), F3  $\rightarrow$  FP1 ( $R^2 = 0.134$ ), and F3  $\rightarrow$  C4 ( $R^2 = 0.130$ ). Between both F7  $\rightarrow$  T7 and T7  $\rightarrow$  F7, highly significant changes of bivariate Granger causalities were obtained ( $R^2 = 0.225$  and  $R^2 = 0.228$ ). Conditional Granger causalities yielded highly significant findings between T7  $\rightarrow$  F7 as well ( $R^2 = 0.168$ ). Table 3.1.37 provides the cognitive task results for all local anterior

**Table 3.1.36:** Significance  $p$  and coefficient of determination  $R^2$  as determined by Fisher's F-test for a least squares quadratic regression model: measures between local anterior channel pairs in the  $\beta_0$ -frequency band during the cognitive task; "\*" and "\*\*\*" indicate  $p < 0.05$  and  $p < 0.01$  respectively

$\beta_0$ -band	Coh.		pCoh.	
	p	$R^2$	p	$R^2$
FP1-F7	0.395	0.031	0.327	0.037
FP2-F8	0.844	0.006	0.887	0.004
FP1-F3	0.136	0.065	0.446	0.027
FP2-F4	0.207	0.052	0.234	0.048
F7-C3	0.467	0.025	0.355	0.035
F8-C4	0.202	0.053	0.530	0.021
F7-T7	0.214	0.051	0.727	0.011
F8-T8	0.104	0.074	0.132	0.066
F3-C3	0.316	0.038	0.733	0.010
F4-C4	0.037*	0.106	0.152	0.062

channel pairs on the whole EEG signals.

**Table 3.1.37:** Significance  $p$  and coefficient of determination  $R^2$  as determined by Fisher's F-test for a least squares quadratic regression model: measures between local anterior channel pairs on the whole EEG signals during the cognitive task; "\*" and "\*\*\*" indicate  $p < 0.05$  and  $p < 0.01$  respectively. For directed measures, the first line per channel pair indicates the first direction of dependence (e.g. from FP1  $\rightarrow$  F7), and the second line indicates the second direction of dependence (e.g. from F7  $\rightarrow$  FP1).

total	Coh.		pCoh.		bGC		cGC	
	p	R <sup>2</sup>	p	R <sup>2</sup>	p	R <sup>2</sup>	p	R <sup>2</sup>
FP1-F7	0.040*	0.103	0.220	0.050	0.031*	0.111	0.538	0.021
					0.770	0.009	0.219	0.050
FP2-F8	0.797	0.008	0.910	0.003	0.462	0.026	0.229	0.049
					0.186	0.055	0.467	0.025
FP1-F3	0.096	0.076	0.132	0.066	0.583	0.018	0.626	0.016
					0.015*	0.134	0.478	0.025
FP2-F4	0.763	0.009	0.040*	0.103	0.831	0.006	0.406	0.030
					0.554	0.020	0.208	0.052
F7-C3	0.691	0.012	0.771	0.009	0.780	0.008	0.710	0.012
					0.745	0.010	0.118	0.070
F8-C4	0.836	0.006	0.438	0.028	0.062	0.090	0.192	0.054
					0.876	0.004	0.071	0.086
F7-T7	0.182	0.056	0.009**	0.147	0.001**	0.225	0.123	0.069
					<0.001**	0.228	0.004**	0.168
F8-T8	0.325	0.037	0.007**	0.153	0.455	0.026	0.894	0.004
					0.222	0.050	0.261	0.044
F3-C3	0.599	0.017	0.348	0.035	0.310	0.039	0.971	0.001
					0.663	0.014	0.066	0.088
F4-C4	0.238	0.048	0.110	0.072	0.017*	0.130	0.579	0.018
					0.182	0.056	0.272	0.043



### Local Posterior

Now, consider the local posterior channel pairs (cf. Figure 2.9.1d). In the  $\delta$ -frequency band, changes of coherences were significant between P7-O1 ( $R^2 = 0.125$ ), C3-P7 ( $R^2 = 0.124$ ), and P4-C4 ( $R^2 = 0.124$ ), and highly significant between C4-P8 ( $R^2 = 0.148$ ), P3-P7 ( $R^2 = 0.171$ ), and P4-P8 ( $R^2 = 0.149$ ). Partial coherences yielded significant results between P4-C4 ( $R^2 = 0.110$ ), P3-P7 ( $R^2 = 0.128$ ), and P4-P8 ( $R^2 = 0.129$ ). Table 3.1.38 provides the cognitive task results for all local posterior channel pairs in the  $\delta$ -frequency band.

**Table 3.1.38:** Significance  $p$  and coefficient of determination  $R^2$  as determined by Fisher's F-test for a least squares quadratic regression model: measures between local posterior channel pairs in the  $\delta$ -frequency band during the cognitive task; "\*" and "\*\*\*" indicate  $p < 0.05$  and  $p < 0.01$  respectively

$\delta$ -band	Coh.		pCoh.	
	$p$	$R^2$	$p$	$R^2$
P7-O1	0.020*	0.125	0.415	0.029
P8-O2	0.233	0.048	0.226	0.049
P3-O1	0.144	0.064	0.394	0.031
P4-O2	0.054	0.094	0.162	0.060
C3-P7	0.020*	0.124	0.418	0.029
C4-P8	0.009**	0.148	0.736	0.010
P3-C3	0.084	0.081	0.314	0.038
P4-C4	0.020*	0.124	0.032*	0.110
P3-P7	0.004**	0.171	0.017*	0.128
P4-P8	0.008**	0.149	0.017*	0.129

In the  $\theta$ -frequency band, significant changes of coherences were observed between C3-P7 ( $R^2 = 0.129$ ), P4-C4 ( $R^2 = 0.118$ ), and P3-P7 ( $R^2 = 0.134$ ); high significances were obtained between C4-P8 ( $R^2 = 0.225$ ), P3-C3 ( $R^2 = 0.171$ ), and P4-P8 ( $R^2 = 0.250$ ). Partial coherences yielded significant findings between C3-P7 ( $R^2 = 0.104$ ), P3-P7 ( $R^2 = 0.099$ ), and P4-P8 ( $R^2 = 0.110$ ). Table 3.1.39 provides the cognitive task results for all local posterior channel pairs in the  $\theta$ -frequency band.

The analysis of coherences in the  $\alpha$ -frequency band yielded significant findings between C4-P8 ( $R^2 = 0.110$ ), and highly significant findings between the parietal channels P3-P7 ( $R^2 = 0.183$ ) and P4-P8 ( $R^2 = 0.161$ ). Changes of partial coherences were significant between P4-P8 as well ( $R^2 = 0.115$ ). Table 3.1.40 provides the cognitive task results for all local posterior channel pairs in the  $\alpha$ -frequency band.

In the  $\beta_0$ -frequency band, quadratic regressions of coherences were significant

**Table 3.1.39:** Significance  $p$  and coefficient of determination  $R^2$  as determined by Fisher's F-test for a least squares quadratic regression model: measures between local posterior channel pairs in the  $\theta$ -frequency band during the cognitive task; "\*" and "\*\*\*" indicate  $p < 0.05$  and  $p < 0.01$  respectively

$\theta$ -band	Coh.		pCoh.	
	p	$R^2$	p	$R^2$
P7-O1	0.235	0.048	0.744	0.010
P8-O2	0.229	0.049	0.163	0.060
P3-O1	0.959	0.001	0.133	0.066
P4-O2	0.107	0.073	0.556	0.020
C3-P7	0.017*	0.129	0.039*	0.104
C4-P8	0.001**	0.225	0.033*	0.109
P3-C3	0.004**	0.171	0.172	0.058
P4-C4	0.025*	0.118	0.145	0.063
P3-P7	0.014*	0.134	0.046*	0.099
P4-P8	<0.001**	0.250	0.032*	0.110

**Table 3.1.40:** Significance  $p$  and coefficient of determination  $R^2$  as determined by Fisher's F-test for a least squares quadratic regression model: measures between local posterior channel pairs in the  $\alpha$ -frequency band during the cognitive task; "\*" and "\*\*\*" indicate  $p < 0.05$  and  $p < 0.01$  respectively

$\alpha$ -band	Coh.		pCoh.	
	p	$R^2$	p	$R^2$
P7-O1	0.068	0.087	0.926	0.003
P8-O2	0.111	0.072	0.419	0.029
P3-O1	0.312	0.039	0.162	0.060
P4-O2	0.052	0.095	0.926	0.003
C3-P7	0.050	0.096	0.284	0.042
C4-P8	0.032*	0.110	0.650	0.014
P3-C3	0.068	0.087	0.148	0.063
P4-C4	0.234	0.048	0.502	0.023
P3-P7	0.003**	0.183	0.056	0.093
P4-P8	0.006**	0.161	0.028*	0.115

between P8-O2 ( $R^2 = 0.100$ ), P4-O2 ( $R^2 = 0.135$ ), C3-P7 ( $R^2 = 0.110$ ), C4-P8 ( $R^2 = 0.100$ ), and P4-P8 ( $R^2 = 0.113$ ), and highly significant between P7-O1 ( $R^2 = 0.188$ ) and P3-P7 ( $R^2 = 0.215$ ). Partial coherences yielded significant findings only between P4-P8 ( $R^2 = 0.101$ ). Table 3.1.41 provides the cognitive task results for all local posterior channel pairs in the  $\beta_0$ -frequency band.

Finally, for the whole EEG signals, significant changes of coherences were observed between P7-O1 ( $R^2 = 0.104$ ), C3-P7 ( $R^2 = 0.131$ ), and P3-C3 ( $R^2 =$

**Table 3.1.41:** Significance  $p$  and coefficient of determination  $R^2$  as determined by Fisher's F-test for a least squares quadratic regression model: measures between local posterior channel pairs in the  $\beta_0$ -frequency band during the cognitive task; "\*" and "\*\*\*" indicate  $p < 0.05$  and  $p < 0.01$  respectively

$\beta_0$ -band	Coh.		pCoh.	
	p	$R^2$	p	$R^2$
P7-O1	0.002**	0.188	0.798	0.008
P8-O2	0.045*	0.100	0.404	0.030
P3-O1	0.079	0.082	0.715	0.011
P4-O2	0.014*	0.135	0.884	0.004
C3-P7	0.032*	0.110	0.393	0.031
C4-P8	0.044*	0.100	0.420	0.029
P3-C3	0.107	0.073	0.341	0.036
P4-C4	0.132	0.066	0.482	0.024
P3-P7	0.001**	0.215	0.107	0.073
P4-P8	0.030*	0.113	0.043*	0.101

0.124); high significance was obtained between C4-P8 ( $R^2 = 0.178$ ), P3-P7 ( $R^2 = 0.194$ ), and P4-P8 ( $R^2 = 0.198$ ). Between the channels P3-P7 and P4-P8, partial coherences yielded significant results as well ( $R^2 = 0.104$  and  $R^2 = 0.120$ ). For bivariate Granger causalities, significant changes were obtained between O2  $\rightarrow$  P8 ( $R^2 = 0.115$ ), and O1  $\rightarrow$  P3 ( $R^2 = 0.108$ ). For conditional Granger causalities, significant findings were observed only between C3  $\rightarrow$  P7 ( $R^2 = 0.099$ ). Table 3.1.42 provides the cognitive task results for all local posterior channel pairs on the whole EEG signals.

**Table 3.1.42:** Significance  $p$  and coefficient of determination  $R^2$  as determined by Fisher's F-test for a least squares quadratic regression model: measures between local posterior channel pairs on the whole EEG signals during the cognitive task; "\*" and "\*\*\*" indicate  $p < 0.05$  and  $p < 0.01$  respectively. For directed measures, the first line per channel pair indicates the first direction of dependence (e.g. from P7  $\rightarrow$  O1), and the second line indicates the second direction of dependence (e.g. from O1  $\rightarrow$  P7).

total	Coh.		pCoh.		bGC		cGC	
	p	R <sup>2</sup>	p	R <sup>2</sup>	p	R <sup>2</sup>	p	R <sup>2</sup>
P7-O1	0.039*	0.104	0.954	0.002	0.180	0.057	0.789	0.008
					0.519	0.022	0.055	0.093
P8-O2	0.160	0.060	0.418	0.029	0.616	0.016	0.313	0.039
					0.027*	0.115	0.377	0.032
P3-O1	0.346	0.035	0.223	0.050	0.724	0.011	0.152	0.062
					0.034*	0.108	0.378	0.032
P4-O2	0.068	0.087	0.802	0.007	0.780	0.008	0.595	0.017
					0.724	0.011	0.880	0.004
C3-P7	0.016*	0.131	0.101	0.075	0.189	0.055	0.046*	0.099
					0.979	0.001	0.257	0.045
C4-P8	0.003**	0.178	0.387	0.032	0.322	0.038	0.496	0.023
					0.371	0.033	0.071	0.086
P3-C3	0.020*	0.124	0.178	0.057	0.814	0.007	0.550	0.020
					0.117	0.070	0.731	0.011
P4-C4	0.057	0.093	0.262	0.044	0.743	0.010	0.480	0.025
					0.800	0.008	0.419	0.029
P3-P7	0.002**	0.194	0.039*	0.104	0.533	0.021	0.166	0.059
					0.849	0.006	0.806	0.007
P4-P8	0.001**	0.198	0.023*	0.120	0.365	0.034	0.321	0.038
					0.170	0.058	0.647	0.015

## 3.2 Synchrony Between Groups of EEG Channels

This section will provide the results for synchrony between the following channel groups (cf. Figures 2.9.2a and 2.9.2b): Anterior (A.)<sup>1</sup>, Central (C.), Posterior (P.), Temporal Left (T.L.), Temporal Right (T.R.), Left (L.) and Right (R.). In the  $\delta$ -,  $\theta$ -,  $\alpha$ -, and  $\beta_0$ -frequency band, coherences and partial coherences were estimated between the respective first and second PCs of each group; dynamic canonical correlations (dynCC) were estimated between the PCS and between the groups in these frequency bands. For the whole bandpass-filtered signals, coherences, partial coherences, bivariate and conditional Granger causalities were estimated between the respective first and second PCs; in addition, static (statCC) and dynamic canonical correlations were computed. Section 3.2.1 will summarize the main findings. In Sections 3.2.2 and 3.2.3, the listing of all resting state and cognitive task results will be provided.

### 3.2.1 Main Results

In resting state, significant changes of coherences between the 1<sup>st</sup> PCs of Central-Posterior ( $R^2 = 0.094$ ) were observed in the  $\delta$ -frequency band. For coherences between the 2<sup>nd</sup> PCs, test results were most significant between Central-Temporal Left in  $\delta$  ( $R^2 = 0.229$ ) and between Central-Temporal Right in  $\delta$  as well ( $R^2 = 0.185$ ). For partial coherences between the 1<sup>st</sup> PCs, the highest significances were observed between Anterior-Posterior in  $\delta$  ( $R^2 = 0.202$ ) and  $\theta$  ( $R^2 = 0.176$ ), Central-Posterior in  $\delta$  ( $R^2 = 0.211$ ) and  $\theta$  ( $R^2 = 0.161$ ), and Anterior-Temporal Left in  $\alpha$  ( $R^2 = 0.143$ ). For partial coherences between the 2<sup>nd</sup> PCs, the group combinations Posterior-Temporal Left in  $\delta$  ( $R^2 = 0.142$ ) and  $\theta$  ( $R^2 = 0.187$ ), and Posterior-Temporal Right in  $\theta$  ( $R^2 = 0.182$ ) showed highly significant findings. Whereas static canonical correlations yielded highly significant test results only between Left-Right ( $R^2 = 0.145$ ), dynamic canonical correlations resulted in significant findings in both lower frequency bands  $\delta$  and  $\theta$  between all channel groups. In  $\delta$ , high significance was observed between Anterior-Temporal Right ( $R^2 = 0.161$ ), Central-Posterior ( $R^2 = 0.159$ ), Central-Temporal Left ( $R^2 = 0.163$ ), Central-Temporal Right ( $R^2 = 0.201$ ), Posterior-Temporal Right ( $R^2 = 0.159$ ), and Temporal Left-Temporal Right ( $R^2 = 0.143$ ). In  $\theta$ , high significance was obtained between Anterior-Posterior ( $R^2 = 0.180$ ), Anterior-Temporal Left ( $R^2 = 0.185$ ), Anterior-Temporal Right ( $R^2 = 0.149$ ), Central-Posterior ( $R^2 = 0.193$ ), Central-Temporal Left ( $R^2 = 0.231$ ), Central-Temporal Right ( $R^2 = 0.194$ ), Posterior-Temporal Left ( $R^2 = 0.252$ ), Posterior-Temporal Right ( $R^2 = 0.235$ ), Temporal Left-Temporal Right ( $R^2 = 0.171$ ), and Left-Right ( $R^2 = 0.268$ ). Additionally, for the whole signal, highly significant results were obtained between Posterior-Temporal Left ( $R^2 = 0.181$ ) and Posterior-Temporal Right ( $R^2 = 0.156$ ). Figure 3.2.1 shows the values of the

<sup>1</sup>The abbreviations in brackets will be used in the tables.

dynamic canonical correlation measure between Posterior-Temporal Left in the  $\theta$ -frequency band as scatterdiagram versus MMSE scores. The quadratic regression ( $p < 0.001$ ,  $R^2 = 0.252$ ) is characterized by an increase of partial coherences for MMSE scores between 26 and 19, and a decrease from 19 downwards.

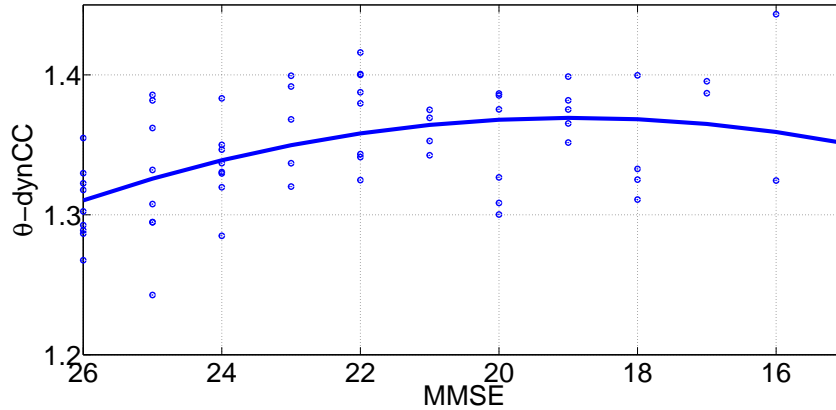


**Figure 3.2.1:** Example for changes of synchrony between groups of channels in **resting state: dynamic canonical correlations** in the  $\theta$ -frequency band for **Posterior-Temporal Left** versus MMSE scores. Low MMSE scores (right side of the abscissa) indicate more severe a higher degree of severity of AD. A quadratic regression was fitted to the data with  $p < 0.001$  and  $R^2 = 0.252$ .

Bivariate Granger causalities between the 1<sup>st</sup> PCs yielded high significance only between Temporal Left  $\rightarrow$  Posterior ( $R^2 = 0.247$ ). None of the group combinations showed highly significant test results between the 2<sup>nd</sup> PCs. Conditional Granger causalities between the 1<sup>st</sup> PCs yielded highly significant findings between all groups, for all of them at least in one direction: Anterior  $\rightarrow$  Central ( $R^2 = 0.206$ ), Central  $\rightarrow$  Anterior ( $R^2 = 0.152$ ), Anterior  $\rightarrow$  Posterior ( $R^2 = 0.264$ ), Anterior  $\rightarrow$  Temporal Left ( $R^2 = 0.201$ ), Temporal Left  $\rightarrow$  Anterior ( $R^2 = 0.208$ ), Anterior  $\rightarrow$  Temporal Right ( $R^2 = 0.168$ ), Central  $\rightarrow$  Posterior ( $R^2 = 0.408$ ), Posterior  $\rightarrow$  Central ( $R^2 = 0.190$ ), Central  $\rightarrow$  Temporal Left ( $R^2 = 0.214$ ), Temporal Left  $\rightarrow$  Central ( $R^2 = 0.213$ ), Central  $\rightarrow$  Temporal Right ( $R^2 = 0.169$ ), Temporal Right  $\rightarrow$  Central ( $R^2 = 0.148$ ), Posterior  $\rightarrow$  Temporal Left ( $R^2 = 0.167$ ), Temporal Left  $\rightarrow$  Posterior ( $R^2 = 0.271$ ), Temporal Right  $\rightarrow$  Posterior ( $R^2 = 0.245$ ), Temporal Left  $\rightarrow$  Temporal Right ( $R^2 = 0.196$ ), and Temporal Right  $\rightarrow$  Temporal Left ( $R^2 = 0.175$ ). In Figure 3.2.2, the values of the conditional Granger causality measure between the 1<sup>st</sup> PCs of Central  $\rightarrow$  Posterior are shown as scatterdiagram versus MMSE scores. The quadratic regression ( $p < 0.001$ ,  $R^2 = 0.408$ ) is characterized by a decrease of conditional Granger causalities for MMSE scores between 26 and 18, and a slight increase from 18 downwards.

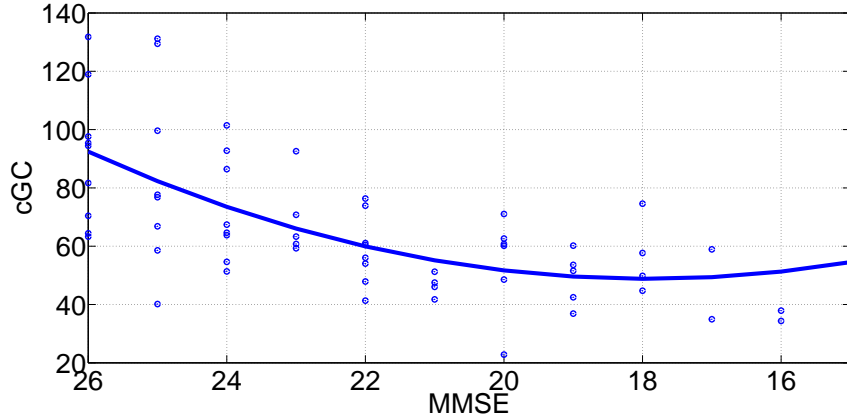


**Figure 3.2.2:** Example for changes of synchrony between channel groups in **resting state**: **conditional Granger causalities** between the 1<sup>st</sup> PCs of **Central**  $\rightarrow$  **Posterior** versus MMSE scores. Low MMSE scores (right side of the abscissa) indicate a higher degree of severity of AD. A quadratic regression was fitted to the data with  $p < 0.001$  and  $R^2 = 0.408$ .

Between the 2<sup>nd</sup> PCs, conditional Granger causalities yielded highly significant results between all groups, each in both directions (denoted by " $\leftrightarrow$ "): Anterior  $\leftrightarrow$  Central ( $R^2 = 0.205, 0.356$ ), Anterior  $\leftrightarrow$  Posterior ( $R^2 = 0.201, 0.313$ ), Anterior  $\leftrightarrow$  Temporal Left ( $R^2 = 0.262, 0.313$ ), Anterior  $\leftrightarrow$  Temporal Right ( $R^2 = 0.253, 0.353$ ), Central  $\leftrightarrow$  Posterior ( $R^2 = 0.245, 0.271$ ), Central  $\leftrightarrow$  Temporal Left ( $R^2 = 0.319, 0.252$ ), Central  $\leftrightarrow$  Temporal Right ( $R^2 = 0.293, 0.303$ ), Posterior  $\leftrightarrow$  Temporal Left ( $R^2 = 0.291, 0.173$ ), Posterior  $\leftrightarrow$  Temporal Right ( $R^2 = 0.304, 0.286$ ), and Temporal Left  $\leftrightarrow$  Temporal Right ( $R^2 = 0.322, 0.344$ ). Figure 3.2.3 displays the values of the conditional Granger causality measure between the 2<sup>nd</sup> PCs of Central  $\rightarrow$  Temporal Left as scatterdiagram versus MMSE scores. In this example, the quadratic regression ( $p < 0.001, R^2 = 0.319$ ) is characterized by a decrease of conditional Granger causalities for MMSE scores between 26 and 17, and a slight increase from 17 downwards.

Table 3.2.1 provides an overview of the significant test results for each measure, frequency band, and channel group combination in resting state. The table shows significances for the measures both between the 1<sup>st</sup> and 2<sup>nd</sup> PCs, and, for canonical coherences, between the channel groups (i.e. multivariate). Those parts of the table with no outcome are grey-colored; canonical correlations, for example, were not calculated between the 1<sup>st</sup> and 2<sup>nd</sup> PCs of each group, but only as multivariate measure.

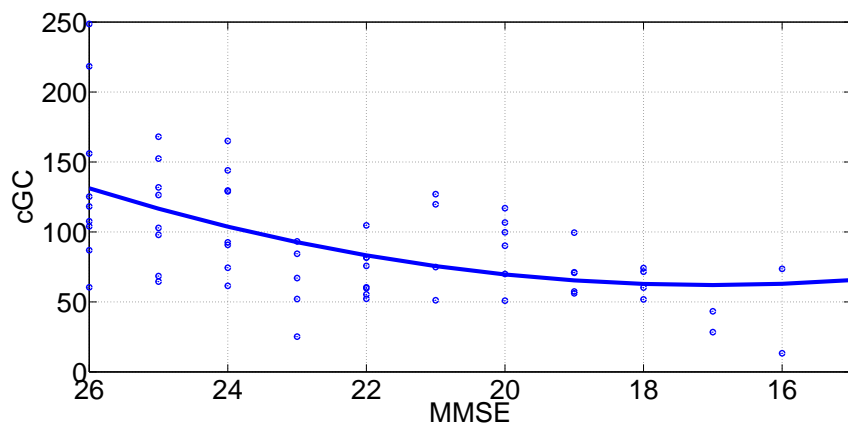


**Figure 3.2.3:** Example for changes of synchrony between channel groups in **resting state**: **conditional Granger causalities** between the 2<sup>nd</sup> PCs of **Central** → **Temporal Left** versus MMSE scores. Low MMSE scores (right side of the abscissa) indicate a higher degree of severity of AD. A quadratic regression was fitted to the data with  $p < 0.001$  and  $R^2 = 0.319$ .





During the cognitive task, highly significant changes of coherences were found between the 2<sup>nd</sup> PCs of Posterior-Temporal Left in  $\theta$  ( $R^2 = 0.249$ ), and of Central-Temporal Left in all frequency bands:  $\delta$  ( $R^2 = 0.413$ ),  $\theta$  ( $R^2 = 0.362$ ),  $\alpha$  ( $R^2 = 0.365$ ),  $\beta_0$  ( $R^2 = 0.216$ ), and for the whole signal ( $R^2 = 0.401$ ). Figure 3.2.4 shows the estimated coherences between the 2<sup>nd</sup> PCs of Central-Temporal Left in the  $\delta$ -frequency band as scatterdiagram versus MMSE scores. The quadratic regression model ( $p < 0.001$ ,  $R^2 = 0.413$ ) is characterized by an increase of coherences for MMSE scores between 26 and 20, and a decrease from 20 downwards.

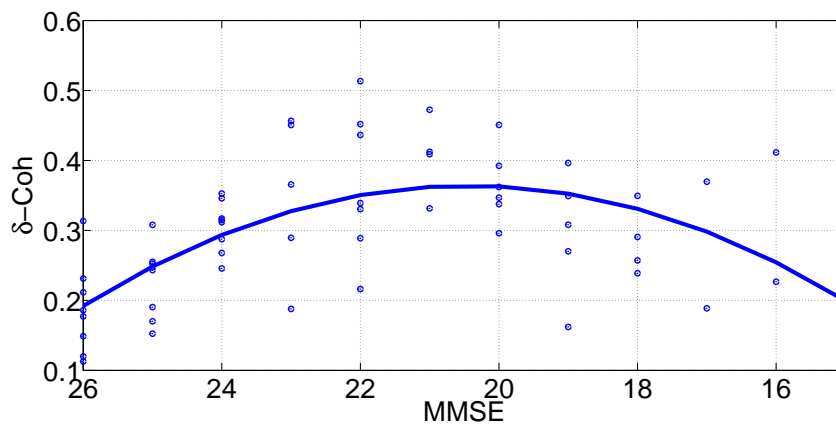


**Figure 3.2.4:** Example for changes of synchrony between channel groups during the **cognitive task**: coherences between the 2<sup>nd</sup> PCs of **Central-Temporal Left** in the  $\delta$ -frequency band versus MMSE scores. Low MMSE scores (right side of the abscissa) indicate a higher degree of severity of AD. A quadratic regression was fitted to the data with  $p < 0.001$  and  $R^2 = 0.413$ .

In contrast to coherences, only partial coherences between the 1<sup>st</sup> PCs yielded highly significant results: between Anterior-Posterior in  $\theta$  ( $R^2 = 0.156$ ), Central-Posterior in  $\delta$  ( $R^2 = 0.190$ ) and  $\theta$  ( $R^2 = 0.165$ ), and Temporal Left-Temporal Right in  $\theta$  ( $R^2 = 0.254$ ). Changes of static canonical correlations were highly significant in the following 8 group combinations: Anterior-Posterior ( $R^2 = 0.197$ ), Anterior-Temporal Left ( $R^2 = 0.207$ ), Central-Posterior ( $R^2 = 0.196$ ), Central-Temporal Left ( $R^2 = 0.405$ ), Central-Temporal Right ( $R^2 = 0.201$ ), Posterior-Temporal Left ( $R^2 = 0.294$ ), Posterior-Temporal Right ( $R^2 = 0.302$ ), and Left-Right ( $R^2 = 0.165$ ). Figure 3.2.5 shows the values of the static canonical correlation measure between Central-Temporal Left as scatterdiagram versus MMSE scores. The quadratic regression model ( $p < 0.001$ ,  $R^2 = 0.405$ ) is characterized by an increase of the canonical correlation measure for MMSE scores between 26 and 20, and a decrease from 20 downwards.

The analysis of dynamic canonical correlations yielded highly significant results in channel group combinations but Anterior-Central and Temporal Left-Temporal Right: Anterior-Posterior in  $\theta$  ( $R^2 = 0.226$ ) and for the whole signal

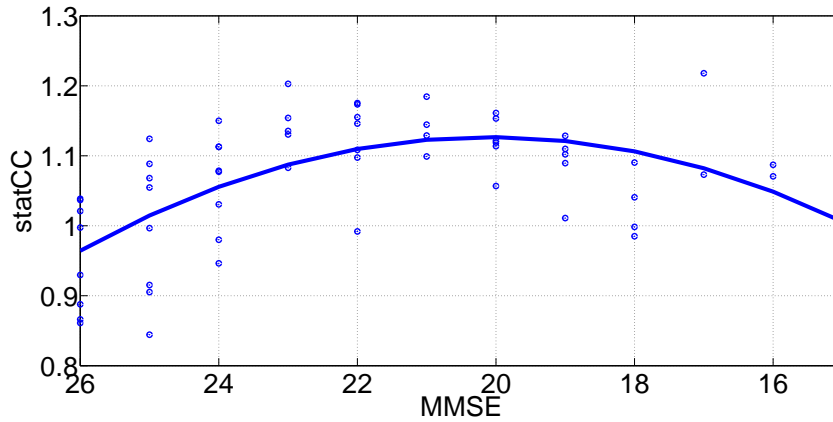


**Figure 3.2.5:** Example for changes of synchrony between channel groups during the **cognitive task: static canonical correlations** between **Central-Temporal Left** versus MMSE scores. Low MMSE scores (right side of the abscissa) indicate a higher degree of severity of AD. A quadratic regression was fitted to the scatterplot with  $p < 0.001$  and  $R^2 = 0.405$ .

( $R^2 = 0.162$ ), Anterior-Temporal Left in  $\theta$  ( $R^2 = 0.278$ ) and for the whole signal ( $R^2 = 0.199$ ), Anterior-Temporal Right in  $\theta$  ( $R^2 = 0.169$ ), Central-Posterior in  $\theta$  ( $R^2 = 0.222$ ) and for the whole signal ( $R^2 = 0.147$ ), Central-Temporal Left in all frequency bands  $\delta$  ( $R^2 = 0.173$ ),  $\theta$  ( $R^2 = 0.390$ ),  $\alpha$  ( $R^2 = 0.195$ ),  $\beta_0$  ( $R^2 = 0.152$ ) and for the whole signal ( $R^2 = 0.294$ ), Central-Temporal Right in  $\delta$  ( $R^2 = 0.172$ ),  $\theta$  ( $R^2 = 0.222$ ),  $\alpha$  ( $R^2 = 0.164$ ) and for the whole signal ( $R^2 = 0.206$ ), Posterior-Temporal Left in  $\theta$  ( $R^2 = 0.266$ ),  $\alpha$  ( $R^2 = 0.252$ ),  $\beta_0$  ( $R^2 = 0.263$ ) and for the whole signal ( $R^2 = 0.278$ ), Posterior-Temporal Right in  $\theta$  ( $R^2 = 0.234$ ),  $\beta_0$  ( $R^2 = 0.212$ ) and for the whole signal ( $R^2 = 0.210$ ), and Left-Right in  $\theta$  ( $R^2 = 0.291$ ). In Figure 3.2.6, the values of the dynamic canonical correlation measure between Central-Temporal Left in the  $\theta$ -frequency band are shown as scatterdiagram versus MMSE scores. The quadratic regression model ( $p < 0.001$ ,  $R^2 = 0.390$ ) is characterized by an increase of dynamic canonical correlations for MMSE scores between 26 and 19, and a decrease from 19 downwards.

Between the 1<sup>st</sup> PCs, changes of the bivariate Granger causality measure were highly significant only between Central  $\rightarrow$  Posterior ( $R^2 = 0.162$ ). Between the 2<sup>nd</sup> PCs, high significance was observed between Central  $\rightarrow$  Temporal Left ( $R^2 = 0.151$ ) and between Temporal Right  $\rightarrow$  Central ( $R^2 = 0.155$ ). For conditional Granger causalities between the 1<sup>st</sup> PCs, highly significant results were obtained between Temporal Left  $\rightarrow$  Anterior ( $R^2 = 0.171$ ), Anterior  $\rightarrow$  Temporal Right ( $R^2 = 0.276$ ), Central  $\rightarrow$  Temporal Right ( $R^2 = 0.197$ ), and Temporal Left  $\rightarrow$  Temporal Right ( $R^2 = 0.185$ ). Between the 2<sup>nd</sup> PCs, high significance was observed between Anterior  $\rightarrow$  Posterior ( $R^2 = 0.206$ ), Temporal Right  $\rightarrow$  Central ( $R^2 = 0.181$ ), Temporal Right  $\rightarrow$  Posterior ( $R^2 = 0.263$ ), and Temporal Right

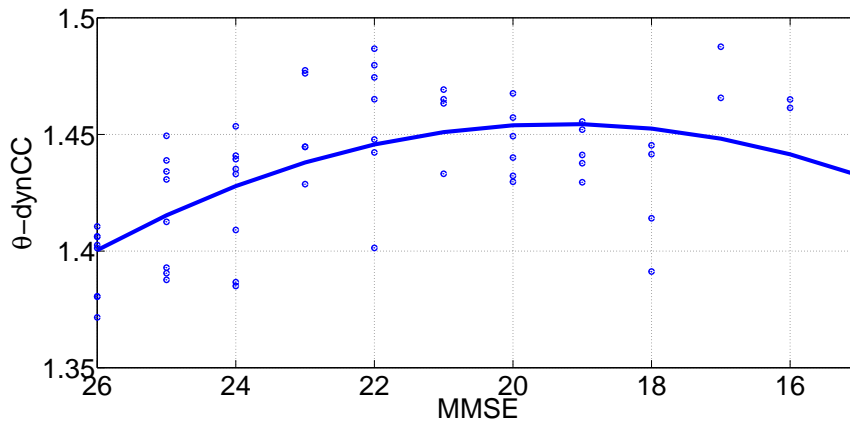


**Figure 3.2.6:** Example for changes of synchrony between channel groups during the **cognitive task: dynamic canonical correlations** between **Central-Temporal Left** in the  $\theta$ -frequency band versus MMSE scores. Low MMSE scores (right side of the abscissa) indicate a higher degree of severity of AD. A quadratic regression was fitted to the scatterplot with  $p < 0.001$  and  $R^2 = 0.390$ .

→ Temporal Left ( $R^2 = 0.248$ ).

Table 3.2.2 provides the significant findings for each measure, frequency band, and channel group combination during the cognitive task. The table shows significances for the measures both between the 1<sup>st</sup> and 2<sup>nd</sup> PCs, and, for canonical coherences, between the channel groups (i.e. multivariate). Those parts of the table with no outcome are grey-colored (cf. Table 3.2.1).



### 3.2.2 Detailed Results: Resting State

Here, the listing of all results from analyzing EEG synchrony between channel groups in resting state will be provided. Starting with the  $\delta$ -frequency band, coherences yielded significant results between the respective first PCs of Central-Posterior ( $R^2 = 0.094$ ). Changes of partial coherences were significant between the first PCs of Central-Temporal Right ( $R^2 = 0.097$ ), and highly significant between the first PCs of Anterior-Posterior ( $R^2 = 0.202$ ) and Central-Posterior ( $R^2 = 0.211$ ). Table 3.2.3 provides the resting state results between the respective first PCs of channel groups in the  $\delta$ -frequency band.

**Table 3.2.3:** Significance  $p$  and coefficient of determination  $R^2$  as determined by Fisher's F-test for a least squares quadratic regression model: measures between the respective first PCs of channel groups in the  $\delta$ -frequency band in resting state; "\*" and "\*\*\*" indicate  $p < 0.05$  and  $p < 0.01$  respectively

$\delta$ -band	p	Coh.	$R^2$	pCoh.	$R^2$
A.-C.	0.670		0.013	0.088	0.077
A.-P.	0.321		0.037	0.001**	0.202
A.-T.L.	0.659		0.014	0.318	0.037
A.-T.R.	0.405		0.029	0.082	0.079
C.-P.	0.049*		0.094	0.001**	0.211
C.-T.L.	0.297		0.039	0.285	0.040
C.-T.R.	0.833		0.006	0.044*	0.097
P.-T.L.	0.107		0.071	0.228	0.047
P.-T.R.	0.515		0.022	0.043*	0.098
T.L.-T.R.	0.329		0.036	0.333	0.035

For the respective second PCs, changes of coherences were significant between Anterior-Temporal Right ( $R^2 = 0.095$ ), Posterior-Temporal Left ( $R^2 = 0.107$ ), and highly significant between Central-Temporal Left ( $R^2 = 0.229$ ) and Central-Temporal Right ( $R^2 = 0.185$ ). Partial coherences yielded significant findings between Central-Temporal Left ( $R^2 = 0.098$ ), and highly significant findings between Posterior-Temporal Left ( $R^2 = 0.142$ ). Table 3.2.4 provides the resting state results between the respective second PCs of channel groups in the  $\delta$ -frequency band.

In the  $\delta$ -frequency band, the analysis of dynamic canonical correlations between the channel groups resulted in significant findings between five group combinations, and in highly significant findings between the remaining six group combinations. The changes of the dynamic canonical correlation measure between the PCs of each channel group yielded highly significant results between Anterior-Temporal Right ( $R^2 = 0.195$ ), Central-Temporal Left ( $R^2 = 0.168$ ), and Central-

**Table 3.2.4:** Significance  $p$  and coefficient of determination  $R^2$  as determined by Fisher's F-test for a least squares quadratic regression model: measures between the respective second PCs of channel groups in the  $\delta$ -frequency band in resting state; "\*" and "\*\*\*" indicate  $p < 0.05$  and  $p < 0.01$  respectively

$\delta$ -band	Coh.		pCoh.	
	p	$R^2$	p	$R^2$
A.-C.	0.187	0.053	0.377	0.032
A.-P.	0.076	0.081	0.239	0.046
A.-T.L.	0.138	0.063	0.581	0.018
A.-T.R.	0.047*	0.095	0.555	0.019
C.-P.	0.759	0.009	0.584	0.018
C.-T.L.	<0.001**	0.229	0.043*	0.098
C.-T.R.	0.002**	0.185	0.146	0.061
P.-T.L.	0.032*	0.107	0.009**	0.142
P.-T.R.	0.270	0.042	0.084	0.078
T.L.-T.R.	0.130	0.065	0.484	0.023

Temporal Right ( $R^2 = 0.171$ ). Table 3.2.5 provides all resting state results between the channel groups in the  $\delta$ -frequency band.

**Table 3.2.5:** Significance  $p$  and coefficient of determination  $R^2$  as determined by Fisher's F-test for a least squares quadratic regression model: measures between channel groups in the  $\delta$ -frequency band in resting state; "\*" and "\*\*\*" indicate  $p < 0.05$  and  $p < 0.01$  respectively

$\delta$ -band	dynCC (betw. groups)		dynCC (betw. PCs)	
	p	$R^2$	p	$R^2$
A.-C.	0.023*	0.117	0.019*	0.123
A.-P.	0.047*	0.095	0.095	0.074
A.-T.L.	0.018*	0.124	0.012*	0.134
A.-T.R.	0.005**	0.161	0.001**	0.195
C.-P.	0.005**	0.159	0.026*	0.113
C.-T.L.	0.004**	0.163	0.004**	0.168
C.-T.R.	0.001**	0.201	0.003**	0.171
P.-T.L.	0.026*	0.113	0.096	0.074
P.-T.R.	0.005**	0.159	0.266	0.042
T.L.-T.R.	0.009**	0.143	0.010*	0.140
L.-R.	0.041*	0.099	0.017*	0.124

Between the respective first PCs in the  $\theta$ -frequency band, no significant changes of coherences were observed. Partial coherences yielded highly significant results between Anterior-Posterior ( $R^2 = 0.176$ ) and Central-Posterior ( $R^2 = 0.161$ ). Table 3.2.6 provides the resting state results between the respective first PCs of

channel groups in the  $\theta$ -frequency band.

**Table 3.2.6:** Significance  $p$  and coefficient of determination  $R^2$  as determined by Fisher's F-test for a least squares quadratic regression model: measures between the respective first PCs of channel groups in the  $\theta$ -frequency band in resting state; "\*" and "\*\*\*" indicate  $p < 0.05$  and  $p < 0.01$  respectively

$\theta$ -band	Coh.		pCoh.	
	p	$R^2$	p	$R^2$
A.-C.	0.984	0.001	0.140	0.062
A.-P.	0.812	0.007	0.003**	0.176
A.-T.L.	0.459	0.025	0.115	0.068
A.-T.R.	0.658	0.014	0.187	0.053
C.-P.	0.234	0.046	0.005**	0.161
C.-T.L.	0.744	0.010	0.293	0.039
C.-T.R.	0.412	0.029	0.070	0.083
P.-T.L.	0.397	0.030	0.635	0.015
P.-T.R.	0.476	0.024	0.085	0.078
T.L.-T.R.	0.283	0.041	0.538	0.020

Coherences yielded significant test results between the respective second PCs of Central-Temporal Left ( $R^2 = 0.137$ ), Central-Temporal Right ( $R^2 = 0.101$ ), Posterior-Temporal Left ( $R^2 = 0.099$ ), and Posterior-Temporal Right ( $R^2 = 0.134$ ). Between the latter two group combinations, highly significant changes of partial coherences were observed as well ( $R^2 = 0.187$  and  $R^2 = 0.182$ ). Table 3.2.7 provides the resting state results between the respective second PCs of channel groups in the  $\theta$ -frequency band.

In the  $\theta$ -frequency band, dynamic canonical correlations yielded significant changes between Anterior-Central, and highly significant changes between the remaining channel combinations. In contrast, dynamic canonical correlations between the PCs showed highly significant changes only between Temporal Left-Temporal Right ( $R^2 = 0.196$ ). Table 3.2.8 provides the resting state results between the channel groups in the  $\theta$ -frequency band.

In the  $\alpha$ -frequency band, no significant changes of coherences between the respective first PCs of channel groups were observed. Partial coherence yielded significant findings between Anterior-Posterior ( $R^2 = 0.096$ ), and highly significant findings between Anterior-Temporal Left ( $R^2 = 0.143$ ). Table 3.2.9 provides the resting state results between the respective first PCs of channel groups in the  $\alpha$ -frequency band.

Neither coherences nor partial coherences yielded statistically significant find-



**Table 3.2.7:** Significance  $p$  and coefficient of determination  $R^2$  as determined by Fisher's F-test for a least squares quadratic regression model: measures between the respective second PCs of channel groups in the  $\theta$ -frequency band in resting state; "\*" and "\*\*\*" indicate  $p < 0.05$  and  $p < 0.01$  respectively

$\theta$ -band	Coh.		pCoh.	
	p	$R^2$	p	$R^2$
A.-C.	0.219	0.049	0.341	0.035
A.-P.	0.235	0.046	0.163	0.058
A.-T.L.	0.650	0.014	0.531	0.021
A.-T.R.	0.340	0.035	0.127	0.065
C.-P.	0.642	0.014	0.645	0.014
C.-T.L.	0.011*	0.137	0.097	0.074
C.-T.R.	0.039*	0.101	0.054	0.091
P.-T.L.	0.041*	0.099	0.002**	0.187
P.-T.R.	0.012*	0.134	0.002**	0.182
T.L.-T.R.	0.535	0.020	0.168	0.057

**Table 3.2.8:** Significance  $p$  and coefficient of determination  $R^2$  as determined by Fisher's F-test for a least squares quadratic regression model: measures between channel groups in the  $\theta$ -frequency band in resting state; "\*" and "\*\*\*" indicate  $p < 0.05$  and  $p < 0.01$  respectively

$\theta$ -band	dynCC (betw. groups)		dynCC (betw. PCs)	
	p	$R^2$	p	$R^2$
A.-C.	0.024*	0.115	0.054	0.091
A.-P.	0.002**	0.180	0.441	0.027
A.-T.L.	0.002**	0.185	0.012*	0.135
A.-T.R.	0.007**	0.149	0.070	0.083
C.-P.	0.001**	0.193	0.143	0.062
C.-T.L.	<0.001**	0.231	0.085	0.077
C.-T.R.	0.001**	0.194	0.159	0.058
P.-T.L.	<0.001**	0.252	0.028*	0.110
P.-T.R.	<0.001**	0.235	0.100	0.073
T.L.-T.R.	0.003**	0.171	0.001**	0.196
L.-R.	<0.001**	0.268	0.145	0.061

ings between the respective second PCs of channel groups in the  $\alpha$ -frequency band. Table 3.2.10 provides all resting state results between the respective second PCs of channel groups in the  $\alpha$ -frequency band.

The analysis of dynamic canonical correlations in the  $\alpha$ -frequency band did not result in significant findings as well, neither between channel groups nor between the respective PCs. Table 3.2.11 provides the resting state results between the

**Table 3.2.9:** Significance  $p$  and coefficient of determination  $R^2$  as determined by Fisher's F-test for a least squares quadratic regression model: measures between the respective first PCs of channel groups in the  $\alpha$ -frequency band in resting state; "\*" and "\*\*\*" indicate  $p < 0.05$  and  $p < 0.01$  respectively

$\alpha$ -band	Coh.		pCoh.	
	p	$R^2$	p	$R^2$
A.-C.	0.767	0.009	0.604	0.016
A.-P.	0.097	0.074	0.046*	0.096
A.-T.L.	0.753	0.009	0.009**	0.143
A.-T.R.	0.397	0.030	0.151	0.060
C.-P.	0.185	0.054	0.271	0.042
C.-T.L.	0.922	0.003	0.388	0.031
C.-T.R.	0.089	0.076	0.383	0.031
P.-T.L.	0.095	0.074	0.891	0.004
P.-T.R.	0.515	0.022	0.113	0.069
T.L.-T.R.	0.160	0.058	0.440	0.027

**Table 3.2.10:** Significance  $p$  and coefficient of determination  $R^2$  as determined by Fisher's F-test for a least squares quadratic regression model: measures between the respective second PCs of channel groups in the  $\alpha$ -frequency band in resting state; "\*" and "\*\*\*" indicate  $p < 0.05$  and  $p < 0.01$  respectively

$\alpha$ -band	Coh.		pCoh.	
	p	$R^2$	p	$R^2$
A.-C.	0.765	0.009	0.660	0.014
A.-P.	0.638	0.015	0.232	0.047
A.-T.L.	0.068	0.084	0.982	0.001
A.-T.R.	0.992	<0.001	0.516	0.021
C.-P.	0.933	0.002	0.727	0.010
C.-T.L.	0.444	0.026	0.813	0.007
C.-T.R.	0.410	0.029	0.735	0.010
P.-T.L.	0.967	0.001	0.233	0.047
P.-T.R.	0.199	0.052	0.098	0.073
T.L.-T.R.	0.687	0.012	0.336	0.035

channel groups in the  $\alpha$ -frequency band.

In the  $\beta_0$ -frequency band, between none of respective first PCs of channel groups, significant test results were observed, neither for coherences nor for partial coherences. Table 3.2.12 provides the resting state results between the respective first PCs of channel groups in the  $\beta_0$ -frequency band.

For the second PCs, coherences yielded significant results between Anterior-

**Table 3.2.11:** Significance  $p$  and coefficient of determination  $R^2$  as determined by Fisher's F-test for a least squares quadratic regression model: measures between channel groups in the  $\alpha$ -frequency band in resting state; "\*" and "\*\*\*" indicate  $p < 0.05$  and  $p < 0.01$  respectively

$\alpha$ -band	dynCC (betw. groups)		dynCC (betw. PCs)	
	p	$R^2$	p	$R^2$
A.-C.	0.909	0.003	0.791	0.008
A.-P.	0.524	0.021	0.173	0.056
A.-T.L.	0.703	0.011	0.397	0.030
A.-T.R.	0.460	0.025	0.788	0.008
C.-P.	0.099	0.073	0.458	0.025
C.-T.L.	0.298	0.039	0.627	0.015
C.-T.R.	0.094	0.074	0.611	0.016
P.-T.L.	0.054	0.091	0.446	0.026
P.-T.R.	0.289	0.040	0.999	<0.001
T.L.-T.R.	0.194	0.052	0.987	<0.001
L.-R.	0.177	0.055	0.533	0.02

**Table 3.2.12:** Significance  $p$  and coefficient of determination  $R^2$  as determined by Fisher's F-test for a least squares quadratic regression model: measures between the respective first PCs of channel groups in the  $\beta_0$ -frequency band in resting state; "\*" and "\*\*\*" indicate  $p < 0.05$  and  $p < 0.01$  respectively

$\beta_0$ -band	Coh.		pCoh.	
	p	$R^2$	p	$R^2$
A.-C.	0.125	0.066	0.345	0.034
A.-P.	0.359	0.033	0.469	0.025
A.-T.L.	0.402	0.029	0.060	0.088
A.-T.R.	0.445	0.026	0.223	0.048
C.-P.	0.052	0.092	0.137	0.063
C.-T.L.	0.638	0.015	0.414	0.029
C.-T.R.	0.136	0.063	0.243	0.045
P.-T.L.	0.386	0.031	0.528	0.021
P.-T.R.	0.899	0.003	0.086	0.077
T.L.-T.R.	0.996	<0.001	0.093	0.075

Temporal Right ( $R^2 = 0.118$ ), and partial coherences between Anterior-Posterior ( $R^2 = 0.117$ ) and Anterior-Temporal Right ( $R^2 = 0.121$ ). Table 3.2.13 provides the resting state results between the respective second PCs of channel groups in the  $\beta_0$ -frequency band.

For dynamic canonical correlations in the  $\beta_0$ -frequency band, significant changes were observed between Central-Posterior ( $R^2 = 0.109$ ), Central Temporal Right

**Table 3.2.13:** Significance  $p$  and coefficient of determination  $R^2$  as determined by Fisher's F-test for a least squares quadratic regression model: measures between the respective second PCs of channel groups in the  $\beta_0$ -frequency band in resting state; "\*" and "\*\*\*" indicate  $p < 0.05$  and  $p < 0.01$  respectively

$\beta_0$ -band	Coh.		pCoh.	
	p	$R^2$	p	$R^2$
A.-C.	0.134	0.064	0.171	0.056
A.-P.	0.133	0.064	0.022*	0.117
A.-T.L.	0.581	0.018	0.368	0.032
A.-T.R.	0.022*	0.118	0.020*	0.121
C.-P.	0.964	0.001	0.738	0.010
C.-T.L.	0.388	0.031	0.839	0.006
C.-T.R.	0.235	0.046	0.549	0.019
P.-T.L.	0.784	0.008	0.261	0.043
P.-T.R.	0.292	0.040	0.805	0.007
T.L.-T.R.	0.165	0.057	0.322	0.036

( $R^2 = 0.111$ ), and Posterior Temporal Left ( $R^2 = 0.100$ ). Table 3.2.14 provides the resting state results between the channel groups in the  $\beta_0$ -frequency band.

**Table 3.2.14:** Significance  $p$  and coefficient of determination  $R^2$  as determined by Fisher's F-test for a least squares quadratic regression model: measures between channel groups in the  $\beta_0$ -frequency band in resting state; "\*" and "\*\*\*" indicate  $p < 0.05$  and  $p < 0.01$  respectively

$\beta_0$ -band	dynCC (betw. groups)		dynCC (betw. PCs)	
	p	$R^2$	p	$R^2$
A.-C.	0.800	0.007	0.108	0.07
A.-P.	0.364	0.033	0.121	0.067
A.-T.L.	0.862	0.005	0.163	0.058
A.-T.R.	0.640	0.015	0.700	0.012
C.-P.	0.030*	0.109	0.389	0.03
C.-T.L.	0.522	0.021	0.135	0.064
C.-T.R.	0.027*	0.111	0.289	0.04
P.-T.L.	0.040*	0.100	0.074	0.082
P.-T.R.	0.394	0.030	0.932	0.002
T.L.-T.R.	0.187	0.053	0.814	0.007
L.-R.	0.205	0.051	0.690	0.012

On the whole EEG signals, the analysis of coherences between the respective first PCs resulted in no significant results. For partial coherences, significance was observed between Anterior-Posterior ( $R^2 = 0.136$ ), and Anterior-Temporal Left ( $R^2 = 0.108$ ). Changes of bivariate Granger causalities were significant between

Anterior  $\rightarrow$  Temporal Left ( $R^2 = 0.121$ ), highly significant between Temporal Left  $\rightarrow$  Posterior ( $R^2 = 0.247$ ). Changes of conditional Granger causalities were (mostly highly) significant for all group combinations. Table 3.2.15 provides the resting state results between the respective first PCs of channel groups in the total frequency band.

**Table 3.2.15:** Significance  $p$  and coefficient of determination  $R^2$  as determined by Fisher's F-test for a least squares quadratic regression model: measures between the respective first PCs of channel groups on the whole EEG signals in resting state; "\*" and "\*\*" indicate  $p < 0.05$  and  $p < 0.01$  respectively

total	Coh.		pCoh.		bGC		cGC	
	p	$R^2$	p	$R^2$	p	$R^2$	p	$R^2$
A.-C.	0.829	0.006	0.399	0.030	0.757	0.009	0.001**	0.206
					0.071	0.083	0.007**	0.152
A.-P.	0.241	0.046	0.012*	0.136	0.191	0.053	<0.001**	0.264
					0.135	0.064	0.036*	0.103
A.-T.L.	0.650	0.014	0.031*	0.108	0.020*	0.121	0.001**	0.201
					0.256	0.044	0.001**	0.208
A.-T.R.	0.480	0.024	0.118	0.068	0.447	0.026	0.004**	0.168
					0.068	0.084	0.050	0.093
C.-P.	0.103	0.072	0.078	0.080	0.416	0.028	<0.001**	0.408
					0.626	0.015	0.002**	0.190
C.-T.L.	0.862	0.005	0.689	0.012	0.286	0.040	0.001**	0.214
					0.157	0.059	0.001**	0.213
C.-T.R.	0.177	0.055	0.073	0.082	0.504	0.022	0.004**	0.169
					0.301	0.039	0.008**	0.148
P.-T.L.	0.191	0.053	0.808	0.007	0.095	0.074	0.004**	0.167
					<0.001**	0.247	<0.001**	0.271
P.-T.R.	0.527	0.021	0.071	0.083	0.933	0.002	0.036*	0.103
					0.677	0.013	<0.001**	0.245
T.L.-T.R.	0.303	0.038	0.334	0.035	0.419	0.028	0.001**	0.196
					0.174	0.056	0.003**	0.175

For the second PCs, significant changes of partial coherences were observed between Posterior-Temporal Left ( $R^2 = 0.104$ ) and Posterior-Temporal Right ( $R^2 = 0.105$ ), and of bivariate Granger causalities between Temporal Right  $\rightarrow$  Temporal Left ( $R^2 = 0.095$ ). Conditional Granger causalities yielded high significance for all group combinations in both directions (several  $R^2 > 0.3$ ). Table 3.2.16 provides the resting state results between the respective second PCs of channel groups in the total frequency band.

Both static and dynamic canonical correlations (between channel groups) yielded significant findings between Central-Temporal Left ( $p = 0.013$ ,  $R^2 = 0.133$  and  $p = 0.021$ ,  $R^2 = 0.119$ ), Posterior-Temporal Left ( $p = 0.026$ ,  $R^2 = 0.113$  and  $p = 0.002$ ,  $R^2 = 0.181$ ), Posterior-Temporal Right ( $p = 0.012$ ,  $R^2 = 0.135$

**Table 3.2.16:** Significance  $p$  and coefficient of determination  $R^2$  as determined by Fisher's F-test for a least squares quadratic regression model: measures between the respective second PCs of channel groups on the whole EEG signals in resting state; "\*" and "\*\*" indicate  $p < 0.05$  and  $p < 0.01$  respectively

total	Coh.		pCoh.		bGC		cGC	
	p	$R^2$	p	$R^2$	p	$R^2$	p	$R^2$
A.-C.	0.359	0.033	0.415	0.028	0.419	0.028	0.001**	0.205
					0.448	0.026	<0.001**	0.356
A.-P.	0.251	0.044	0.129	0.065	0.224	0.048	0.001**	0.201
					0.317	0.037	<0.001**	0.313
A.-T.L.	0.922	0.003	0.696	0.012	0.051	0.093	<0.001**	0.262
					0.479	0.024	<0.001**	0.313
A.-T.R.	0.214	0.049	0.193	0.053	0.528	0.021	<0.001**	0.253
					0.524	0.021	<0.001**	0.353
C.-P.	0.942	0.002	0.726	0.010	0.239	0.046	<0.001**	0.245
					0.202	0.051	<0.001**	0.271
C.-T.L.	0.063	0.087	0.361	0.033	0.880	0.004	<0.001**	0.319
					0.205	0.051	<0.001**	0.252
C.-T.R.	0.097	0.074	0.240	0.046	0.179	0.055	<0.001**	0.293
					0.128	0.065	<0.001**	0.303
P.-T.L.	0.405	0.029	0.035*	0.104	0.138	0.063	<0.001**	0.291
					0.840	0.006	0.003**	0.173
P.-T.R.	0.133	0.064	0.034*	0.105	0.706	0.011	<0.001**	0.304
					0.586	0.017	<0.001**	0.286
T.L.-T.R.	0.389	0.030	0.267	0.042	0.086	0.077	<0.001**	0.322
					0.047*	0.095	<0.001**	0.344

and  $p = 0.006$ ,  $R^2 = 0.156$ ), and Left-Right ( $p = 0.008$ ,  $R^2 = 0.145$  and  $p = 0.011$ ,  $R^2 = 0.137$ ). In addition, significant changes of dynamic canonical correlations were observed between Central-Posterior ( $R^2 = 0.140$ ), and Central-Temporal Right ( $R^2 = 0.134$ ). For static canonical correlations between PCs, changes were significant between Central-Temporal Left ( $R^2 = 0.133$ ), Posterior-Temporal Left ( $R^2 = 0.113$ ), and Posterior-Temporal Right ( $R^2 = 0.135$ ). Table 3.2.17 provides the resting state results between the channel groups on the whole EEG signals.

**Table 3.2.17:** Significance  $p$  and coefficient of determination  $R^2$  as determined by Fisher's F-test for a least squares quadratic regression model: measures between channel groups on the whole EEG signals in resting state; "\*" and "\*\*\*" indicate  $p < 0.05$  and  $p < 0.01$  respectively

total	statCC (groups)		statCC (PCs)		dynCC (groups)		dynCC (PCs)	
	p	R <sup>2</sup>	p	R <sup>2</sup>	p	R <sup>2</sup>	p	R <sup>2</sup>
A.-C.	0.171	0.056	0.191	0.053	0.373	0.032	0.154	0.059
A.-P.	0.312	0.037	0.491	0.023	0.215	0.049	0.324	0.036
A.-T.L.	0.077	0.081	0.076	0.081	0.132	0.064	0.061	0.087
A.-T.R.	0.120	0.067	0.222	0.048	0.209	0.050	0.255	0.044
C.-P.	0.061	0.088	0.206	0.050	0.010*	0.140	0.319	0.037
C.-T.L.	0.013*	0.289	0.040*	0.133	0.021*	0.119	0.164	0.058
C.-T.R.	0.062	0.087	0.475	0.024	0.012*	0.134	0.397	0.030
P.-T.L.	0.026*	0.464	0.025*	0.113	0.002**	0.181	0.111	0.07
P.-T.R.	0.012*	0.723	0.011*	0.135	0.006**	0.156	0.620	0.016
TL-TR	0.106	0.071	0.137	0.063	0.120	0.067	0.189	0.053
L.-R.	0.008**	0.145	0.167	0.057	0.011*	0.137	0.233	0.047

### 3.2.3 Detailed Results: Cognitive Task

In this section, the listing of all results from analyzing EEG synchrony between channel groups during the cognitive task will be provided. In the  $\delta$ -frequency band, changes of partial coherences were significant between the respective first PCs of Central-Temporal Right ( $R^2 = 0.139$ ) and Temporal Left-Temporal Right ( $R^2 = 0.109$ ), and highly significant between Central-Posterior ( $R^2 = 0.190$ ). No significant changes of coherences were observed. Table 3.2.18 provides the cognitive task results between the respective first PCs of channel groups in the  $\delta$ -frequency band.

**Table 3.2.18:** Significance  $p$  and coefficient of determination  $R^2$  as determined by Fisher's F-test for a least squares quadratic regression model: measures between the respective first PCs of channel groups in the  $\delta$ -frequency band during the cognitive task; "\*" and "\*\*" indicate  $p < 0.05$  and  $p < 0.01$  respectively

$\delta$ -band	Coh.		pCoh.	
	p	$R^2$	p	$R^2$
A.-C.	0.533	0.021	0.903	0.003
A.-P.	0.789	0.008	0.164	0.060
A.-T.L.	0.574	0.019	0.214	0.051
A.-T.R.	0.981	0.001	0.909	0.003
C.-P.	0.082	0.081	0.002**	0.190
C.-T.L.	0.472	0.025	0.167	0.059
C.-T.R.	0.224	0.049	0.012*	0.139
P.-T.L.	0.321	0.038	0.590	0.018
P.-T.R.	0.984	0.001	0.153	0.062
T.L.-T.R.	0.917	0.003	0.033*	0.109

For the second PCs, coherences yielded significant findings between Posterior-Temporal Right ( $R^2 = 0.107$ ), and highly significant findings between Central-Temporal Left ( $R^2 = 0.413$ ). No significances were observed for partial coherences. Table 3.2.19 provides the cognitive task results between the respective second PCs of channel groups in the  $\delta$ -frequency band.

Dynamic canonical correlations (between channel groups) yielded significant test results between Anterior-Central ( $R^2 = 0.105$ ), Anterior-Temporal Right ( $R^2 = 0.110$ ), Central-Posterior ( $R^2 = 0.104$ ), Posterior-Temporal Right ( $R^2 = 0.131$ ), and Temporal Left-Temporal Right ( $R^2 = 0.098$ ), and highly significant results between Central-Temporal Left ( $R^2 = 0.173$ ), and Central-Temporal Right ( $R^2 = 0.172$ ). Significant changes of dynamic canonical correlations between the PCs were observed between Anterior-Temporal Right ( $R^2 = 0.130$ ), Central-Temporal Left ( $R^2 = 0.110$ ), and Central Temporal Right ( $R^2 = 0.126$ ). Table 3.2.20 provides the cognitive task results between the channel groups in the  $\delta$ -



**Table 3.2.19:** Significance  $p$  and coefficient of determination  $R^2$  as determined by Fisher's F-test for a least squares quadratic regression model: measures between the respective second PCs of channel groups in the  $\delta$ -frequency band during the cognitive task; "\*" and "\*\*\*" indicate  $p < 0.05$  and  $p < 0.01$  respectively

$\delta$ -band	Coh.		pCoh.	
	p	$R^2$	p	$R^2$
A.-C.	0.089	0.079	0.922	0.003
A.-P.	0.712	0.011	0.969	0.001
A.-T.L.	0.129	0.067	0.216	0.051
A.-T.R.	0.640	0.015	0.585	0.018
C.-P.	0.980	0.001	0.309	0.039
C.-T.L.	<0.001**	0.413	0.072	0.085
C.-T.R.	0.138	0.065	0.748	0.010
P.-T.L.	0.530	0.021	0.214	0.051
P.-T.R.	0.035*	0.107	0.675	0.013
T.L.-T.R.	0.796	0.008	0.299	0.040

frequency band.

**Table 3.2.20:** Significance  $p$  and coefficient of determination  $R^2$  as determined by Fisher's F-test for a least squares quadratic regression model: measures between channel groups in the  $\delta$ -frequency band during the cognitive task; "\*" and "\*\*\*" indicate  $p < 0.05$  and  $p < 0.01$  respectively

$\delta$ -band	dynCC (betw. groups)		dynCC (betw. PCs)	
	p	$R^2$	p	$R^2$
A.-C.	0.038*	0.105	0.332	0.037
A.-P.	0.094	0.077	0.768	0.009
A.-T.L.	0.057	0.093	0.097	0.076
A.-T.R.	0.033*	0.110	0.017*	0.130
C.-P.	0.040*	0.104	0.595	0.017
C.-T.L.	0.004**	0.173	0.032*	0.110
C.-T.R.	0.004**	0.172	0.019*	0.126
P.-T.L.	0.077	0.083	0.993	0.001
P.-T.R.	0.016*	0.131	0.267	0.044
T.L.-T.R.	0.048*	0.098	0.198	0.053
L.-R.	0.242	0.047	0.087	0.079

In the  $\theta$ -frequency band, changes of coherences were significant between the respective first PCs of ( $R^2 = 0.117$ ). Partial coherences yielded high significance between Central-Posterior ( $R^2 = 0.165$ ), Anterior-Posterior ( $R^2 = 0.156$ ), and Temporal Left-Temporal Right ( $R^2 = 0.254$ ); additionally, significant changes were

observed between Anterior-Temporal Left ( $R^2 = 0.109$ ) and Central-Temporal Right ( $R^2 = 0.113$ ). Table 3.2.21 provides the cognitive task results between the respective first PCs of channel groups in the  $\theta$ -frequency band.

**Table 3.2.21:** Significance  $p$  and coefficient of determination  $R^2$  as determined by Fisher's F-test for a least squares quadratic regression model: measures between the respective first PCs of channel groups in the  $\theta$ -frequency band during the cognitive task; "\*" and "\*\*" indicate  $p < 0.05$  and  $p < 0.01$  respectively

$\theta$ -band	Coh.		pCoh.	
	$p$	$R^2$	$p$	$R^2$
A.-C.	0.845	0.006	0.517	0.022
A.-P.	0.574	0.019	0.007**	0.156
A.-T.L.	0.281	0.042	0.034*	0.109
A.-T.R.	0.446	0.027	0.990	<0.001
C.-P.	0.026*	0.117	0.005**	0.165
C.-T.L.	0.599	0.017	0.076	0.084
C.-T.R.	0.143	0.064	0.029*	0.113
P.-T.L.	0.533	0.021	0.767	0.009
P.-T.R.	0.957	0.001	0.118	0.070
T.L.-T.R.	0.265	0.044	<0.001**	0.254

For the second PCs, highly significant results were observed for coherences between Central-Temporal Left ( $R^2 = 0.362$ ) and between Posterior-Temporal Left ( $R^2 = 0.249$ ). Partial coherences yielded significant findings between Posterior-Temporal Left as well ( $p = 0.029$ ,  $R^2 = 0.113$ ). Table 3.2.22 provides the cognitive task results between the respective second PCs of channel groups in the  $\theta$ -frequency band.

The analysis of dynamic canonical correlations (between channel groups) in the  $\theta$ -frequency band resulted in highly significant findings for all but two group combinations, and significant findings for the remaining two combinations. The highest value  $R^2 = 0.390$  was observed between Central-Temporal Left. Dynamic canonical correlations between the PCs yielded high significance between Temporal Left and Temporal Right ( $R^2 = 0.153$ ), and significance for seven further group combinations. Table 3.2.23 provides the cognitive task results between the channel groups in the  $\theta$ -frequency band.

In the  $\alpha$ -frequency band, neither coherences nor partial coherences yielded significant findings between the first PCs of channel groups. Table 3.2.24 provides the cognitive task results between the respective first PCs of channel groups in the  $\alpha$ -frequency band.

**Table 3.2.22:** Significance  $p$  and coefficient of determination  $R^2$  as determined by Fisher's F-test for a least squares quadratic regression model: measures between the respective second PCs of channel groups in the  $\theta$ -frequency band during the cognitive task; "\*" and "\*\*\*" indicate  $p < 0.05$  and  $p < 0.01$  respectively

$\theta$ -band	Coh.		pCoh.	
	p	$R^2$	p	$R^2$
A.-C.	0.360	0.034	0.643	0.015
A.-P.	0.309	0.039	0.725	0.011
A.-T.L.	0.504	0.023	0.748	0.010
A.-T.R.	0.197	0.054	0.216	0.051
C.-P.	0.121	0.069	0.176	0.057
C.-T.L.	<0.001**	0.362	0.100	0.075
C.-T.R.	0.174	0.058	0.923	0.003
P.-T.L.	<0.001**	0.249	0.029*	0.113
P.-T.R.	0.278	0.043	0.394	0.031
T.L.-T.R.	0.633	0.015	0.228	0.049

**Table 3.2.23:** Significance  $p$  and coefficient of determination  $R^2$  as determined by Fisher's F-test for a least squares quadratic regression model: measures between channel groups in the  $\theta$ -frequency band during the cognitive task; "\*" and "\*\*\*" indicate  $p < 0.05$  and  $p < 0.01$  respectively

$\theta$ -band	dynCC (betw. groups)		dynCC (betw. PCs)	
	p	$R^2$	p	$R^2$
A.-C.	0.032*	0.110	0.284	0.042
A.-P.	0.001**	0.226	0.661	0.014
A.-T.L.	<0.001**	0.278	0.015*	0.133
A.-T.R.	0.004**	0.169	0.029*	0.113
C.-P.	0.001**	0.222	0.125	0.068
C.-T.L.	<0.001**	0.390	0.013*	0.138
C.-T.R.	0.001**	0.222	0.015*	0.134
P.-T.L.	<0.001**	0.266	0.038*	0.105
P.-T.R.	<0.001**	0.234	0.028*	0.114
T.L.-T.R.	0.013*	0.138	0.008**	0.153
L.-R.	<0.001**	0.291	0.036*	0.106

For the second PCs of the channel groups, the quadratic regression of coherences was highly significant between Central-Temporal Left ( $R^2 = 0.365$ ). For partial coherences, it was significant between Central-Temporal Left as well ( $R^2 = 0.105$ ). Additionally, coherences yielded significance between Central-Temporal Right ( $R^2 = 0.142$ ). Table 3.2.25 provides the cognitive task results between the respective second PCs of channel groups in the  $\alpha$ -frequency band.

**Table 3.2.24:** Significance  $p$  and coefficient of determination  $R^2$  as determined by Fisher's F-test for a least squares quadratic regression model: measures between the respective first PCs of channel groups in the  $\alpha$ -frequency band during the cognitive task; "\*" and "\*\*\*" indicate  $p < 0.05$  and  $p < 0.01$  respectively

$\alpha$ -band	Coh.		pCoh.	
	p	$R^2$	p	$R^2$
A.-C.	0.891	0.004	0.709	0.012
A.-P.	0.440	0.027	0.098	0.076
A.-T.L.	0.235	0.048	0.068	0.087
A.-T.R.	0.325	0.037	0.755	0.009
C.-P.	0.177	0.057	0.603	0.017
C.-T.L.	0.729	0.011	0.361	0.034
C.-T.R.	0.293	0.041	0.491	0.024
P.-T.L.	0.760	0.009	0.422	0.029
P.-T.R.	0.704	0.012	0.526	0.022
T.L.-T.R.	0.550	0.020	0.234	0.048

**Table 3.2.25:** Significance  $p$  and coefficient of determination  $R^2$  as determined by Fisher's F-test for a least squares quadratic regression model: measures between the respective second PCs of channel groups in the  $\alpha$ -frequency band during the cognitive task; "\*" and "\*\*\*" indicate  $p < 0.05$  and  $p < 0.01$  respectively

$\alpha$ -band	Coh.		pCoh.	
	p	$R^2$	p	$R^2$
A.-C.	0.467	0.025	0.747	0.010
A.-P.	0.106	0.073	0.485	0.024
A.-T.L.	0.406	0.030	0.467	0.025
A.-T.R.	0.115	0.071	0.312	0.039
C.-P.	0.746	0.010	0.898	0.004
C.-T.L.	<0.001**	0.365	0.038*	0.105
C.-T.R.	0.011*	0.142	0.405	0.030
P.-T.L.	0.559	0.020	0.808	0.007
P.-T.R.	0.567	0.019	0.566	0.019
T.L.-T.R.	0.174	0.058	0.133	0.066

The analysis of dynamic canonical correlations (between channel groups) resulted in significant findings between Anterior-Temporal Left ( $R^2 = 0.140$ ), Posterior-Temporal Right ( $R^2 = 0.140$ ) and Left-Right ( $R^2 = 0.105$ ), and in highly significant findings between Central-Temporal Left ( $R^2 = 0.195$ ), Central-Temporal Right ( $R^2 = 0.164$ ) and Posterior-Temporal Left ( $R^2 = 0.252$ ). Changes of dynamic canonical correlations between the PCs were highly significant between

Central-Temporal Left ( $R^2 = 0.254$ ). Table 3.2.26 provides the cognitive task results between the channel groups in the  $\alpha$ -frequency band.

**Table 3.2.26:** Significance  $p$  and coefficient of determination  $R^2$  as determined by Fisher's F-test for a least squares quadratic regression model: measures between channel groups in the  $\alpha$ -frequency band during the cognitive task; "\*" and "\*\*" indicate  $p < 0.05$  and  $p < 0.01$  respectively

$\alpha$ -band	dynCC (betw. groups)		dynCC (betw. PCs)	
	p	$R^2$	p	$R^2$
A.-C.	0.132	0.066	0.260	0.045
A.-P.	0.092	0.078	0.370	0.033
A.-T.L.	0.012*	0.140	0.072	0.085
A.-T.R.	0.356	0.034	0.110	0.072
C.-P.	0.065	0.088	0.433	0.028
C.-T.L.	0.002**	0.195	<0.001**	0.254
C.-T.R.	0.005**	0.164	0.038*	0.105
P.-T.L.	<0.001**	0.252	0.107	0.073
P.-T.R.	0.012*	0.140	0.213	0.051
T.L.-T.R.	0.098	0.076	0.035*	0.108
L.-R.	0.037*	0.105	0.057	0.093

In the  $\beta_0$ -frequency band, neither coherences nor partial coherences between the respective first PCs of channel groups yielded significant results. Table 3.2.27 provides all cognitive task results between the respective first PCs of channel groups in the  $\beta_0$ -frequency band.

For the second PCs, changes of coherences were observed to be highly significant between Central-Temporal Left ( $R^2 = 0.216$ ). Significant results were obtained for coherences between Temporal Left-Temporal Right ( $R^2 = 0.137$ ), and for partial coherences between Anterior-Temporal Right ( $R^2 = 0.100$ ) and Central-Temporal Right ( $R^2 = 0.121$ ). Table 3.2.28 provides the cognitive task results between the respective second PCs of channel groups in the  $\beta_0$ -frequency band.

Dynamic canonical correlations (between channel groups) yielded significance between Anterior-Posterior ( $R^2 = 0.108$ ), Anterior-Temporal Right ( $R^2 = 0.102$ ), Central-Posterior ( $R^2 = 0.121$ ) and Central-Temporal Right ( $R^2 = 0.114$ ), and high significance between Central-Temporal Left ( $R^2 = 0.152$ ), Posterior-Temporal Left ( $R^2 = 0.263$ ) and Posterior-Temporal Right ( $R^2 = 0.212$ ). Changes of dynamic canonical correlations between the PCs were highly significant between Central-Temporal Left ( $R^2 = 0.203$ ). Table 3.2.29 provides the cognitive task results between the channel groups in the  $\beta_0$ -frequency band.

**Table 3.2.27:** Significance  $p$  and coefficient of determination  $R^2$  as determined by Fisher's F-test for a least squares quadratic regression model: measures between the respective first PCs of channel groups in the  $\beta_0$ -frequency band during the cognitive task; "\*" and "\*\*\*" indicate  $p < 0.05$  and  $p < 0.01$  respectively

$\beta_0$ -band	Coh.		pCoh.	
	p	$R^2$	p	$R^2$
A.-C.	0.416	0.029	0.376	0.033
A.-P.	0.467	0.025	0.518	0.022
A.-T.L.	0.142	0.064	0.414	0.029
A.-T.R.	0.226	0.049	0.522	0.022
C.-P.	0.311	0.039	0.205	0.052
C.-T.L.	0.163	0.060	0.338	0.036
C.-T.R.	0.073	0.085	0.939	0.002
P.-T.L.	0.741	0.010	0.825	0.007
P.-T.R.	0.300	0.040	0.757	0.009
T.L.-T.R.	0.487	0.024	0.786	0.008

**Table 3.2.28:** Significance  $p$  and coefficient of determination  $R^2$  as determined by Fisher's F-test for a least squares quadratic regression model: measures between the respective second PCs of channel groups in the  $\beta_0$ -frequency band during the cognitive task; "\*" and "\*\*\*" indicate  $p < 0.05$  and  $p < 0.01$  respectively

$\beta_0$ -band	Coh.		pCoh.	
	p	$R^2$	p	$R^2$
A.-C.	0.293	0.041	0.289	0.041
A.-P.	0.772	0.009	0.498	0.023
A.-T.L.	0.087	0.079	0.147	0.063
A.-T.R.	0.057	0.093	0.045*	0.100
C.-P.	0.879	0.004	0.742	0.010
C.-T.L.	0.001**	0.216	0.063	0.089
C.-T.R.	0.032	0.110	0.022*	0.121
P.-T.L.	0.574	0.019	0.433	0.028
P.-T.R.	0.676	0.013	0.280	0.042
T.L.-T.R.	0.013*	0.137	0.328	0.037

On the whole EEG signals, changes of partial coherences were significant between Anterior-Posterior ( $R^2 = 0.119$ ) and Temporal Left-Temporal Right ( $R^2 = 0.116$ ). Bivariate Granger causalities yielded significant findings between Anterior  $\rightarrow$  Posterior ( $R^2 = 0.099$ ), Temporal Right  $\rightarrow$  Central ( $R^2 = 0.104$ ) and Posterior  $\rightarrow$  Temporal Left ( $R^2 = 0.136$ ), and highly significant findings between Central  $\rightarrow$  Posterior ( $R^2 = 0.162$ ). Changes of conditional Granger causalities were significant between Central  $\rightarrow$  Anterior ( $R^2 = 0.129$ ), Posterior  $\rightarrow$  Anterior

**Table 3.2.29:** Significance  $p$  and coefficient of determination  $R^2$  as determined by Fisher's F-test for a least squares quadratic regression model: measures between channel groups in the  $\beta_0$ -frequency band during the cognitive task; "\*" and "\*\*" indicate  $p < 0.05$  and  $p < 0.01$  respectively

$\beta_0$ -band	dynCC (betw. groups)		dynCC (betw. PCs)	
	p	$R^2$	p	$R^2$
A.-C.	0.099	0.075	0.206	0.052
A.-P.	0.034*	0.108	0.197	0.054
A.-T.L.	0.089	0.079	0.042*	0.102
A.-T.R.	0.042*	0.102	0.196	0.054
C.-P.	0.022*	0.121	0.487	0.024
C.-T.L.	0.008**	0.152	0.001**	0.203
C.-T.R.	0.028*	0.114	0.017*	0.129
P.-T.L.	<0.001**	0.263	0.157	0.061
P.-T.R.	0.001**	0.212	0.106	0.073
T.L.-T.R.	0.178	0.057	0.047*	0.099
L.-R.	0.080	0.082	0.037*	0.106

( $R^2 = 0.112$ ), Temporal Left  $\rightarrow$  Posterior ( $R^2 = 0.109$ ) and Posterior  $\rightarrow$  Temporal Right ( $R^2 = 0.117$ ), and highly significant between Temporal Left  $\rightarrow$  Anterior ( $R^2 = 0.171$ ), Anterior  $\rightarrow$  Temporal Right ( $R^2 = 0.276$ ), Central  $\rightarrow$  Temporal Right ( $R^2 = 0.197$ ) and Temporal Left  $\rightarrow$  Temporal Right ( $R^2 = 0.185$ ). Table 3.2.30 provides the cognitive task results between the respective first PCs of channel groups in the total frequency band.

For the second PCs, changes of coherences were significant between Central-Temporal Right ( $R^2 = 0.107$ ), and highly significant between Central-Temporal Left ( $R^2 = 0.401$ ). For the latter group combination, partial coherences yielded significant results as well ( $R^2 = 0.101$ ). The analysis of bivariate Granger causalities showed significant findings between Central  $\rightarrow$  Posterior ( $R^2 = 0.116$ ), and highly significant findings between Central  $\rightarrow$  Temporal Left ( $R^2 = 0.151$ ), and Temporal Right  $\rightarrow$  Central ( $R^2 = 0.155$ ). For conditional Granger causalities, significance was observed all but two group combinations; high significance between Anterior  $\rightarrow$  Posterior ( $R^2 = 0.206$ ), Temporal Right  $\rightarrow$  Central ( $R^2 = 0.181$ ), Temporal Right  $\rightarrow$  Posterior ( $R^2 = 0.263$ ), and Temporal Right  $\rightarrow$  Temporal Left ( $R^2 = 0.248$ ). Table 3.2.31 provides the cognitive task results between the respective second PCs of channel groups in the total frequency band.

Finally, both static and dynamic canonical correlations showed significant changes for all group combinations but Anterior-Temporal Right and Anterior-Central respectively. Between Central-Temporal Left, a coefficient of determination  $R^2 = 0.405$  was derived. Changes of both static and dynamic canonical corre-

**Table 3.2.30:** Significance  $p$  and coefficient of determination  $R^2$  as determined by Fisher's F-test for a least squares quadratic regression model: measures between the respective first PCs of channel groups on the whole EEG signals during the cognitive task; "\*" and "\*\*\*" indicate  $p < 0.05$  and  $p < 0.01$  respectively

total	Coh.		pCoh.		bGC		cGC	
	p	$R^2$	p	$R^2$	p	$R^2$	p	$R^2$
A.-C.	0.973	0.001	0.852	0.005	0.307 0.830	0.039 0.006	0.287 0.017*	0.041 0.129
A.-P.	0.452	0.027	0.024*	0.119	0.046* 0.340	0.099 0.036	0.470 0.031*	0.025 0.112
A.-T.L.	0.236	0.048	0.071	0.086	0.584 0.835	0.018 0.006	0.248 0.004**	0.046 0.171
A.-T.R.	0.405	0.030	0.943	0.002	0.876 0.879	0.004 0.004	<0.001** 0.294	0.276 0.041
C.-P.	0.060	0.091	0.071	0.086	0.005** 0.090	0.162 0.078	0.217 0.225	0.051 0.049
C.-T.L.	0.902	0.003	0.102	0.075	0.136 0.177	0.065 0.057	0.419 0.134	0.029 0.066
C.-T.R.	0.198	0.053	0.085	0.080	0.831 0.039*	0.006 0.104	0.002** 0.508	0.197 0.023
P.-T.L.	0.626	0.016	0.658	0.014	0.013* 0.920	0.136 0.003	0.280 0.033*	0.042 0.109
P.-T.R.	0.746	0.010	0.320	0.038	0.074 0.368	0.084 0.033	0.025* 0.493	0.117 0.024
T.L.-T.R.	0.407	0.030	0.027*	0.116	0.459 0.786	0.026 0.008	0.002** 0.495	0.185 0.024

lations were highly significant between Central-Temporal Left as well ( $R^2 = 0.179$  and  $R^2 = 0.232$ ). Table 3.2.32 provides the cognitive task results between the channel groups on the whole EEG signals.



**Table 3.2.31:** Significance  $p$  and coefficient of determination  $R^2$  as determined by Fisher's F-test for a least squares quadratic regression model: measures between the respective second PCs of channel groups on the whole EEG signals during the cognitive task; "\*" and "\*\*\*" indicate  $p < 0.05$  and  $p < 0.01$  respectively

total	Coh.		pCoh.		bGC		cGC	
	p	R <sup>2</sup>	p	R <sup>2</sup>	p	R <sup>2</sup>	p	R <sup>2</sup>
A.-C.	0.317	0.038	0.721	0.011	0.340 0.892	0.036 0.004	0.047* 0.024*	0.099 0.119
A.-P.	0.333	0.037	0.726	0.011	0.854 0.577	0.005 0.018	0.001** 0.019*	0.206 0.126
A.-T.L.	0.310	0.039	0.529	0.021	0.674 0.579	0.013 0.018	0.079 0.107	0.082 0.073
A.-T.R.	0.116	0.070	0.192	0.054	0.540 0.381	0.021 0.032	0.034* 0.075	0.109 0.084
C.-P.	0.584	0.018	0.735	0.010	0.027* 0.271	0.116 0.043	0.017* 0.013*	0.129 0.137
C.-T.L.	<0.001**	0.401	0.043*	0.101	0.008** 0.937	0.151 0.002	0.203 0.014*	0.053 0.134
C.-T.R.	0.035*	0.107	0.759	0.009	0.358 0.007**	0.034 0.155	0.075 0.003**	0.084 0.181
P.-T.L.	0.056	0.093	0.382	0.032	0.483 0.197	0.024 0.054	0.145 0.094	0.063 0.077
P.-T.R.	0.415	0.029	0.539	0.021	0.283 0.188	0.042 0.055	0.148 <0.001**	0.063 0.263
T.L.-T.R.	0.381	0.032	0.152	0.062	0.075 0.637	0.084 0.015	0.056 <0.001**	0.093 0.248

**Table 3.2.32:** Significance  $p$  and coefficient of determination  $R^2$  as determined by Fisher's F-test for a least squares quadratic regression model: measures between channel groups on the whole EEG signals during the cognitive task; "\*" and "\*\*\*" indicate  $p < 0.05$  and  $p < 0.01$  respectively

total	statCC (groups)		statCC (PCs)		dynCC (groups)		dynCC (PCs)	
	p	R <sup>2</sup>	p	R <sup>2</sup>	p	R <sup>2</sup>	p	R <sup>2</sup>
A.-C.	0.034*	0.108	0.152	0.062	0.060	0.091	0.290	0.041
A.-P.	0.002**	0.197	0.199	0.053	0.005**	0.162	0.488	0.024
A.-T.L.	0.001**	0.207	0.046*	0.099	0.001**	0.199	0.032*	0.110
A.-T.R.	0.125	0.068	0.367	0.033	0.061	0.090	0.040*	0.103
C.-P.	0.002**	0.196	0.266	0.044	0.009**	0.147	0.340	0.036
C.-T.L.	<0.001**	0.405	0.003**	0.179	<0.001**	0.294	<0.001**	0.232
C.-T.R.	0.001**	0.201	0.085	0.080	0.001**	0.206	0.012*	0.139
P.-T.L.	<0.001**	0.294	0.084	0.081	<0.001**	0.278	0.122	0.069
P.-T.R.	<0.001**	0.302	0.015*	0.133	0.001**	0.210	0.140	0.064
TL-TR	0.011*	0.141	0.03*	0.112	0.022*	0.121	0.013*	0.136
L.-R.	0.005**	0.165	0.089	0.079	0.010*	0.146	0.036*	0.107

### 3.3 Synchrony Within Groups of EEG Channels

This section will provide the results for synchrony between the following channel groups (cf. Figures 2.9.2a and 2.9.2b): Anterior (A.)<sup>2</sup>, Central (C.), Posterior (P.), Temporal Left (T.L.), Temporal Right (T.R.), Left (L.), Right (R.) and All. In the  $\delta$ -,  $\theta$ -,  $\alpha$ -, and  $\beta_0$ -frequency bands, the information explained by the respective first dynamic PC was investigated. For the whole signal, the information content of the respective first static and dynamic PCs was estimated. Section 3.3.1 will summarize the findings, whereas Sections 3.3.2 and 3.3.3 will present the listing of all results.

#### 3.3.1 Main Results

In resting state, no highly significant changes were observed, neither of the static nor the dynamic PCA measure. Occasionally, the latter yielded significant findings in Anterior in  $\delta$ , Posterior in  $\theta$  and for the whole signal, in Temporal Right in  $\beta_0$ , and in Right in  $\beta_0$ . Table 3.3.1 provides an overview of the significant test results for each measure, frequency band, and channel group in resting state.

**Table 3.3.1:** Overview of the significances derived for a least squares quadratic regression model of synchrony measures within channel groups in resting state; "\*" and "\*\*\*" indicate  $p < 0.05$  and  $p < 0.01$  respectively.

REC	Ant.	Cent.	Post.	Temp.L.	Temp.R.	L.	R.	All
<b>dynPCA</b>								
$\delta$	*							
$\theta$			*					
$\alpha$								
$\beta_0$					*		*	
total			*					
<b>statPCA</b>								

During the cognitive task, highly significant changes were observed only in the  $\beta_0$ -frequency band for the dynamic PCA measure in Temporal Right ( $R^2 = 0.208$ ), Right ( $R^2 = 0.160$ ), and All ( $R^2 = 0.159$ ). Figure 3.3.1 displays the values of the dynamic PCA measure in Temporal Right in the  $\beta_0$ -frequency band as scatterdiagram versus MMSE scores. The quadratic regression model ( $p = 0.001$ ,  $R^2 = 0.208$ ) is characterized by an increase for MMSE scores between 26 and 20, and a decrease from 20 downwards.

Table 3.3.2 provides an overview of the significant test results for each measure, frequency band, and channel group during the cognitive task.

<sup>2</sup>The abbreviations in brackets will be used in the tables.

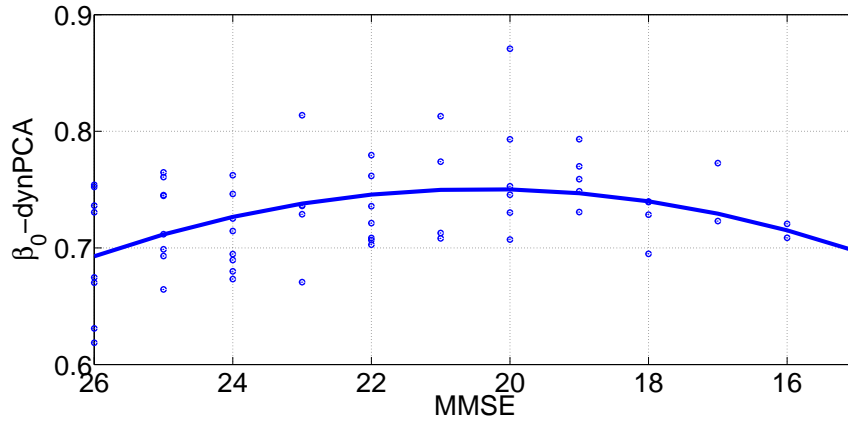


**Figure 3.3.1:** Example for changes of synchrony within channel groups during the **cognitive task: dynamic PCA in Temporal Right** in the  $\beta_0$ -frequency band versus MMSE scores. Low MMSE scores (right side of the abscissa) indicate a higher degree of severity of AD. A quadratic regression was fitted to the scatterplot with  $p = 0.001$  and  $R^2 = 0.208$ .

**Table 3.3.2:** Overview of the significances derived for a least squares quadratic regression model of synchrony measures within channel groups during the cognitive state; "\*" and "\*\*" indicate  $p < 0.05$  and  $p < 0.01$  respectively.

FN	Ant.	Cent.	Post.	Temp.L.	Temp.R.	L.	R.	All
<b>dynPCA</b>								
$\delta$								
$\theta$								
$\alpha$								
$\beta_0$					**	*	**	**
total								
<b>statPCA</b>								
			*					

### 3.3.2 Detailed Results: Resting State

Here, the listing of all results from analyzing EEG synchrony within channel groups in resting state will be provided, starting with the  $\delta$ -frequency band. Quadratic regression of the variance explained by the first dynamic PC was significant only in Anterior ( $R^2 = 0.111$ ). Table 3.3.3 provides the resting state results within channel groups in the  $\delta$ -frequency band.

**Table 3.3.3:** Significance  $p$  and coefficient of determination  $R^2$  as determined by Fisher's F-test for a least squares quadratic regression model: measures within channel groups in the  $\delta$ -frequency band in resting state; "\*" and "\*\*" indicate  $p < 0.05$  and  $p < 0.01$  respectively

$\delta$ -band	$p$	dynPCA	$R^2$
A.	0.028*		0.111
C.	0.594		0.017
P.	0.087		0.077
T.L.	0.510		0.022
T.R.	0.886		0.004
L.	0.832		0.006
R.	0.561		0.019
All	0.435		0.027

In the  $\theta$ -frequency band, changes of the dynamic PCA measure yielded significant test results only in Posterior ( $R^2 = 0.101$ ). Table 3.3.4 provides the resting state results within channel groups in the  $\theta$ -frequency band.

**Table 3.3.4:** Significance  $p$  and coefficient of determination  $R^2$  as determined by Fisher's F-test for a least squares quadratic regression model: measures within channel groups in the  $\theta$ -frequency band in resting state; "\*" and "\*\*" indicate  $p < 0.05$  and  $p < 0.01$  respectively

$\theta$ -band	$p$	dynPCA	$R^2$
A.	0.295		0.039
C.	0.841		0.006
P.	0.039*		0.101
T.L.	0.775		0.008
T.R.	0.962		0.001
L.	0.967		0.001
R.	0.882		0.004
All	0.736		0.010

In the  $\alpha$ -frequency band, no statistically significant findings could be observed.

Table 3.3.5 provides the resting state results within channel groups in the  $\alpha$ -frequency band.

**Table 3.3.5:** Significance  $p$  and coefficient of determination  $R^2$  as determined by Fisher's F-test for a least squares quadratic regression model: measures within channel groups in the  $\alpha$ -frequency band in resting state; "\*" and "\*\*" indicate  $p < 0.05$  and  $p < 0.01$  respectively

$\alpha$ -band	p	dynPCA	$R^2$
A.	0.901		0.003
C.	0.441		0.026
P.	0.075		0.081
T.L.	0.786		0.008
T.R.	0.700		0.012
L.	0.305		0.038
R.	0.380		0.031
All	0.387		0.031

In the  $\beta_0$ -frequency band, the analysis revealed significant findings in Temporal Right ( $R^2 = 0.100$ ), and Right ( $R^2 = 0.128$ ). Table 3.3.6 provides the resting state results within channel groups in the  $\beta_0$ -frequency band.

**Table 3.3.6:** Significance  $p$  and coefficient of determination  $R^2$  as determined by Fisher's F-test for a least squares quadratic regression model: measures within channel groups in the  $\beta_0$ -frequency band in resting state; "\*" and "\*\*" indicate  $p < 0.05$  and  $p < 0.01$  respectively

$\beta_0$ -band	p	dynPCA	$R^2$
A.	0.881		0.004
C.	0.209		0.050
P.	0.088		0.077
T.L.	0.209		0.050
T.R.	0.041*		0.100
L.	0.228		0.047
R.	0.015*		0.128
All	0.099		0.073

On the whole EEG signals, changes of the static PCA measure were significant in none of the channel groups. For dynamic PCs, significant results were obtained only in Posterior ( $R^2 = 0.101$ ). Table 3.3.7 provides the resting state findings within channel groups in the total frequency band.

**Table 3.3.7:** Significance  $p$  and coefficient of determination  $R^2$  as determined by Fisher's F-test for a least squares quadratic regression model: measures within channel groups on the whole EEG signals in resting state; "\*" and "\*\*\*" indicate  $p < 0.05$  and  $p < 0.01$  respectively

total	statPCA		dynPCA	
	p	R <sup>2</sup>	p	R <sup>2</sup>
A.	0.674	0.013	0.629	0.015
C.	0.528	0.021	0.521	0.021
P.	0.086	0.077	0.038*	0.101
T.L.	0.969	0.001	0.923	0.003
T.R.	0.931	0.002	0.622	0.015
L.	0.659	0.014	0.843	0.006
R.	0.628	0.015	0.355	0.033
All	0.522	0.021	0.448	0.026

### 3.3.3 Detailed Results: Cognitive Task

Here, finally, the listing of all results from analyzing EEG synchrony within channel groups during the cognitive task will be provided. In the  $\delta$ -frequency band, no significance was found. Table 3.3.8 provides the cognitive task results within channel groups in the  $\delta$ -frequency band.

**Table 3.3.8:** Significance  $p$  and coefficient of determination  $R^2$  as determined by Fisher's F-test for a least squares quadratic regression model: measures within channel groups in the  $\delta$ -frequency band during the cognitive task; "\*" and "\*\*\*" indicate  $p < 0.05$  and  $p < 0.01$  respectively

$\delta$ -band	$p$	dynPCA	$R^2$
A.	0.159		0.061
C.	0.674		0.013
P.	0.098		0.076
T.L.	0.916		0.003
T.R.	0.616		0.016
L.	0.866		0.005
R.	0.213		0.051
All	0.563		0.019

Also in the  $\theta$ -frequency band, none of the channel groups showed significant test results. Table 3.3.9 provides the cognitive task results within channel groups in the  $\theta$ -frequency band.

**Table 3.3.9:** Significance  $p$  and coefficient of determination  $R^2$  as determined by Fisher's F-test for a least squares quadratic regression model: measures within channel groups in the  $\theta$ -frequency band during the cognitive task; "\*" and "\*\*\*" indicate  $p < 0.05$  and  $p < 0.01$  respectively

$\theta$ -band	$p$	dynPCA	$R^2$
A.	0.375		0.033
C.	0.748		0.010
P.	0.056		0.093
T.L.	0.306		0.039
T.R.	0.554		0.020
L.	0.530		0.021
R.	0.229		0.049
All	0.320		0.038

In the  $\alpha$ -frequency band, no significant changes of synchrony were found as well. Table 3.3.10 provides the cognitive task results within channel groups in the

$\alpha$ -frequency band.

**Table 3.3.10:** Significance  $p$  and coefficient of determination  $R^2$  as determined by Fisher's F-test for a least squares quadratic regression model: measures within channel groups in the  $\alpha$ -frequency band during the cognitive task; "\*" and "\*\*\*" indicate  $p < 0.05$  and  $p < 0.01$  respectively

$\alpha$ -band	$p$	dynPCA	$R^2$
A.	0.667		0.014
C.	0.257		0.045
P.	0.112		0.071
T.L.	0.245		0.047
T.R.	0.082		0.081
L.	0.159		0.060
R.	0.438		0.028
All	0.143		0.064

In the  $\beta_0$ -frequency band, the dynamic PCA measure yielded significant findings in Left ( $R^2 = 0.118$ ), and highly significant findings in Temporal Right ( $R^2 = 0.208$ ), Right ( $R^2 = 0.160$ ), and All ( $R^2 = 0.159$ ). Table 3.3.11 provides the cognitive task results within channel groups in the  $\beta_0$ -frequency band.

**Table 3.3.11:** Significance  $p$  and coefficient of determination  $R^2$  as determined by Fisher's F-test for a least squares quadratic regression model: measures within channel groups in the  $\beta_0$ -frequency band during the cognitive task; "\*" and "\*\*\*" indicate  $p < 0.05$  and  $p < 0.01$  respectively

$\beta_0$ -band	$p$	dynPCA	$R^2$
A.	0.148		0.063
C.	0.103		0.074
P.	0.075		0.084
T.L.	0.068		0.087
T.R.	0.001**		0.208
L.	0.024*		0.118
R.	0.006**		0.160
All	0.006**		0.159

Finally, the analysis on the whole EEG signals indicated significant changes of the amount of variance explained by the first static PC in Posterior ( $R^2 = 0.117$ ). No significant changes of the dynamic PCA measure could be observed. Table 3.3.12 provides the cognitive task results within channel groups on the whole EEG signal.



**Table 3.3.12:** Significance  $p$  and coefficient of determination  $R^2$  as determined by Fisher's F-test for a least squares quadratic regression model: measures within channel groups on the whole EEG signals during the cognitive task; "\*" and "\*\*" indicate  $p < 0.05$  and  $p < 0.01$  respectively

total	statPCA		dynPCA	
	p	$R^2$	p	$R^2$
A.	0.397	0.031	0.571	0.019
C.	0.621	0.016	0.299	0.040
P.	0.025*	0.117	0.055	0.094
T.L.	0.110	0.072	0.170	0.058
T.R.	0.146	0.063	0.116	0.070
L.	0.823	0.007	0.135	0.066
R.	0.874	0.005	0.270	0.043
All	0.763	0.009	0.106	0.073



---

### Discussion and Conclusion

---

This chapter will provide a summary of the findings and discuss them in light of the research questions. Then, the findings will be compared to the scientific status quo. Comments and critical thoughts about the applied methods will follow. Finally, suggestions for further research will conclude this work. Throughout this chapter, the terms *significant* and *highly significant* will be used for the F-test results of quadratic regression on the levels  $p = 0.05$  and  $p = 0.01$  respectively.

#### 4.1 Discussion

$H_0^1$ : *Synchronies between single EEG channels change in the course of AD.*

The resting state analysis of EEG synchrony between single electrode channels showed only scattered significances. The most promising results were observed for partial coherences in left-hemispheric electrode channel pairs FP1-O1, F3-O1, F7-T7, and C3-P7. During the cognitive task, coherences yielded the most significant results, especially in local posterior channel pairs C4-P8, P3-P7, and P4-P8. For the channel pair F7-T7, partial coherences, bivariate and conditional Granger causalities showed highly significant results. However, the number of promising findings between channel pairs is small; thus, the observed, mostly isolated correlations of the mentioned synchrony measures with the MMSE should not be overrated as they could be attributed to random multiple testing errors.

$H_0^2$ : *Synchronies between EEG channel groups change in the course of AD.*

Dividing the channels into groups yielded higher significances than the investigation of channel pairs. In resting state, dynamic canonical correlations showed constantly significant results in the  $\delta$ - and  $\theta$ -frequency band with  $R^2 > 0.20$ . Additionally, the changes of conditional Granger causalities were highly significant for all group combinations with most  $R^2$  larger than 0.25. During the cognitive task, coherences between the 2<sup>nd</sup> PCs of the Central and Temporal Left channel groups yielded highly significant results in all frequency bands with relatively high  $R^2 > 0.35$ . For these group combinations, both static ( $R^2 = 0.405$ ) and dynamic

canonical correlations (especially in  $\theta$  with  $R^2 = 0.390$ ) showed high significances as well; highly significant changes of these two measures were observed for most group combinations. In general, canonical correlations between the channel groups were more significant than between the PCs. Partial coherences and the Granger measures showed only scattered significances. However, dynamic canonical correlations and conditional Granger causalities in resting state, and coherences and static/dynamic canonical correlations during the cognitive task turned out to be promising measures for EEG synchrony changes.

*$H_0^3$ : Synchronies within EEG channel groups change in the course of AD.*

In resting state, the investigation of EEG synchrony within the predefined channel groups yielded no highly significant results. Neither for the dynamic PCA measure in the different frequency bands nor for the static PCA measure results supporting  $H_0^3$  were observed. During the cognitive task, analyses showed high significances for the dynamic PCA measure in the channel groups Temporal Right ( $R^2 = 0.208$ ), Right ( $R^2 = 0.160$ ), and All ( $R^2 = 0.159$ ) in the  $\beta_0$ -frequency band. The applied measures do not definitely support  $H_0^3$ ; however, an investigation of higher frequencies and other PCs than the first may be expedient in this matter.

There is only a small number of studies that are directly comparable to this work as most works perform group comparisons (e.g. NOLD/MCI/AD) instead of correlating EEG synchrony markers with AD severity. However, a major share of these group comparisons suggested a decrease of EEG synchrony in resting state (e.g. [11], [12], [13], [14], [16], [18], [20], [22], [23], [24], [26]), and an increase during cognitive tasks for MCI and in few cases also for AD patients as compared to controls (e.g. [32], [33]). This increase was attributed to compensatory mechanisms in the brain (cf. [38]). These synchrony changes were mostly reported for the left hemisphere, often between Temporal and Parietal, or Temporal and Central electrode channels. The mainly applied synchrony measures were coherences and, in more recent studies, nonlinear measures originating from information theory. Studies that are directly comparable to this work reported no significant correlations between the degree of AD and coherences, neither in resting state ([16], [36]) nor during a working memory task ([36]). However, significant correlations were observed between the degree of AD and synchronization likelihood ([23], [24], [39]), and global field synchronization ([28]), respectively.

In this work, an increase of synchrony in the initial stages and a decrease in the later stages of AD was observed for several measures both in resting state and during a cognitive task. This increase of EEG synchrony may be attributed to the same compensatory mechanisms in the brain that have been reported in the former mentioned group comparison studies. This phenomenon was more prominent during the cognitive task than in resting state. In the latter, a decrease of Granger

causalities between channel groups was observed also in the initial stage of AD. Whereas no significant correlations between AD severity and coherences have been reported in e.g. [16] and [36], coherences yielded highly significant results during the cognitive task in this study. This may be due to the applied quadratic regression model that allowed to model increases at the initial stage of AD as well. The most significant changes of coherences were observed between Central and Temporal Left channel groups, and Central and Posterior groups. These findings correspond to the majority of mentioned group studies. Altogether, the investigation between channel groups showed by far more significant results than between single channels. The accumulation of several channels resulted in a more stable analysis of synchrony, maybe because single EEG channels can easily be disturbed.

Applying different measures for synchrony proved to be justified; some of the measures described synchrony changes in one of the EEG stages better than in the other, or could emphasize the compensatory mechanisms in the brain. Also, by using both time-static and -dynamic measures, valuable information could be gained. In resting state, the investigation of dynamic canonical correlations yielded additional information as compared to the static analysis. Synchrony changes were significant only in the low frequency bands  $\delta$  and  $\theta$ . During the cognitive task, the information gain from using the dynamic measure was neglectable. This may suggest that the neuronal transmission during a cognitive task happens at high speed and, thus, measuring time-dynamic changes cannot provide additional insights.

In the following paragraphs, critical thoughts on the applied methods will follow, starting with the sample data. The EEG samples from the PRODEM-AUSTRIA database were all conducted in a uniform setting and according to a clinically predefined paradigm. Clinical assessments included neuropsychological tests and the enrollment of demographic parameters sex, age, degree of education, and duration of AD. These properties, together with the integration of both resting state and a cognitive task, make high quality data of these samples. The sample consisting of 79 EEG datasets from probable AD patients is, compared to scientific literature, among the largest; a comparable or higher number was applied only in [22] (103 AD patients, 124 controls), [20] (73 AD patients, 69 subjects with MCI, 64 controls) and [39] (109 AD patients, 88 subjects with MCI, 69 controls). The small sample size used in various studies is often owed to the limited accessibility to clinical databases; however, access to high quality databases such as the PRODEM-AUSTRIA database is of decisive importance for these types of studies.

In this study, MMSE scores were used for quantifying the severity of AD. This neuropsychological test score is applied in most studies that are comparable to this work (e.g. [16], [23]). However, different testing scores such as CDR, NPI, DAD, or CERAD could serve as alternative quantifications of AD severity (cf. e.g. [28]).

For capturing the EEG synchrony changes as compared with MMSE, a quadratic least squares regression was applied. The usage of the quadratic form is, to the best of the author's knowledge, a novelty in this field. It allows to capture non-monotonical synchrony changes such as those from compensatory mechanisms in the brain. The demographic variables sex, age, degree of education, and duration of AD were used as covariables. From the directly comparable studies listed above, [16] and [24] include the covariable age in the analysis. However, there are studies that have observed significant correlations between one or more of the four covariables and AD (e.g. [28]); thus, including them in the analyses is reasonable.

A crucial step in automated EEG analysis is the preprocessing procedure for minimizing deteriorations due to artefacts. Eliminating low-frequency artefacts by high-pass filtering is common practice in EEG analysis. The border frequency of 2 Hz was empirically determined. EEG recordings that contain cardiac artefacts are often discarded from further analyses; here, in order to maintain a large sample size, algorithms for the detection and elimination of cardiac artefacts (cf. [52]) were applied and verified by visual examination. There is a broad range of alternative algorithms for the removal of cardiac artefacts, both relying solely on the EEG (e.g. [75], [76]) and relying on a simultaneously recorded ECG channel (e.g. [77], [78]). For the removal of eye artefacts, the simultaneously recorded EOG channels were utilized. The removal of high-frequency oscillations from the EOGs by low-pass filtering was empirically developed and fine-tuned. A static regression of each EEG channel on the EOG channels is straight-forward. Other procedures – often in the absence of additional EOG channels – such as blind source separation have been applied in several studies (e.g. [76]). In the final preprocessing step, the EEG data were low-pass filtered. Most studies investigate the signals up to 20 or 30 Hz; however, in order to minimize interfering muscular artefacts without discarding EEG channels, a border frequency of 15 Hz was determined by comparing the spectra of channels with and without muscular artefacts. Thus, all further analyses were limited to the band-pass filtered signal (2 – 15 Hz).

As the EEG is a non-stationary signal, analyses were carried out on quasi-stationary EEG segments. The EEG recordings were divided in segments of equal length of 4 seconds with an overlap of 2 seconds. Alternatively, adaptive segmentation procedures have been described in scientific literature (e.g. [54], [55]). However, these procedures require structural breaks in the data, e.g. when the patient is opening the eyes. Within the EEG stages resting state and cognitive task, no severe structural breaks were observed and, thus, the uniform-length segments applied. The EEG synchrony measures were calculated for each segment and averaged over all segments corresponding to resting state and cognitive task respectively.

In this work, an indirect spectral estimation procedure with a Parzen window function was applied. Comparable studies have often used the periodogram and

direct approaches like the Welch method (e.g. [17]). For averaging of measures in frequency bands, both estimates are consistent. For analyses and automated detection of characteristic single EEG frequencies such as the individual alpha frequency, the presented indirect approach is better suited than the periodogram due to its "irregular" shape (cf. Section 2.7.1).

Dividing the frequency domain in frequency bands is common practice in EEG analysis; however, frequency borders vary in literature and the transition frequencies between the four frequency bands may differ from the transition frequencies used here by  $\pm 1$  Hz. The lower frequency border of the  $\delta$ -band is often defined as 0 or 0.5 Hz. The upper  $\beta$ -border is usually defined in a range of 20 to 30 Hz; here, the border of 15 Hz was chosen in order to make sure that no artefacts deteriorate the analyses. An alternative to fixed frequency bands would be an individualization by means of the individual position of peaks such as the individual alpha frequency and the transition frequencies between these peaks. As these peaks and the transition between them vary widely amongst different subjects, electrode channels, and cognitive phases, an individualization of frequency bands is a non-trivial task that would have complicated the analyses.

The channel pairs in the four categories far intra- and interhemispheric, and local anterior and posterior were defined from medical experts with the aim to cover all major neuronal connections that may be affected by AD. Additional channel pairs are conceivable. The clustering of EEG channels in channel groups was partly done according to [38] and was inspired by the brain's lobe structure. This approach allows to quantify EEG synchrony more robustly than between EEG channel pairs as single EEG channels are much more prone to interferences.

All measures for EEG synchrony were derived from the spectral density and, thus, only the first and second moments were utilized. Due to the complexity of neuronal processes, recent studies have considered nonlinear measures such as mutual information or synchronization likelihood (cf. e.g. [39]). The application of these nonlinear measures could provide additional aspects on the changes of EEG synchrony. For several of the applied measures, minor modifications are conceivable: for the investigation of Granger causalities, the Euklidean norm of the matrix-entries of the AR coefficients was used. Another norm such as the Manhattan norm could be applied instead. The same applies to the Euklidean norm of canonical correlation coefficients. Here, the maximum norm could be an alternative. Whereas the estimation of EEG synchrony measures between single channels is straightforward, estimating them between groups of channels can be done in different ways. Here, the measures were calculated between the respective first and second PCs of each group. Interestingly, synchrony between the second PCs yielded the highest significances, most of them in the left hemisphere. Synchrony changes between the first PCs were mostly significant between Anterior-Central and Central-Posterior. Thus, the first and the second PCs may describe different

neuronal patterns that change with the severity of AD. The usage of more than the first two PCs was ruled out due to the small amount of variance explained by other than the first two PCs. Another possibility would be to use a different factor model instead of PCA. An alternative approach would be to calculate the measures between each channel from one group and each channel from another group, and to average over all these channel pairs (e.g. [38]). The same considerations apply to the measurement of EEG synchrony within channel groups.

For diagnostic purposes, a steep incline or decline of the synchrony measures with decreasing MMSE would be preferable. The only measures that showed a rather monotonous decrease with decreasing MMSE were Granger causalities. For the remaining synchrony measures, diagnostic ambiguity arises due to the initial increase for MMSE scores between 26 and 20/19, and the decrease from 20/19 downwards. However, especially during the cognitive task, a steep initial incline of e.g. coherences was observed. Thus, the synchrony measures could provide valuable information for characterizing the AD severity in an initial stage of AD.

## 4.2 Conclusion

In conclusion, this study indicates that several of the applied synchrony measures relate to AD severity as measured by MMSE score. This relation was observed to be more significant between the EEG channel groups than between single channels. The accumulation of channels allowed a more stable analysis of synchrony, maybe because single EEG channels are more easily disturbed. The most prominent significant results were observed in the EEG of the left hemisphere, especially between temporal and central, temporal and parietal, and central and parietal regions. In the resting state EEG, dynamic canonical correlations and Granger causalities related to MMSE scores most significantly. During the cognitive task, coherences and both static and dynamic canonical correlations showed the highest significances. Thus, the different measures – although closely related to each other – seem to capture different aspects of EEG synchrony. Synchrony changes were observed to be most prominent during the cognitive task and, thus, the clinical recording paradigm yielded a valuable information gain. The usage of the demographic features age, sex, degree of education, and duration of AD as covariables improved the analysis in terms of significance. Another key aspect of this study is the utilization of a quadratic regression model instead of common linear regression. The non-monotonicity allowed to model ambiguous trends of EEG synchrony that cannot be characterized by a linear model. As a matter of fact, all synchrony measures but Granger causalities displayed an increase of EEG synchrony in the initial stage ( $MMSE > 20$ ) of AD and a decrease in later stages. This effect was most prominent during the cognitive task and may be owed to compensatory mechanisms in the brain. Although this phenomenon causes diagnostic ambiguity, its analysis may provide supplementary information for understanding the neuronal



changes in AD.

Future studies should combine the presented EEG synchrony measures with others from e.g. information theory in order to capture additional aspects of EEG synchrony. As EEG slowing and reduced EEG complexity are associated with AD as well, the application of measures for these phenomena should be another approach. Longitudinal studies need to determine as to whether the EEG measures are also capable of predicting AD progression. A combination of EEG measures with other markers for AD severity, e.g. from clinical imaging procedures, could improve the understanding of functional and structural neuronal changes that come along with AD.



---

## Bibliography

---

- [1] R. Schmidt and et al., "Consensus statement 'Dementia 2010' of the Austrian Alzheimer Society," *Neuropsychiatr*, vol. 24, no. 2, pp. 67–87, 2010.
- [2] K. Jellinger, "The enigma of mixed dementia," *Alzheimers Dement.*, vol. 3, no. 1, pp. 40–53, 2007.
- [3] H. Braak, U. Rub, C. Schultz, and K. Del Tredici, "Vulnerability of cortical neurons to Alzheimer's and Parkinson's diseases," *Alzheimer's disease: a century of scientific and clinical research*, pp. 35–44, 2006.
- [4] G. McKhann, D. Drachman, M. Folstein, R. Katzman, D. Price, and E. Stadlan, "Clinical diagnosis of Alzheimer's disease: report of the NINCDS-ADRDA Work Group under the auspices of Department of Health and Human Services Task Force on Alzheimer's Disease," *Neurology*, vol. 34, no. 7, pp. 939–944, 1984.
- [5] J. Jeong, "EEG dynamics in patients with Alzheimer's disease," *Clinical Neurophysiology*, vol. 115, p. 1490–1505, 2004.
- [6] L. Bracco, R. Gallato, F. Grigoletto, A. Lippi, V. Lepore, G. Bino, M. Lazzaro, F. Carella, T. Piccolo, and C. Pozzilli, "Factors affecting course and survival in Alzheimer's disease: a 9-year longitudinal study," *Arch Neurol.*, vol. 51, pp. 1213–1219, 1994.
- [7] J. Wancata, M. Musalek, R. Alexandrowicz, and M. Krautgartner, "Number of dementia sufferers in Europe between the years 2000 and 2050," *European Psychiatry*, vol. 18, no. 6, pp. 306–313, 2003.
- [8] Alzheimer's Disease International, "World Alzheimer Report 2010: The Global Economic Impact of Dementia," 2010.
- [9] World Health Organization and Alzheimer's Disease International, "Dementia: A public health priority," 2012.
- [10] Alzheimer's Disease International, "World Alzheimer Report 2011: The benefits of early diagnosis and intervention," 2011.

- [11] J. Dauwels, F. Vialatte, and A. Cichocki, "Diagnosis of Alzheimer's disease from EEG signals: where are we standing?," *Curr Alzheimer Res.*, vol. 7, no. 6, pp. 487–505, 2010.
- [12] T. Locatelli, M. Cursi, D. Liberati, M. Franceschi, and G. Comi, "EEG coherence in Alzheimer's disease," *Electroencephalogr. Clin. Neurophysiol.*, vol. 106, pp. 229–237, 1998.
- [13] Y. Wada, Y. Nanbu, Y. Koshino, N. Yamaguchi, and T. Hashimoto, "Reduced interhemispheric EEG coherence in Alzheimer's disease: analysis during rest and photic stimulation," *Alzheimer Dis. Assoc. Disord.*, vol. 12, pp. 175–181, 1998.
- [14] R. Anghinah, P. Kanda, M. Jorge, E. De Lima, L. Pascuzzi, and A. De Paiva Melo, "Alpha band coherence analysis of EEG in healthy adult and Alzheimer's type dementia subjects," *Arq. Neuropsiquiatr.*, vol. 58, pp. 272–275, 2000.
- [15] A. Stevens, T. Kircher, M. Nickola, M. Bartels, N. Rosellen, and H. Wormstall, "Dynamic regulation of EEG power and coherence is lost early and globally in probable DAT," *Eur. Arch. Psychiatry Clin. Neurosci.*, vol. 251, p. 199–204, 2001.
- [16] G. Adler, S. Brassens, and A. Jajcevic, "EEG coherence in Alzheimer's dementia," *J Neural Transm.*, vol. 110, no. 9, pp. 1051–1058, 2003.
- [17] K. van der Hiele, A. Vein, R. Reijntjes, R. Westendorp, E. Bollen, M. van Buchem, J. van Dijk, and H. Middelkoop, "EEG correlates in the spectrum of cognitive decline," *Clin Neurophysiol.*, vol. 118, no. 9, pp. 1931–1939, 2007.
- [18] B. Jelles, P. Scheltens, W. van der Flier, E. Jonkman, F. da Silva, and C. Stam, "Global dynamical analysis of the EEG in Alzheimer's disease: frequency-specific changes of functional interactions," *Clin. Neurophysiol.*, vol. 119, no. 4, p. 837–841, 2008.
- [19] K. Akrofi, M. Baker, M. O'Boyle, and R. Schiffer, "A Model of Alzheimer's disease and mild cognitive impairment based on EEG coherence," *ICME International Conference on Complex Medical Engineering*, pp. 1–6, 2009.
- [20] C. Babiloni, R. Ferri, G. Binetti, F. Vecchio, G. Frisoni, B. Lanuzza, C. Miniussi, F. Nobili, G. Rodriguez, F. Rundo, A. Cassarino, F. Infarinato, E. Cassetta, S. Salinari, F. Eusebi, and P. Rossini, "Directionality of EEG synchronization in Alzheimer's disease subjects," *Neurobiol Aging*, vol. 30, no. 1, pp. 93–102, 2009.
- [21] J. Jeong, J. Gore, and B. Peterson, "Mutual information analysis of the EEG in patients with Alzheimer's disease," *Clinical Neurophysiology*, vol. 112, pp. 827–835, 2001.

- [22] B. Wan, D. Ming, H. Qi, Z. Xue, Y. Yin, Z. Zhou, and L. Cheng, "Linear and nonlinear quantitative EEG analysis," *IEEE Eng. Med. Biol. Mag.*, vol. 27, no. 5, pp. 58–63, 2008.
- [23] C. J. Stam, Y. van der Made, Y. A. L. Pijnenburg, and P. Scheltens, "EEG synchronization in mild cognitive impairment and Alzheimer's disease," *Acta Neurologica Scandinavica*, vol. 108, p. 90–96, 2003.
- [24] Y. A. Pijnenburg, Y. van de Made, A. M. van Cappellen van Walsum, D. L. Knol, P. Scheltens, and C. J. Stam, "EEG Synchronization likelihood in mild cognitive impairment and Alzheimer's disease during a working memory task," *Clin. Neurophysiol.*, vol. 115, pp. 1332–1339, 2004.
- [25] C. J. Stam, T. Montez, B. F. Jones, S. A. R. B. Rombouts, Y. van der Made, Y. A. L. Pijnenburg, and P. Scheltens, "Disturbed fluctuations of resting state EEG synchronization in Alzheimer's disease," *Clinical Neurophysiology*, vol. 116, pp. 708–715, 2005.
- [26] M. Kramer, F. L. Chang, M. Cohen, D. Hudson, and A. Szeri, "Synchronization measures of the scalp EEG can discriminate healthy from Alzheimer's subjects," *International Journal of Neural Systems*, vol. 17, pp. 1–9, 2007.
- [27] C. Stam, G. Nolte, and A. Daffertshofer, "Phase lag index: assessment of functional connectivity from multi channel EEG and MEG with diminished bias from common sources," *Hum. Brain Mapp.*, vol. 28, no. 11, p. 1178–1193, 2007.
- [28] Y. Park, H. Che, C. Im, H. Jung, S. Bae, and S. Lee, "Decreased EEG synchronization and its correlation with symptom severity in Alzheimer's disease," *Neurosci Res.*, vol. 62, no. 2.
- [29] Y. Pijnenburg, R. Strijers, Y. Made, W. van der Flier, P. Scheltens, and C. Stam, "Investigation of resting-state EEG functional connectivity in frontotemporal lobar degeneration," *Clin Neurophysiol.*, vol. 119, no. 8, pp. 1732–1738, 2008.
- [30] J. Dauwels, F. Vialatte, T. Rutkowski, and A. Cichocki, "Measuring neural synchrony by message passing," *Advances in Neural Information Processing Systems*, vol. 20, 2007.
- [31] M. J. Hogan, G. R. Swanwick, J. Kaiser, M. Rowan, and B. Lawlor, "Memory-related EEG power and coherence reductions in mild Alzheimer's disease," *Int. J. Psychophysiol.*, vol. 49, no. 2, pp. 147–163, 2003.
- [32] Z. Y. Jiang, "Study on EEG Power and Coherence in Patients with Mild Cognitive Impairment During Working Memory Task," *J. Zhejiang Univ. Sci B.*, vol. 6, pp. 1213–1219, 2005.

- [33] Z. Y. Jiang and L. L. Zheng, "Inter- and intra-hemispheric EEG coherence in patients with mild cognitive impairment at rest and during working memory task," *J. Zhejiang Univ Sci B.*, vol. 7, pp. 357–364, 2006.
- [34] Z. Hidasi, B. Czigler, P. Salacz, E. Csibri, and M. Molnár, "Changes of EEG spectra and coherence following performance in a cognitive task in Alzheimer's disease," *Int. J. Psychophysiol.*, vol. 65, no. 3.
- [35] B. Güntekin, E. Saatçi, and G. Yener, "Decrease of evoked delta, theta and alpha coherences in Alzheimer patients during a visual oddball paradigm," *Brain Res.*, vol. 1235, pp. 109–116, 2009.
- [36] M. Kikuchi, Y. Wada, T. Takeda, H. Oe, T. Hashimoto, and Y. Koshino, "EEG harmonic responses to photic stimulation in normal aging and Alzheimer's disease: differences in interhemispheric coherence," *Clin Neurophysiol.*, vol. 113, no. 7.
- [37] Z. Y. Jiang, "Abnormal Cortical Functional Connections in Alzheimer's Disease: Analysis of Inter- and Intra-Hemispheric EEG Coherence," *J Zhejiang Univ Sci B.*, vol. 6, p. 259–264, 2005.
- [38] J. Dauwels, F. Vialatte, T. Musha, and A. Cichocki, "A comparative study of synchrony measures for the early diagnosis of Alzheimer's disease based on EEG," *NeuroImage*, vol. 49, p. 668–693, 2010.
- [39] C. Babiloni, R. Ferri, G. Binetti, A. Cassarino, G. D. Forno, M. Ercolani, F. Ferreri, G. B. Frisoni, B. Lanuzza, C. Miniussi, F. Nobili, G. Rodriguez, F. Rundo, C. J. Stam, T. Musha, F. Vecchio, and P. M. Rossini, "Fronto-parietal coupling of brain rhythms in mild cognitive impairment: a multicentric EEG study," *Brain Res. Bull.*, vol. 69, pp. 63–73, 2006.
- [40] M. Folstein, S. Folstein, and P. McHugh, "'Mini-mental state'. A practical method for grading the cognitive state of patients for the clinician," *Journal of psychiatric research*, vol. 12, no. 3, pp. 189–198, 1975.
- [41] M. Deistler and W. Scherrer, "The prague lectures, ECONOMETRICS II," 1992. Lecture notes for a course in Econometrics, Time Series Analysis, given at CERGE Prag, January – May 1992.
- [42] M. Waser, M. Deistler, H. Garn, T. Benke, P. Dal-Bianco, G. Ransmayr, D. Grossegger, and R. Schmidt, "EEG in the diagnostics of Alzheimer's disease," *Statistical Papers*, pp. 1–13, 2013.
- [43] C. Hughes, L. Berg, W. Danziger, L. Coben, and R. Martin, "A new clinical scale for the staging of dementia," *Br J Psychiatry*, vol. 140, pp. 566–572, 1982.

- [44] I. Gélinas, L. Gauthier, and M. McIntyre, "Development of a functional measure for persons with Alzheimer's disease: the Disability Assessment for Dementia," *American Journal of Occupational Therapy*, vol. 53, pp. 471–481, 1999.
- [45] J. Cummings, M. Mega, K. Gray, S. Rosenberg-Thompson, D. Carusi, and J. Gornbein, "The Neuropsychiatric Inventory: comprehensive assessment of psychopathology in dementia," *Neurology*, vol. 44, no. 12, pp. 2308–14, 1994.
- [46] J. Yesavage, T. Brink, T. Rose, O. Lum, V. Huang, M. Adey, and V. Leirer, "Development and validation of a geriatric depression screening scale: a preliminary report," *J Psychiatr Res.*, vol. 17, no. 1, pp. 37–49, 1982–1983.
- [47] J. Morris, A. Heyman, R. Mohs, J. Hughes, G. van Belle, and G. Fillenbaum, "The Consortium to Establish a Registry for Alzheimer's Disease (CERAD): part 1 — clinical and neuropsychological assessment of Alzheimer's disease," *Neurology*, vol. 39, pp. 1159–1165, 1989.
- [48] S. Mirra, A. Heyman, D. McKeel, S. Sumi, B. Crain, and L. Brownlee, "The Consortium to Establish a Registry for Alzheimer's Disease (CERAD): part 2 — clinical and neuropsychological assessment of Alzheimer's disease," *Neurology*, vol. 41, pp. 479–486, 1991.
- [49] H. H. Jasper, "The ten-twenty electrode system of the International Federation," *Electroencephalography and Clinical Neurophysiology*, vol. 10, no. 2, pp. 371–375, 1958.
- [50] H.-J. Park, D.-U. Jeong, and K.-S. Park, "Automated detection and elimination of periodic ECG artifacts in EEG using the energy interval histogram method," *IEEE Transactions on Biomedical Engineering*, vol. 49, no. 12, pp. 1526–1533, 2002.
- [51] S. Mukhopadhyay and G. C. Ray, "A new interpretation of non-linear energy operator and its efficacy in spike detection," *IEEE Transactions on Biomedical Engineering*, vol. 45, no. 2, pp. 180–187, 1998.
- [52] M. Waser and H. Garn, "Removing Cardiac Interference from the Electroencephalogram Using a Modified Pan-Tompkins Algorithm and Linear Regression," *35th Annual International IEEE EMBS Conference*, 2013.
- [53] A. Y. Kaplan, A. A. Fingelkurts, A. A. Fingelkurts, S. V. Borisov, and B. S. Darkhovsky, "Nonstationary nature of the brain activity as revealed by EEG/MEG: Methodological, practical and conceptual challenges," *Signal Processing*, vol. 85, no. 11, pp. 2190–2212, 2005.

- [54] G. Bodenstein and H. M. Praetorius, "Feature extraction from the electroencephalogram by adaptive segmentation," *Proceedings of the IEEE*, vol. 65, no. 5, p. 642–652, 1977.
- [55] M. Deistler, O. Prohaska, E. Reschenhofer, and R. Vollmer, "Procedure for identification of different stages of EEG background activity and its application to the detection of drug effects," *Electroencephalogr Clin Neurophysiol.*, vol. 64, no. 4, pp. 294–300, 1986.
- [56] P. J. Brockwell and R. A. Davis, *Time series: Theory and Methods*. Springer, 1991.
- [57] E. J. Hannan, *Multiple Time Series*. Wiley, 1970.
- [58] E. J. Hannan and M. Deistler, *The statistical theory of linear systems*. Wiley, 1988.
- [59] Y. A. Rozanov, *Stationary Random Processes*. Holden-Day, 1967.
- [60] D. R. Brillinger, *Time Series: Data Analysis and Theory*. Holden-Day, 1981.
- [61] R. Dahlhaus, "Graphical interaction models for multivariate time series," *Metrika*, vol. 51, pp. 157–172, 2000.
- [62] C. W. J. Granger, "Investigating causal relations by econometric models and cross-spectral methods," *Econometrica*, vol. 37, pp. 424–438, 1969.
- [63] C. Flamm, U. Kalliauer, M. Deistler, M. Waser, and A. Graef, "Graphs for Dependence and Causality in Multivariate Time Series," in *System Identification, Environmental Modelling, and Control System Design*, pp. 133–151, Springer London, 2012.
- [64] M. Eichler, "Graphical modeling of dynamic relationships in multivariate time series," in *Handbook of Time Series Analysis*, p. 335–372, Wiley-VCH, 2006.
- [65] H. Hotelling, "Relations Between Two Sets of Variates," *Biometrika*, vol. 28, no. 3–4, pp. 321–377, 1936.
- [66] K. Pearson, "On Lines and Planes of Closest Fit to Systems of Points in Space," *Philosophical Magazine*, vol. 2, no. 11.
- [67] H. Hotelling, "Analysis of a complex of statistical variables into principal components," *Journal of Educational Psychology*, vol. 24, pp. 417–441, 498–520, 1933.
- [68] R. Schlittgen and B. H. J. Streitberg, *Zeitreihenanalyse*. Oldenbourg Wissenschaftsverlag GmbH, 2001.



- [69] A. Schuster, "On the investigation of hidden periodicities with application to a supposed 26 day period of meteorological phenomena," *Terrestrial Magnetism and Atmospheric Electricity*, vol. 3, no. 13–14, 1898.
- [70] J. W. Tukey, "An introduction to the calculations of numerical spectrum analysis," *Spectral Analysis of Time Series*, pp. 25–46, 1967.
- [71] R. B. Blackman and J. W. Tukey, "Particular Pairs of Windows," *The Measurement of Power Spectra, From the Point of View of Communications Engineering*, pp. 98–99, 1959.
- [72] E. Parzen, "On Estimation of a Probability Density Function and Mode," *The Annals of Mathematical Statistics*, vol. 33, no. 3, pp. 1065–1076, 1962.
- [73] R. Dahlhaus, M. Eichler, and J. Sankühler, "Identification of synaptic connections in neural ensembles by graphical models," *Journal of Neuroscience Methods*, vol. 77, pp. 93–107, 1997.
- [74] H. Akaike, "A new look at the statistical model identification," *IEEE Transactions on Automatic Control*, vol. 19, no. 6, p. 716–723, 1974.
- [75] J. A. Jiang, C. F. Chao, M. J. Chiu, R. G. Lee, C. L. Tseng, and R. Lin, "An automatic analysis method for detecting and eliminating ECG artifacts in EEG," *Computers Biol. Med.*, vol. 37, pp. 1660–1671, 2007.
- [76] T. P. Jung, S. Makeig, C. Humphries, T. W. Lee, M. J. McKeown, V. Iragui, and T. J. Sejnowski, "Removing electroencephalographic artifacts by blind source separation," *Psychophysiology*, vol. 37, no. 2, pp. 163–178, 2000.
- [77] M. Nakamura and H. Shibasaki, "Elimination of EKG artifacts from EEG recordings: a new method of noncephalic referential EEG recording," *Electroenceph. and Clin. Neurophysiol.*, vol. 66, pp. 89–92, 1987.
- [78] H.-J. Park, J.-M. Han, D.-U. Jeong, and K.-S. Park, "A study on the elimination of the ECG artifact in the polysomnographic EEG and EOG using AR model," *20th Int. Conf. IEEE EMBS*, pp. 1632–1635, 1998.



# Curriculum Vitae

## Personal information

First name(s) / Surname(s) **Dipl.-Ing. Markus WASER**  
Address(es) Promenadegasse 11-13/3/11, 1170 Vienna, Austria  
Telephone(s) Mobile: +43 6504685333  
E-mail markus.waser@gmx.at  
Nationality Austrian  
Date of birth 04.06.1985  
Gender Male

## Education and training

Dates May 2010 onwards  
Title of qualification awarded Dr. techn.  
Principal subjects/occupational skills covered Econometrics, time series analysis, and system theory with a focus on biomedical signal analysis  
Name and type of organisation providing education and training Vienna University of Technology, Institute of Mathematical Methods in Economics  
Level in national or international classification ISCED 6

Dates 2004 - 2010  
Title of qualification awarded Dipl.-Ing., (with honors)  
Principal subjects/occupational skills covered - Technical Mathematics  
- Mathematical Methods in Economics  
Name and type of organisation providing education and training Vienna University of Technology  
Level in national or international classification ISCED 5

Dates August 2008 – January 2009  
(Exchange term)  
Title of qualification awarded -  
Principal subjects/occupational skills covered Economics  
Name and type of organisation providing education and training City College of New York (CCNY)

Dates 2009 - 2010  
Title of qualification awarded -  
Principal subjects/occupational skills covered - Interaction between technology, innovation, and markets  
- Benchmarking, marketing, and business management  
Name and type of organisation providing education and training Top Industrial Managers Europe (T.I.M.E.) European Management Program (T.E.M.P.)  
- Vienna University of Technology (September 2009)  
- Universidad Politécnica de Madrid (February 2010)  
- University of Sevilla (September 2010)

Dates 2009 - 2010  
 Title of qualification awarded -  
 Principal subjects/occupational skills covered - Use-of-potential analysis  
 - Establishing interdisciplinary network  
 Name and type of organisation providing education and training Vienna University of Technology, TUtheTOP – High Potential Program

**Professional experience**

Dates January 2011 onwards  
 Occupation or position held Scientist  
 Main activities and responsibilities - Developing algorithms for biosignal processing with focus on electroencephalogram (EEG)  
 - Statistical evaluation of biomarkers for neurodegenerative disorders with focus on Alzheimer's disease  
 Name and address of employer AIT Austrian Institute of Technology, Donau-City-Straße 1, 1220 Vienna, Austria  
 Type of business or sector Research

Dates 2010 - 2011  
 Occupation or position held Project Assistant  
 Main activities and responsibilities Analysing methods in econometrics, time series analysis, and system theory  
 Name and address of employer Vienna University of Technology, Institute of Mathematical Methods in Economics, Argentinierstr. 8, 1040 Vienna, Austria  
 Type of business or sector Research

Dates 2009 - 2011  
 Occupation or position held Software Developer  
 Main activities and responsibilities Developing algorithms for financial time series analysis and automated trading systems  
 Name and address of employer TeleTrader Software GmbH, Salzgies 15, 1010 Vienna, Austria  
 Type of business or sector Finance

Dates 2005 - 2008  
 Occupation or position held Private Tutor  
 Main activities and responsibilities Assisting children in all academic years with Mathematics, English, and Latin  
 Name and address of employer LernQuadrat OG und Bildungsmanagement GmbH, Mariahilfer Straße 103, 1060 Vienna, Austria  
 Type of business or sector Tutoring

**Language competences**

Mother tongue(s) **German**

Other language(s)

Self-assessment  
 European level (\*)

**English**

**French**

**Spanish**

**Latin**

Understanding				Speaking				Writing	
Listening		Reading		Spoken interaction		Spoken production			
C1	Proficient	C1	Proficient	C1	Proficient	C1	Proficient	C1	Proficient
B2	Ind. user	B2	Ind. user	B2	Ind. user	B2	Ind. user	B2	Ind. user
A1	Beginner	A1	Beginner	A1	Beginner	A1	Beginner	A1	Beginner
-	-	B2	Ind. user	-	-	-	-	B2	Ind. user

(\*) *Common European Framework of Reference for Languages*

## Publications

### Journal papers

M. Waser, M. Deistler, H. Garn, T. Benke, P. Dal-Bianco, G. Ransmayr, D. Grossegger, and R. Schmidt, "EEG in the diagnostics of Alzheimer's disease," *Statistical Papers*, pp. 1–13, 2013.

### Conferences with proceedings

M. Waser and H. Garn, "Removing cardiac interference from the electroencephalogram using a modified Pan-Tompkins algorithm and linear regression," 35th Annual International IEEE EMBS Conference, 2013.

H. Garn, M. Waser, M. Lechner, M. Dorfer, and D. Grossegger, "Robust, automatic real-time monitoring of the time course of the individual alpha frequency in the time and frequency domain," 34th Annual International IEEE EMBS Conference, 2012.

### Conferences with abstract

H. Garn, M. Waser, T. Benke, P. Dal-Bianco, G. Ransmayr, M. Deistler, D. Grossegger, and R. Schmidt, "Using cognitive qEEG to characterize disease severity in the PROspective DEMentia registry Austria (PRODEM)," 21st World Congress of Neurology, 2013.

### Book chapters

C. Flamm, U. Kalliauer, M. Deistler, M. Waser, and A. Graef, "Graphs for dependence and causality in multivariate time series," in *System Identification, Environmental Modelling, and Control System Design*, pp. 133–151, Springer London, 2012.



---

(Markus Waser)